AAAS

Science

19 FEBRUARY 2026

AUDACIOUS ANGLER

Tall-crested *Spinosaurus* species discovered in the Sahara **p. 782**

RESEARCH ARTICLE SUMMARY

PALEONTOLOGY

Scimitar-crested *Spinosaurus* species from the Sahara caps stepwise spinosaurid radiation

Paul C. Sereno *et al.*

Full article and list of author affiliations: https://doi.org/10.1126/science.adx5486

INTRODUCTION: The fossils of *Spinosaurus aegyptiacus*, a giant sail-backed, fish-eating theropod dinosaur from northern Africa, have inspired competing lifestyle interpretations, either as a semiaquatic ambush predator stalking shorelines and shallows or a fully aquatic predator in pursuit of prey underwater. Its bones and teeth have been found only in coastal deposits near marine margins, a locale potentially consistent with either lifestyle interpretation.

RATIONALE: In the central Sahara, a new fossiliferous area (Jenguebi) was discovered in beds equivalent in age [Farak Formation; Cenomanian ~95 million years ago (Mya)] to those yielding fossil remains of *S. aegyptiacus*. We describe from this area a new species, *Spinosaurus mirabilis* sp. nov., which is very similar to *S. aegyptiacus* in skeletal form but with a much taller, scimitar-shaped cranial crest. Two new sauropods were found in close association with the new spinosaurid buried in fluvial sediments indicative of an inland riparian habitat.

RESULTS: *S. mirabilis* sp. nov. is distinguished by the low profile of its snout, a hypertrophied nasal-prefrontal crest, greater spacing of posterior maxillary teeth, and other features. Its features highlight the extraordinary specializations of both species of the genus *Spinosaurus*, including interdigitating upper and lower teeth. Principal component analysis of body proportions places spinosaurids between semiaquatic waders (e.g., herons) and aquatic divers (e.g., darters) distant from all other predatory dinosaurs. A time-calibrated phylogenetic analysis resolves three evolutionary phases: an initial Jurassic radiation when their distinctive elongate fish-snaring skull evolved and split into two distinctive designs, baryonychine and spinosaurine; an Early Cretaceous circum-Tethyan diversification when both reigned as dominant predators; and a final early Late Cretaceous phase when spinosaurines attained maximum body size as shallow water ambush specialists limited geographically to northern Africa and South America.

CONCLUSION: The discovery of the tall-crested *S. mirabilis* sp. nov. in a riparian setting within an inland basin supports a lifestyle interpretation of a wading, shoreline predator with visual display an important aspect of its biology. At the end of the Cenomanian about 95 million years ago, an abrupt eustatic rise in sea level and the attendant climate change brought the spinosaurid radiation to an end. □

Corresponding authors: dinosaur@uchicago.edu (Paul C. Sereno); eoalulavis@gmail.com (Daniel Vidal) Cite this article as P. C. Sereno *et al.*, *Science* **391**, eadx5486 (2026). DOI: 10.1126/science.adx5486

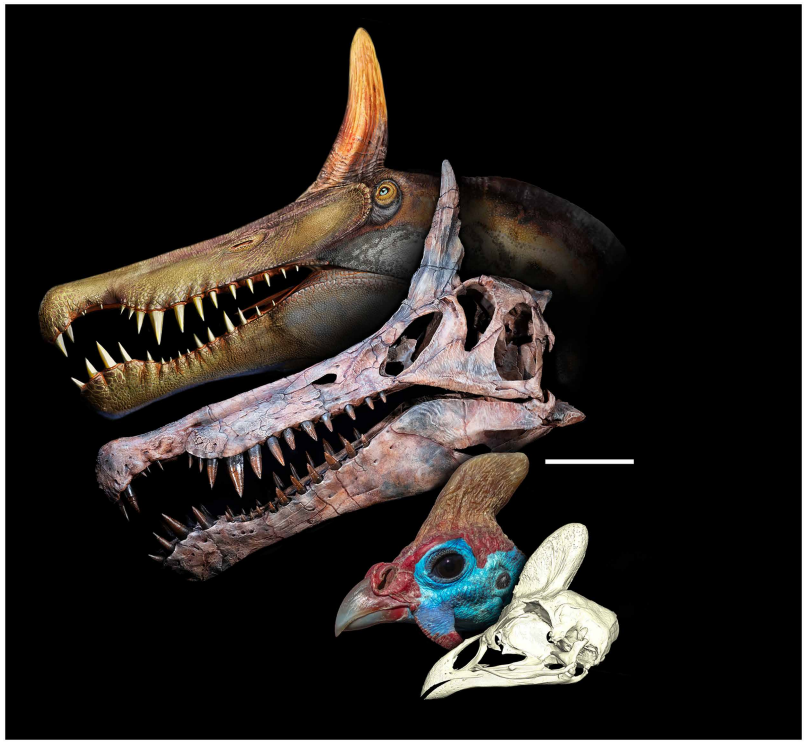

Sheathed bony head crests ~~and~~ extinct and living dinosaurs. *S. mirabilis* sp. nov., evolved the tallest head crest of any theropod dinosaur, drawing attention to the midline ornamentation that characterizes the cranium and axial skeleton of all spinosaurids. In life, the crest would have been extended to some degree by a keratinous sheath, as in the living helmeted guinea fowl (*Numida meleagris*). Visual signaling, as is the case in guinea fowl and other crested avians, was likely the function of spinosaurid cranial crests and trunk and tail sails. Scale bar, 20 cm for *S. mirabilis* and 3 cm for *N. meleagris*.

FLESH RENDERING AND LAYOUT BY DANI NAVARRO; ADULT SKULL CAST BY THE FOSSIL LAB; HELMETED GUINEA FOWL IMAGES BY TODD GREENE

PALEONTOLOGY

Scimitar-crested *Spinosaurus* species from the Sahara caps stepwise spinosaurid radiation

Paul C. Sereno[1,2]*, Daniel Vidal[1,3]*, Nathan P. Myhrvold[4], Evan Johnson-Ransom[1], María Ciudad Real[3], Stephanie L. Baumgart[5], Noelia Sánchez Fontela[6], Todd L. Green[7], Evan T. Saitta[1], Boubé Adamou[8], Lauren L. Bop[1], Tyler M. Keillor[1], Erin C. Fitzgerald[1], Didier B. Dutheil[9], Robert A. S. Laroche[10], Alexandre V. Demers-Potvin[11], Álvaro Simarro[3], Francesc Gascó-Lluna[12], Ana Lázaro[13], Arturo Gamonal[3], Charles V. Beightol[14], Vincent Reneleau[9], Rachel Vautrin[9], Filippo Bertozzo[15], Alejandro Granados[16], Grace Kinney-Broderick[17], Jordan C. Mallon[18], Rafael M. Lindoso[19], Jahandar Ramezani[20]

We describe a close relative of *Spinosaurus aegyptiacus*, the sail-backed, fish-eating giant from nearshore deposits of northern Africa. *Spinosaurus mirabilis* sp. nov., discovered in the central Sahara alongside long-necked dinosaurs in a riparian habitat, is distinguished by a scimitar-shaped bony crest projecting far above its skull roof. We discern three discrete phases in spinosaurid evolution. During the first phase with roots in the Jurassic, an elongate fish-snaring skull emerged that soon was modified along divergent paths. During a second Early Cretaceous phase, spinosaurids became the dominant predators in circum-Tethyan habitats. The final phase began just before the Late Cretaceous during the opening of the Atlantic Ocean, when spinosaurines attained maximum body size as shallow water ambush specialists limited geographically to northern Africa and South America.

Spinosaurus aegyptiacus, a sail-backed fish-eating giant from nearshore deposits of northern Africa, has attracted renewed attention over its skeletal form and lifestyle interpretations (*1*–*3*). Secondarily aquatic vertebrates arose multiple times among reptiles, including ichthyosaurs, plesiosaurs, mosasaurs, fluked sea-faring crocodylomorphs, and diving penguins (*4*), but apparently never among nonavian dinosaurs that inhabited all major continental areas for nearly 150 million years. That is, unless *S. aegyptiacus* and some of its forebears were more than semiaquatic shoreline ambush predators wading into shallow waters (*2*, *3*, *5*, *6*) and instead were aquatic divers pursuing prey underwater with severely reduced functional capacity on land (*7*–*9*).

To date, *Spinosaurus* fossils are known only from nearshore deposits along Africa's margin of the Tethys Sea (*1*–*3*, *10*, *11*). Finding ~7-tonne *Spinosaurus* (*3*) within a terrestrial basin at distance from a marine shoreline could provide key evidence for a semiaquatic lifestyle, because all large-bodied (>1 tonne) secondarily aquatic tetrapods, living and extinct, are marine (*4*). Here, we describe a new *Spinosaurus* species with a scimitar-shaped cranial crest that otherwise is close in size and skeletal form to *S. aegyptiacus* (Figs. 1 to 3). Its remains were discovered in an inland basin in the central Sahara at the end of the final phase of spinosaurid evolution.

Results

Systematic paleontology

Dinosauria Owen, 1842
Theropoda Marsh, 1884
Spinosauridae Stromer, 1915
Spinosaurinae Stromer, 1915
Spinosaurini Stromer, 1915
Spinosaurus Stromer, 1915

Revised generic diagnosis

Large-bodied spinosaurine (skeletal length ~10 to 14 m) characterized by relatively small external naris and narial fossa (maximum diameter less than half that of the orbit) that are retracted to a position closer to the orbit than the anterior end of the snout, exclusion of the premaxilla from the border of the external naris*, blade-shaped, fused nasal crest lapped laterally along its base by a subtriangular prefrontal process*, "mushroom-shaped" snout where the anterior end of premaxillae is wider than long with a constriction after pm3*, interdigitating mid and posterior maxillary and dentary teeth with festooned alveolar external margins*, notch for dentary tooth 1 in the premaxillae at the height of the second alveoli*, diastema in maxillary and dentary tooth rows with paired tooth pairs*, anterior edge of dentary protruding, with a chin-like process more anterior than dentary tooth 1 that is directed anterodorsally*, midcervical neural spines (~C5) anteroposteriorly broadened (equal to centrum length without the condyle), anterior dorsal neural spines strap shaped (parallel sided); mid and posterior dorsal neural spines with an expanded spine base*, anterior caudal neural spines with cruciate cross section*, tibial medial malleolar edge not covered by astragalus. Asterisks indicate unambiguous generic synapomorphies.

Holotype

The holotype of *S. mirabilis* (MNBH JEN1, where MNBH is Musée National Boubou Hama, Niamey, Niger) is an associated right premaxilla, both maxillae, the base and the bottom half of the fused nasal crest with portions of both prefrontals, the alveolar edge of the right dentary, and five maxillary teeth found in association with the maxillae.

Referred specimens

Referred specimens come from Jenguebi (MNBH JEN2–9) and Iguidi (MNBH IGU11, IGU25, and IGU38) (Fig. 1A, "Fossil materials" section in the supplementary materials, and table S1).

Etymology

The species name *mirabilis*, meaning "astonishing" in Latin, is in reference to the hypertrophied nasal-prefrontal crest.

Type locality and horizon

The holotype was found in Sirig Taghat (meaning "no water, no goat" in Tamasheq), Jenguebi area, Agadez Region, Republic of the Niger, Farak Formation (*12*).

The arc of Mesozoic sediments to the south of the Aïr Massif infilling the Iullemeden Basin (*13*), initially informally described as "Continentale intercalaire" (*14*), includes four successive terrestrial formations of

[1]Department of Organismal Biology and Anatomy, University of Chicago, Chicago, IL, USA. [2]Committee on Evolutionary Biology, University of Chicago, Chicago, IL, USA. [3]Grupo de Biología Evolutiva, UNED, Madrid, Spain. [4]Intellectual Ventures, Bellevue, WA, USA. [5]Department of Physiological Sciences, University of Florida, College of Veterinary Medicine, Gainesville, FL, USA. [6]Independent researcher, Navalcarnero, Madrid, Spain. [7]Department of Biomedical and Anatomical Sciences, New York Institute of Technology College of Osteopathic Medicine at Arkansas State University, Jonesboro, AR, USA. [8]Institute for Research in the Humanities, Abdou Moumouni University, Niamey, République du Niger. [9]Centre de Recherche en Paléontologie – Paris, Muséum National d'Histoire Naturelle, Paris, France. [10]Department of BioSciences, Rice University, Houston, TX, USA. [11]Department of Bioengineering, McGill University, Montreal, Canada. [12]Museo de Benagéber, Benagéber, Valencia, Spain. [13]Universidad de Valencia, Valencia, Spain. [14]Vicksburg National Military Park, Vicksburg, MS, USA. [15]Operational Directorate Earth and History of Life, Royal Belgian Institute of Natural Sciences, Brussels, Belgium. [16]Departamento de Ecología y Geología, University of Málaga, Málaga, Spain. [17]Department of Earth Sciences, University of Cambridge, Cambridge, UK. [18]Beaty Centre for Species Discovery and Palaeobiology Section, Canadian Museum of Nature, Ottawa, Canada. [19]Instituto Federal de Educação, Ciência e Tecnologia do Maranhão, Departamento Acadêmico de Biologia, Campus Monte Castelo, São Luís-MA, Brasil. [20]Department of Earth, Atmospheric and Planetary Sciences, Massachusetts Institute of Technology, Cambridge, MA, USA. ***Corresponding author. Email: dinosaur@uchicago.edu (P.C.S.); eoalulavis@gmail.com (D.V.)**

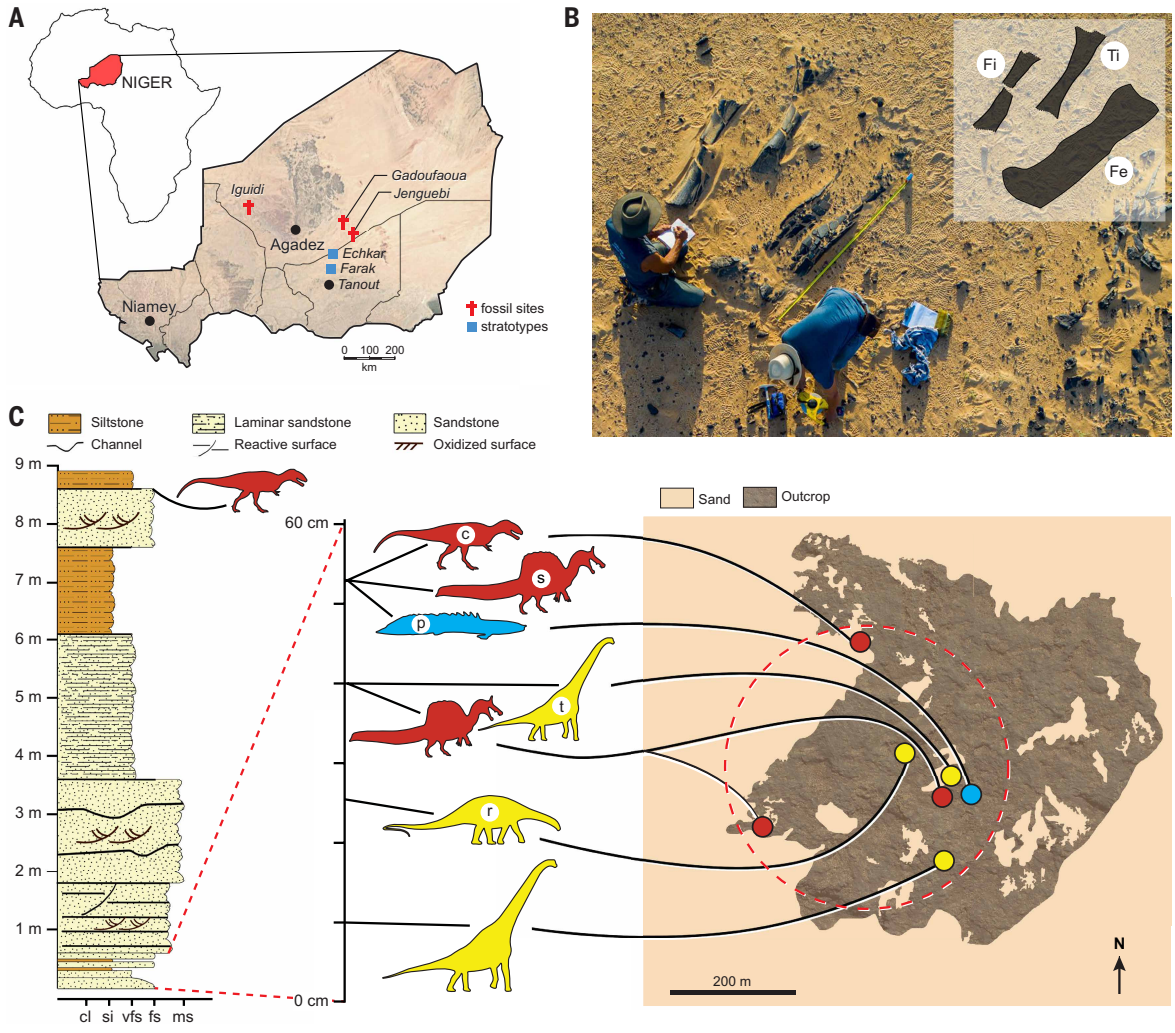

Fig. 1. Locality of *S. mirabilis* sp. nov. in Niger. (**A**) Location of the fossil areas Jenguebi, Gadoufaoua, and Iguidi (In Abangharit) and the stratotype sections of the Echkar and Farak Formations. (**B**) Drone photograph of the Sirig Taghat locality in the Jenguebi area showing the associated hind leg of a partial skeleton of a large unnamed titanosaurian. (**C**) Stratigraphic section (left) of the Farak Formation in the vicinity of the type locality for *S. mirabilis* with a map of key specimens from the lowermost 60 cm. Also shown in an ~8- to 9-m upsection is an associated carcharodontosaurid skeleton collected nearby. A map (right) of the central exposure at Sirig Taghat shows the proximity of the large-bodied fauna (dashed circle, 450 m diameter). c, *Carcharodontosaurus* sp.; cl, clay; Fe, femur; Fi, fibula; fs, fine sand; ms, medium sand; p, unnamed polypterid; r, unnamed rebbachisaurid; s, *S. mirabilis*; si, silt; t, unnamed titanosaurian; Ti, tibia; vfs, very fine sand.

Cretaceous age, Tazolé, Elrhaz, Echkar, and Farak (*15*), the last underlying the well-dated Cenomanian-Turonian limestone (*16*). We revisited the name-bearing sections for both the Echkar and Farak Formations and exposures of the overlying Cenomanian-Turonian limestone in terrain near Tanout (Fig. 1A). We conclude that both the Jenguebi and Iguidi (In Abangharit) fossil areas represent exposures of the Farak Formation (*12*). The collected vertebrate fauna at both locales compares closely with the Kem Kem Group of Morocco (*10*, *17*) [Early to Middle Cenomanian, 100 to 95 million years ago (Mya); see the "Local stratigraphy and associated fauna" section in the supplementary materials].

Diagnosis

Spinosaurine with a low snout (parallel dorsal and ventral margins in profile)*, greater spacing of posterior maxillary (and presumably opposing dentary) teeth*, a scimitar-shaped nasal-prefrontal crest arching upward and backward with a lateral eminence offset toward the anterior margin*, postaxial cervical pleurocoels with greater anteroposterior diameter than adjacent parapophyseal articular facets, and a tibial articular depression for the ascending process of the astragalus reduced in area with the edge of the medial malleolus exposed in anterior view (Figs. 2, A and B and 3A and the "Fossil materials" section in the supplementary materials). Asterisks above indicate autapomorphies of *S. mirabilis* sp. nov.

Saharan fossil trove

In the 1950s, French uranium geologists discovered abundant vertebrate fossils on the western edge of a vast Saharan sand sea in Niger (*18*). Called Gadoufaoua (Fig. 1A), the area soon attracted return expeditions that have unearthed a landmark vertebrate fauna of mid-Cretaceous age (~110 Mya, Aptian-Albian), including the most completely known spinosaurid *Suchomimus tenerensis* (*3*, *19*). Also in the 1950s, French geologist H. Faure (*12*, *20*) discovered fossils in Cretaceous rocks of younger age (~95 Mya, Cenomanian). Akarazeras, his small, remote locale, yielded a few sabre-shaped teeth resembling those of the giant predator *Carcharodontosaurus saharicus* from similar-age rocks in the Western Desert of Egypt (*17*). Unlike Gadoufaoua, no one returned, and Faure's fossil teeth were lost.

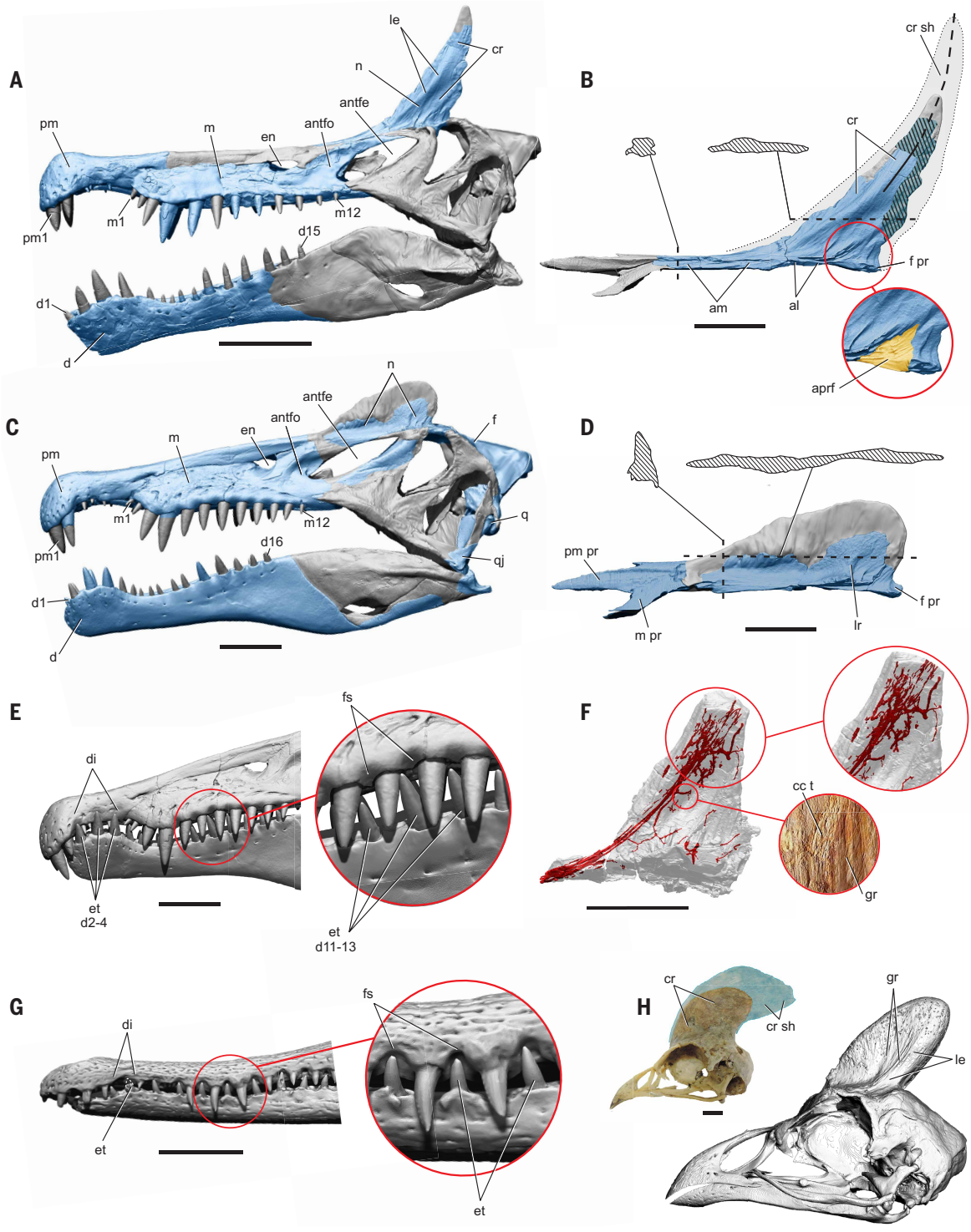

Fig. 2. Skull of *S. mirabilis* sp. nov. compared with *S. aegyptiacus* and modern analogs. (**A**) Composite skull reconstruction of *S. mirabilis* showing preserved bones (blue) with the occiput and posterior lower jaw based on *Irritator challengeri* (*43*,*48*). (**B**) Fused nasals of *S. mirabilis* (MNBH JEN3) are shown in left lateral view with transverse (anterior) and horizontal (posterior) cross sections of the anterior process and crest, respectively. Portions of the crest known in other specimens (MNBH JEN1, JEN2) are shown (cross-hatched blue) as well as reconstructed portions that are currently unknown (dark gray). The estimated extension of the crest as a keratinous sheath is shown (light gray). A magnified view of the articular surface for the prefrontal is shown (yellow). (**C**) Composite skull reconstruction of *S. aegyptiacus* showing preserved bones (blue) with most of the occiput and posterior lower jaw (dark gray) based on *I. challengeri* (*43*). (**D**) Fused nasals of *S. aegyptiacus* (UCRC PV14, 15, 192 scaled to match) with transverse (anterior) and horizontal (posterior) cross sections of the anterior process and crest, respectively, and the thin broken dorsal margin restored (dark gray). (**E**) Interdigitating teeth in *S. aegyptiacus* with magnified view showing alveolar festoons to accommodate everted dentary crowns (MSNM V4047, UCRC PV4). (**F**) CT-based digital rendering of neurovascular canals within the nasal crest of *S. mirabilis* in left lateral view with magnified views of vascularity at mid length and surface striations (MNBH JEN1). (**G**) Optical scan of the end of the snout of an African slender-snouted crocodile (*Mecistops cataphractus*, UF Herp 145926) in left lateral view showing a one-tooth upper diastema and festooned alveolar margins accommodating everted teeth. (**H**) Skull of the helmeted guineafowl (*Numida meleagris*, TLG NM007) in lateral view from a CT scan

(*25*) and with lateral view of an adult male skull (*27*) showing the fused frontal crest and its extension by a keratinous crest sheath (green). MSNM, Museo Civico di Storia Naturale, Milan; TLG, T. L. Green Research Collection, Denver; UCRC, University of Chicago Research Collection, Chicago; UF, University of Florida, Gainesville. al, articular surface for the lacrimal; am, articular surface for the maxilla; antfe, antorbital fenestra; antfo, antorbital fossa; aprf, articular surface for the prefrontal; cc t, crisscross texture; cr, crest; cr sh, crest sheath; d, dentary; d1 to 4, 11 to 13, 15, and 16, dentary tooth 1 to 4, 11 to 13, 15, and 16; di, diastema; en, external naris; et, everted tooth; et, everted tooth; f, frontal; f pr, frontal process; fs, festoon; gr, groove; le, lateral eminence; lr, lateral ridge; m, maxilla; m1, 12, maxillary tooth 1, 12; m pr, maxillary process; n, nasal; pm, premaxilla; pm1, premaxillary tooth 1; pm pr, premaxillary process; q, quadrate; qj, quadratojugal. Scale bars, 20 cm in (A), (C) and (E); 10 cm in (B), (D) and (F); 5 cm in (G); and 1 cm in (H).

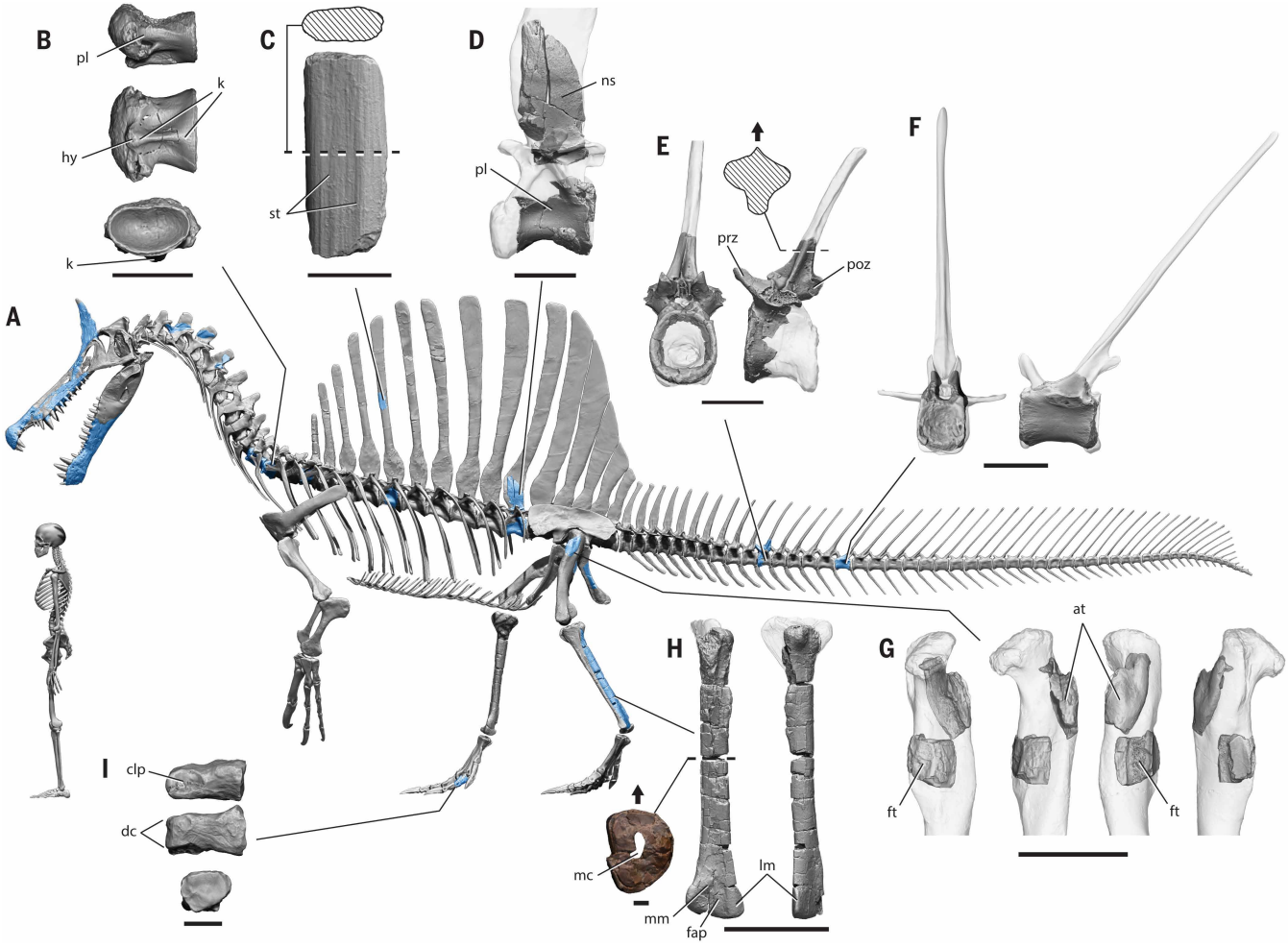

Fig. 3. Preserved postcranial bones of *S. mirabilis* sp. nov. (**A**) Composite skeletal silhouette showing preserved bones (blue) of *S. mirabilis* with skeletal length of ~8 m scaled to the size of the subadult holotype (MNBH JEN1). Missing bone is based on *S. aegyptiacus* (*3*). (**B**) First dorsal centrum in lateral, ventral, and posterior views (MNBH IGU11). (**C**) Dorsal neural spine section in lateral view with cross section (MNBH JEN2). (**D**) Partial posterior dorsal vertebra in left lateral view (MNBH JEN2). (**E**) Partial anterior caudal vertebra in anterior and left lateral views with cross section (MNBH JEN9). (**F**) Midcaudal centrum in anterior and left lateral views (MNBH IGU32). (**G**) Anterior and fourth trochanters of the left femur in lateral, medial, anterior, and posterior views (MNBH JEN2). (**H**) Left tibia in anterior, lateral, and midshaft cross-sectional views (arrow, anterior; MNBH JEN2). (**I**) Pedal digit II-1 phalanx in lateral, dorsal, and proximal views (MNBH IGU40). at, anterior trochanter; clp, collateral ligament pit; dc, distal condyle; fap, fossa for the ascending process of the astragalus; ft, fourth trochanter; hy, hypapophysis; k, keel; lm, lateral malleolus; mc, medullary cavity; mm, medial malleolus; ns, neural spine; pl, pleurocoel; poz, postzygapophysis; prz, prezygapophysis; st, striation. Human skeleton height, 170 cm. Scale bars, 5 cm in (B), (C), and (F); 10 cm in (D), (E), (G), and (H); and 3 cm in (I).

Nearly 70 years later, we rediscovered Akarazeras and, venturing farther into the sand sea, found a fossiliferous area called Jenguebi comparable in fossil preservation and faunal significance to Gadoufaoua (Fig. 1A). In addition to *S. mirabilis*, finds included a partial skull and skeleton of *Carcharodontosaurus* sp., new titanosaurian and rebbachisaurid sauropods, and the skull of a large polypterid fish (Fig. 1, B and C).

Riparian habitat

Multiple specimens of *S. mirabilis* were found in fluvial sediments near rebbachisaurid and titanosaurian sauropod skeletons indicative of a riparian habitat (Fig. 1, B and C). The proximity of the vertebrate fauna on site and within section and the degree of association and articulation of the skeletal remains leave no doubt about their coexistence in the same habitat (see the "Local stratigraphy and associated fauna" section in the supplementary materials). Specimens of *S. mirabilis* from the Jenguebi and Iguidi fossil areas (Fig. 1A) in the inland Iullemmeden Basin (*13*) were ~500 to 1000 km distant, respectively, from the closest marine margin in the Benue Trough during Early to Middle Cenomanian time [~100 to 95 Mya (*21*)]. Later, toward the close of the Cenomanian and dawn of the Turonian (~ 94.5 Mya),

the sea level rose abruptly, flooding low-lying continental areas to create the Trans-Saharan seaway (*16*, *22*). The inland setting during Early to Middle Cenomanian time suggests that *S. mirabilis* was a wading ambush piscivore (*3*, *5*). Given its detailed resemblance to contemporary *S. aegyptiacus* of northern Africa, it is unlikely the latter was a diving pursuit predator in marginal marine waters (*7*–*9*).

Discussion

Skull

The skull of *S. mirabilis* closely resembles that of its northern African relative *S. aegyptiacus* (Fig. 2, A and C). The diastema in the upper tooth row of *S. mirabilis* is broad with fossae accommodating three large dentary teeth, and the jaw margins are festooned to accommodate interdigitating crowns as in *S. aegyptiacus* and long-snouted crocodylians (Fig. 2, E and G). The snout end has a slightly different shape in profile, the premaxilla arching slightly above the rest of the snout and the expanded dentary end having more of a subquadrate than oval shape. The posterior half of the snout of *S. mirabilis* also has a lower profile toward the orbit with parallel rather than diverging dorsal and ventral margins (Fig. 2, A and C). Although the tooth count of *S. mirabilis* is similar to that of *S. aegyptiacus*, spacing between teeth in the posterior half of the snout is greater (see the "Skeletal reconstruction" section in the supplementary materials).

The scimitar-shaped nasal crest, the signature cranial feature of *S. mirabilis*, is gently upturned to an apex over the orbit and has a longitudinal thickening, or lateral eminence, along its length between thinning anterior and posterior margins (Fig. 2, A and B). It lacks the raised, vertical fluting present in the midsection of the nasal crest in *S. aegyptiacus* (Fig. 2D). The fused nasals that form the body of the crest are lapped laterally by a subtriangular process of the prefrontal (Fig. 2B, magnified view) as in *S. aegyptiacus*. The crest in *Spinosaurus*, thus, is accurately described as a nasal-prefrontal composite rather than fused nasals alone as occurs in baryonychine spinosaurids (*23*, *24*).

Paired vessels provide vascular supply to the dense bone of the crest in *S. mirabilis*, ramifying at midlength with very few canals opening externally (Fig. 2F). Unlike avian cranial casques, which are very porous and pneumatized (*25*, *26*), spinosaurid crests are composed of solid bone. Fine longitudinal, and in some areas crisscrossing, striations and deeper longitudinal grooves are present over sections of the crest (Fig. 2F). These surface details suggest that the bony crest in *S. mirabilis* was enveloped and likely extended by a keratinous sheath with its own vascular supply (Fig. 2B), based on extant avian analogs such as *Casuarius*, *Macrocephalon*, and *Numida* (Fig. 2H and supplementary materials) (*26*–*28*).

Asymmetry unrelated to taphonomic factors is present in all three crests of *S. mirabilis* and is most pronounced in the laterally deflected crest of the subadult holotype (MNBH JEN1; see the supplementary materials and fig. S7). Side-to-side asymmetry is also present in the crest flutings of *S. aegyptiacus* (Fig. 2D) and is common condition in cassowary casques [*Casuarius* (*28*)]. With only three examples from disparately aged individuals, it is not possible to assess crest dimorphism in *S. mirabilis*. The holotype and largest individual known has by far the most robust crest.

In nonavian theropods, the most common and sometimes flamboyant design of cranial ornamentation involves parasagittal, often pneumatized, crests along the dorsolateral edges of the snout (paired nasal, lacrimal, and prefrontal) as in *Dilophosaurus* (*29*) and *Cryolophosaurus* (*30*). A second design involves sagittal solid ornaments generated by fusion of paired bones as in the nasal crests in *Proceratosaurus* (*31*) and *Ceratosaurus* (*32*) or the cone-shaped frontal horn in *Majungasaurus* (*33*). This sagittal design characterizes spinosaurids (fused nasals) with minor contribution to each side by the prefrontal in *Spinosaurus* (Fig. 2B). Rarely in nonavian theropods has cranial ornamentation involved a combination of parasagittal and sagittal designs as in *Monolophosaurus* (*34*) and *Citipati* (*35*) or the elaboration of bilateral, cone-shaped horns on the skull roof (frontals) as in *Carnotaurus* (*36*).

The many examples of cranial ornamentation cited above in predatory (or omnivorous) nonavian theropods characterize individual species or select genera rather than all members of their more inclusive clades. A fused nasal or nasal-prefrontal crest, by contrast, is present in all spinosaurids in which that portion of the skull is known. The crest in *S. mirabilis* is relatively taller than in any other nonavian dinosaur, exceeding the height of the rest of the cranium at the orbits (Fig. 2A). If *S. mirabilis* grew to the size of *S. aegyptiacus*, then the bony cranial crest scaled isometrically would measure ~40 cm in length and perhaps >50 cm in life with a keratinous sheath.

Equally widespread among spinosaurids are heightened trunk and caudal sails, the primary function of which was likely visual display. Visual signaling (*3*, *5*, *37*, *38*) thus seems to have been enhanced in spinosaurids, possibly a consequence of their habitual presence in narrow shoreline habitats with less obstructed sightlines (*39*). The prominent sagittal cranial crest in *S. mirabilis* adds to the evidence that visual display, rather than aquatic propulsion (*6*), was the primary function of the heightened trunk and caudal sails (*3*, *5*).

Skeleton

Several vertebrae of *S. mirabilis* bear derived hallmarks of the axial column of *S. aegyptiacus*, including the advanced cervicalization and broad proportions of the first dorsal centrum, the presence of a trunk sail of unknown shape with striated neural spines, anterior caudal neural spines with a cruciate cross section, and short midcaudal centra with subquadrate articular faces (Fig. 3, A to F). Portions of the proximal end of the femur, including the narrow anterior and hypertrophied fourth trochanters, and a pedal phalanx with a low profile and reduced distal condyles are also similar to those in *S. aegyptiacus* (Fig. 3, G and I). Differences include relatively larger anterior dorsal pleurocoels and a proportionately longer tibia with an open, albeit reduced, medullary cavity (Fig. 3, A, B, and H, and supplementary materials).

We estimate the subadult skeletal length of the holotype at ~8 m, with adult length in *S. mirabilis* uncertain given the immaturity of all known individuals (Fig. 3A and supplementary materials). As in *S. aegyptiacus*, the holotype and most referred specimens are also immature. Cranial crest fusion occurs early in growth in spinosaurids (an unfused nasal has never been found), with later closure of other cranial and axial sutures (e.g., interpremaxillary and neural arch–centrum) with maturity. The holotype of *S. mirabilis* is ~15% smaller than the neotype subadult skeleton of *S. aegyptiacus*, or ~61% the size of the largest known specimen of *S. aegyptiacus* (see the supplementary materials and table S2).

Predatory mode

Long-snouted shoreline piscivores such as gharials among crocodylians and herons among waterbirds have been cited as modern analogs for spinosaurids (*1*–*3*, *5*, *40*), although these have starkly different postures (quadrupedal versus bipedal) and feeding modes (toothed lateral versus toothless vertical strike). Likewise, parallels have been drawn to the toothy snout end (terminal rosette and tooth-filled diastema) of the pike conger eel [*Muraenesox* (*41*)], although its body design (no head-neck mobility) and feeding setting (submerged bottom feeding in darkness) could not be more different. However, measurements of skull form with no other consideration (*5*, *42*) have not been able to clearly distinguish spinosaurids from other carnivorous archosaurs or to link them decisively with heron-like shoreline predators.

Although drawing attention by functional analogy to aspects of spinosaurid cranial anatomy (e.g., snout length, terminal rosette, and crest) can be informative, their presumed wading predatory mode (long snout, neck, and hind legs) should ally them with extant bipedal wading predators such as herons in a quantitative analysis. To test for the existence of such a predatory mode, we conducted a principal component analysis (PCA) of seven measures that capture cranial dimensions and neck and hind limb length in the two best known spinosaurids,

S. tenerensis and *S. aegyptiacus*, and 41 additional extinct and extant carnivorous archosaurs (Fig. 4, fig. S18, and table S6).

Five predatory modes cluster discretely using minimum convex hulls in a plot of PC2 and PC3 (Fig. 4). PC1 captures overall size variation and accounts for most of the variance (91%) given body size range in sampled taxa across four orders of magnitude (see the supplementary materials and fig. S18). Spinosaurids plot far from short-necked, short-limbed crocodylians and all other nonavian terrestrial and aerial avian predators and between semiaquatic long-necked, long-limbed birds such as herons (Fig. 4, number 28), which capture prey while wading in shallow water (*43*, *44*), and the least modified of aquatic divers such as darters (Fig. 4, number 38). These two subgroups, waders and divers, hunt for prey in distinctive, nonoverlapping modes, although both avian subgroups share a relatively long neck with spinosaurids (Fig. 4, variable 1).

Divers have proportionately longer skulls than either avian waders or spinosaurids (Fig. 4, variable 3). These three aquaphilic groups differ in relative hind limb length, which is shortest in divers and longest in waders (Fig. 4, variable 2). For avian waders, long hind limbs allow prey capture in water depths up to ~50 cm (*43*, *44*), which is slightly less than the hip height (~60 cm) of a wading adult blue heron (Fig. 4, number 28). Spinosaurids are positioned just outside of the wading bird polygon, with proportionately shorter hind limbs due to their much greater body mass. Spinosaurid hind limbs, of course, have much greater absolute length than any avian wader, facilitating fish capture in water more than three times as deep (>150 cm) (*3*). Spinosaurid skeletal form is therefore the most consistent with predation of fish through wading in shallow waters.

Spinosaurid evolution

We augment a previous spinosauroid dataset (*3*) by one-third, incorporating new and recently introduced character data (*24*, *45*–*47*). In a maximum parsimony analysis, a basal baryonychine-spinosaurine split is resolved, the latter clade increasingly diversified by recent finds including a new Brazilian spinosaurine (Fig. 5B, Materials and methods, and supplementary materials). We recognize three distinct phases in spinosaurid evolution (Fig. 5B, phases I to III).

The first 35-million-year (Myr) phase (Fig. 5B, phase I and node 1), comprising approximately half of the spinosaurid fossil record, is currently known only from isolated teeth in Jurassic and lowermost Cretaceous

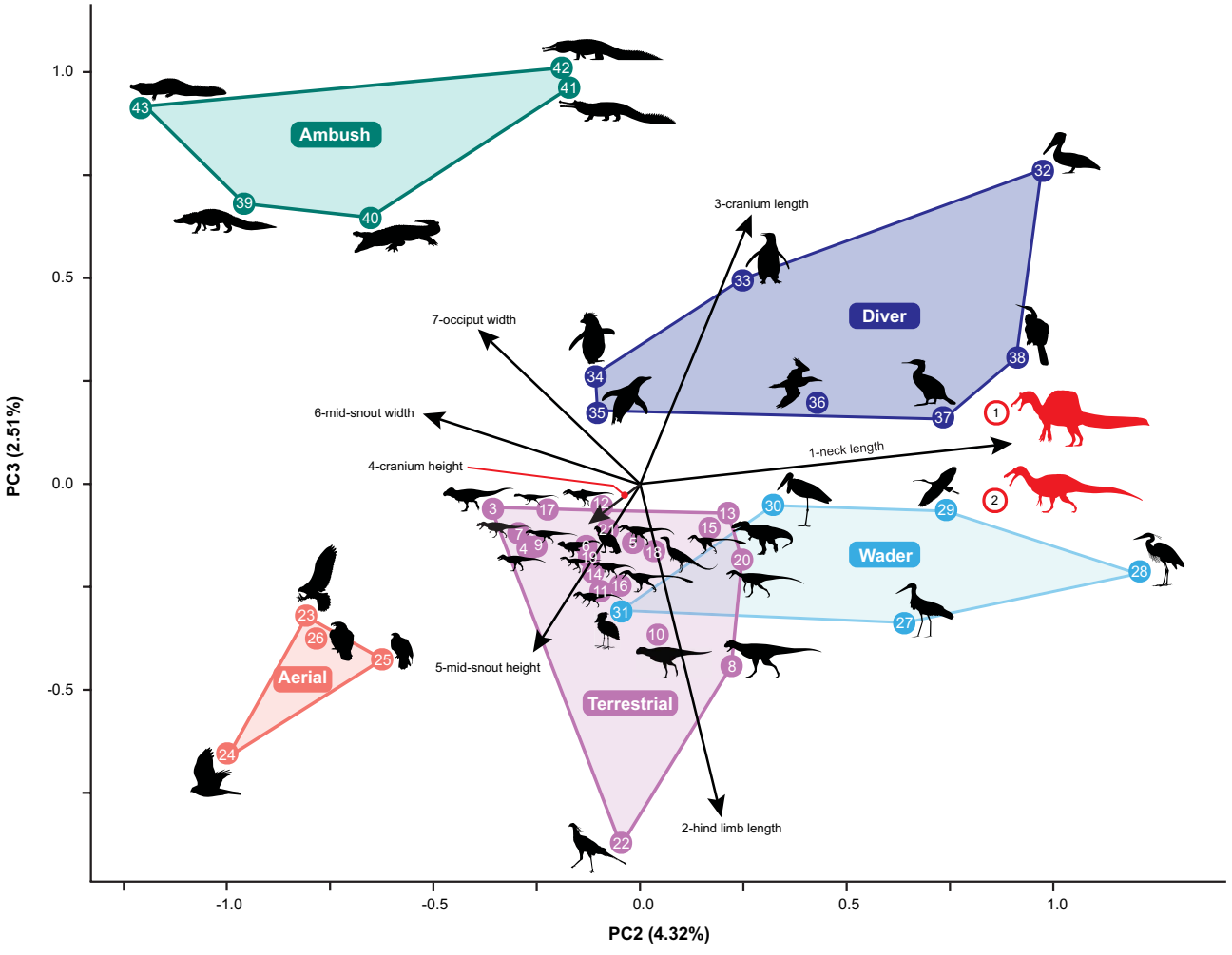

Fig. 4. Plot of predatory modes among archosaurs distinguishes spinosaurids. PCA (PC2 and PC3) of snout, neck, and hind limb dimensions (seven variables) with minimum convex hulls identifying five predatory modes (ambush, aerial, terrestrial, wader, and diver) in 43 extant and extinct carnivorous archosaurs including two spinosaurids (1 and 2), 18 other nonavian dinosaurs (3 to 20), two ground-based avian scavengers (21 and 22), four aerial birds of prey (23 to 26), six semiaquatic wading birds (27 to 32), six aquatic diving birds (33 to 38), and five crocodylians (39 to 43). Spinosaurids (*Suchomimus* and *Spinosaurus*) plot between avian waders and divers far from other nonavian dinosaurs and crocodylians. Arrows identify vectors for the loadings of seven variables: 1, cranium length; 2, cranium height; 3, occiput width; 4, midsnout height; 5, midsnout width; 6, neck length; and 7, hind limb length (for species and measurements, see the Materials and methods and the supplementary materials).

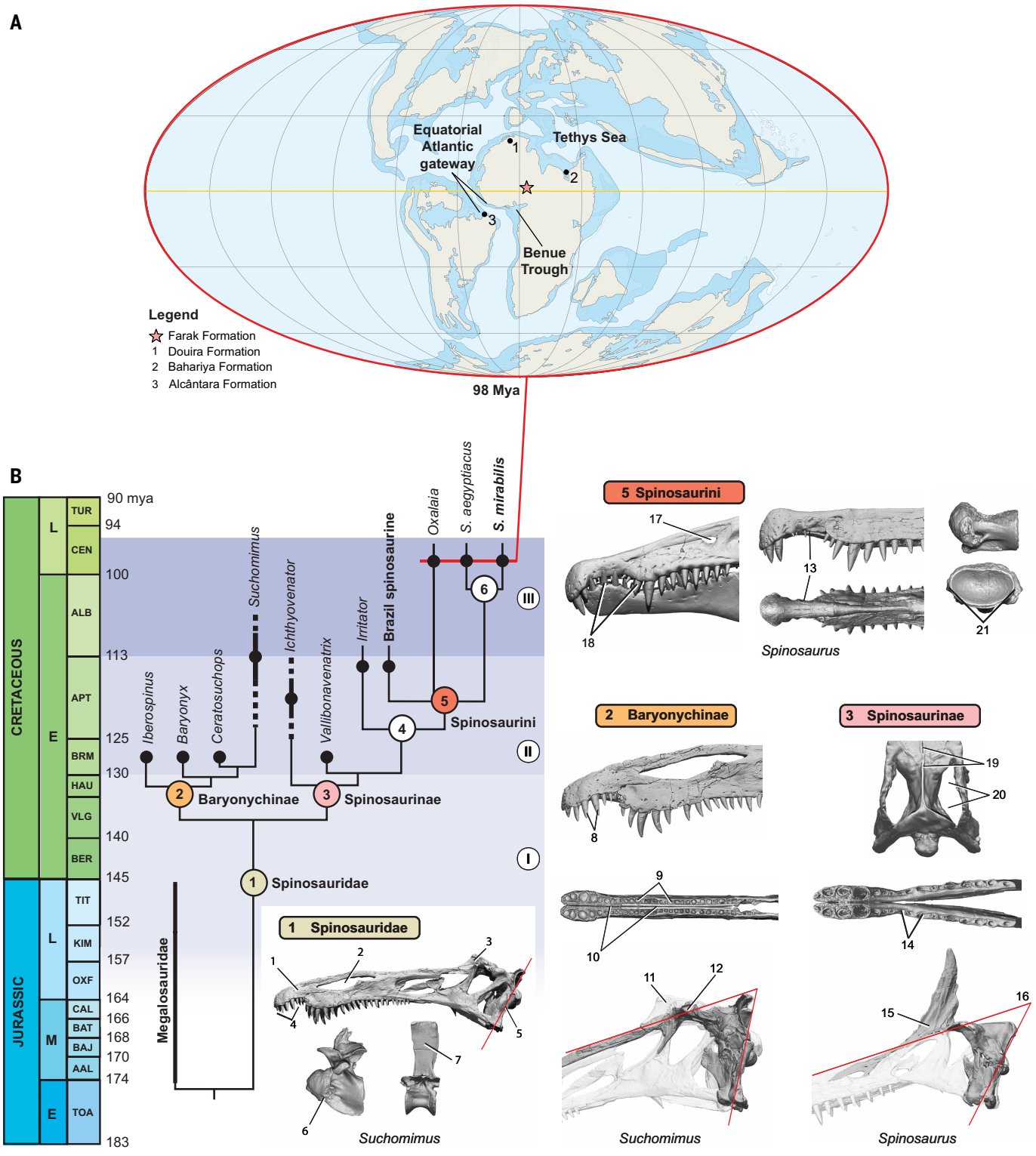

Fig. 5. Three-phase model for spinosaurid evolution. (**A**) Early-Middle Cenomanian paleobiogeographic map (~98 Mya) showing the formations and localities yielding the last known spinosaurines. (**B**) Time-calibrated phylogeny of spinosaurids highlighting 21 key features that arose during three successive evolutionary phases (I, II, and III). Dots sometimes extended by thick lines indicate estimated temporal age. 1, elongate snout; 2, partial retraction of external naris; 3, fused median nasal crest; 4, terminal rosette; 5, occiput-basipterygoid in a single plane; 6, cervical-like anterior dorsal vertebrae (D2 shown); 7, elevated dorsal-sacral-caudal neural spines; 8, elevated premaxillary dentition; 9, smaller, more numerous dentary teeth; 10, long dentary symphysis; 11, stout, cruciate nasal crest; 12, swollen lacrimal-postorbital brow; 13, diastema lengthening and transverse constriction; 14, spaced teeth in maxillary and dentary; 15, elevated sagittal nasal crest; 16, snout-occiput angle decreased to ~40°; 17, external nares small, more retracted; 18, interdigitating teeth with festooned alveolar margins; 19, frontal sagittal crest; 20, supratemporal fossa lengthened, removed from frontal; and 21, cervicodorsal centra wider than deep. Paleogeographic map is based on (*71*) with modifications after recent local paleogeographic research (*16*, *72*). The Brazil spinosaurine (UFMA ITA1, where UFMA is Universidade Federal do Maranhão, São Luís, Brazil) is based on a partial skeleton under study.

horizons (*48*). Nonetheless, the array of shared piscivorous features of all later spinosaurids arose during this initial phase, when spinosaurids evidently remained relatively uncommon or in habitats less suitable to preservation. These features include an elongate snout with some narial retraction, a terminal rosette of premaxillary teeth, and a median nasal crest (Fig. 5B, features 1 to 4). Other distinctive features include a very large prefrontal that forms the anterior roof of the orbit; an extremely deep, short braincase; and a reduced fossa for the olfactory bulb. The vertebral column is distinctive in the lengthening of the neck; cervicalization of the anterior dorsal vertebrae for enhanced dorsoventral flexion; and at least moderate heightening of the dorsal, sacral, and caudal neural spines (Fig. 5B, features 6 and 7). Increased forelimb strength for prey manipulation is shown by the strong deltopectoral crest, hypertrophied olecranon, and flaring forearm epicondyles in all known spinosaurids (Fig. 3A).

This array of trophic, structural, and sociosexual adaptations have masked major differences in skull and dental form that arose between baryonychines and spinosaurines during this poorly documented phase. In baryonychines, the dentary teeth are smaller and more numerous than the maxillary teeth and are anchored in dentary rami that lie immediately adjacent to one another in the midline (Fig. 5B, node 2 and features 9 and 10). This very narrow, gharial-like jaw occludes within a very narrow snout composed of maxillae that are joined in rugose suture for half their length (*19*, *24*), unlike spinosaurines or any other nonavian dinosaurs. In baryonychines, both the premaxillary rosette and the opposing large dentary teeth that insert within the rosette are set above the principal tooth rows (Fig. 5B, feature 8). In addition, the orbital margin is greatly thickened by swellings of the lacrimal and postorbital (Fig. 5B, feature 12) (*3*, *24*), closely resembling the condition in carcharodontosaurids (*17*).

In spinosaurines, by contrast, the dentary symphysis is limited to the ramus underlying the premaxillary rosette. More posteriorly, the dentary rami diverge from the midline to engage a broader posterior snout with fewer spaced teeth (Fig. 5B, node 3 and feature 14). The frontal thickens medially toward the midline, not laterally toward a thickened orbit margin, and fuses with its opposite to form a sagittal crest, joining the midline crest formed by fused nasals anteriorly and parietals posteriorly (Fig. 5B, feature 19). The occiput is tilted backward, narrowing the angle to the snout and lengthening the parietal and supratemporal fossa, the latter no longer extending onto the frontal (Fig. 5B, features 16 and 20). The nasal crest is further developed in the sagittal plane with reduction of the prominent lateral ridge that in baryonychines rises to the apex of the crest (Fig. 5B, feature 15).

During a second 20-Myr phase in the Early Cretaceous (Fig. 5B, phase II), spinosaurids diversified in habitats bordering the Tethys Sea, where they were the largest and most common predators. This holds to the south on Gondwana for the African baryonychine *Suchomimus* (*3*, *19*) and Brazilian spinosaurine *Irritator* (*45*, *49*–*51*) and to the north on Laurasia, with increasingly diverse baryonychines in Europe (*23*, *24*, *52*–*54*) and the spinosaurine *Ichthyovenator* in southern Asia (*55*). Evidence for both baryonychines and spinosaurines in the same fauna has also come to light in Iberia (*56*, *57*) and possibly also in Thailand (*58*).

With less head weight than most large-bodied bipedal theropods, spinosaurids emphasized the reach and power of the forelimb for prey capture and manipulation beyond that seen in any other theropod group. The 1.4-m-long forelimb in *Suchomimus* is characterized by exceptionally stout shafts, hypertrophied flexor and extensor processes, and unguals measuring up to 32 cm along the outer curve. Although specialized jaws and small-sized posterior teeth in baryonychines suggest piscivory, the remainder of the baryonychine skeleton is that of a "generalist predator" (*59*). *Suchomimus,* possibly the last surviving baryonychine (Fig. 5B), dominated the large predator niche on land in central Africa while competing for fish along riverways with the 11-m-long crocodyliform *Sarcosuchus* (*60*). The best known spinosaurine of this phase, *Irritator* (*45*, *49*–*51*) from the adjacent Araripe Basin of Brazil (*61*), has further piscivorous adaptations, including teeth with increased spacing and a more retracted external naris, while remaining the largest predator of its day.

A final 15-Myr phase (Fig. 5B, phase III) began during the latest Aptian or early Albian with a subset of spinosaurines here recognized as Spinosaurini. They survived only on the southern margin of the Tethys Sea on South America and Africa, areas that by 110 Mya were separated by a deep water straight (>500 m depth) called the Equatorial Atlantic gateway [(*62*); Fig. 5A]. The earliest representative is a yet unnamed late Aptian or early Albian genus from the Parnaíba Basin of Brazil (Fig. 5B). By the Early to Middle Cenomanian (~98 Mya), spinosaurines reached maximum body size as specialized fish eaters with a hypertrophied trunk sail (Fig. 3C), ceding inland predation to equal-sized carcharodontosaurids (*17*). *Oxalaia*, discovered on a coastal island in Brazil, is known from a snout end and isolated teeth and bones (*63*, *64*). Across northern Africa, a better fossil record includes abundant teeth and skeletal remains provisionally referred to *S. aegyptiacus* (*1*–*3*, *8*, *65*, *66*).

Increased piscivorous specializations include a lengthened upper diastema that accommodates three large dentary teeth (*67*) and the interdigitation of more posterior upper and lower tooth rows (Fig. 2E), as in long-snouted crocodilians (Fig. 2F), fish-eating pterosaurs (*68*), and secondarily aquatic tetrapods such as ichthyosaurs and plesiosaurs (*4*). The neck appears to have a tighter "S" shape with enhanced ventroflexion at the neck-trunk junction, and the manus has gently recurved unguals for raking (Fig. 5B, features 13, 18, and 21). Also present are tall trunk neural spines indicative of a hypertrophied sail (Fig. 3C).

Just before the close of the Cenomanian, a fast-paced global transgression (~94.5 Mya) flooded low-lying continental areas, creating a shallow seaway spanning the Sahara north to south (*16*, *21*). The abrupt sea-level change was synchronous with global temperature flux and marked marine biotic turnover (*22*) that on land appears to have resulted in the extinction of these large-bodied piscivores. This discovery of *S. mirabilis* in an inland basin in the Sahara establishes a still poorly known inland presence for spinosaurines near the end of their reign.

Materials and methods

Structure from motion photogrammetry

Photogrammetry was conducted on cranial and postcranial bones of *S. mirabilis* and other spinosaurid remains to obtain three-dimensional (3D) digital meshes using a Fujifilm XT-4 camera and AgiSoft Metashape to compose the cranial and postcranial skeletal reconstructions.

Computed tomographic scanning

Computed tomography (CT) scans were taken at the University of Chicago Hospital (RRID:SCR_018372; N. Gruszauskas) using a Philips Brilliance iCT 256-slice multidetector scanner and at the University of Chicago PaleoCT facility (RRID:SCR_024763) using a Waygate Phoenix V|tomex|s microCT scanner.

PCA

We took seven linear measurements (cranium length, cranium height, occiput width, midsnout height, midsnout width, neck length, and hind limb length, all in centimeters) that capture key aspects of head and body form critical to predatory mode in 43 extant and extinct carnivorous archosaurs (Fig. 4, supplementary materials, and table S3). We plotted the two spinosaurids (spinosaurine *S. aegyptiacus* and baryonychine *S. tenerensis*) as unknown for the purposes of the analysis and group taxa into five predatory modes: ambush (semiaquatic), terrestrial, aerial, wader (semiaquatic), and diver (aquatic).

The sampled taxa range in body mass across four orders of magnitude (*Accipiter nisus*, ~0.2 kg; *Tyrannosaurus rex*, ~8000 to 9000 kg). To address skewness when considering such profound scaling, we

log_{10}-transformed the dataset to linearize the relationship between variables. Then, we normalized the measurements by standardizing each variable to unit variance (i.e., mean of zero, SD of 1) to ensure that individual morphometric variables did not dominate the others. We performed PCA using R version 4.4.1 [setting scale=TRUE in the command prcomp()].

The seven morphometric variables have a negative loading of −0.367 to −0.392 on the first principal component (see the "Principal component analysis" section in the supplementary materials and table S4). This consistent pattern across the morphometric variables means that PC1 represents size, as expected, and captures most of the variation in the dataset (91.06%). Most of the rest of the variation involves cranium, neck, and hind limb proportions.

Spinosaurids plot between long and narrow snouted, long-necked semiaquatic waders and aquatic divers well separated from other (terrestrial) nonavian dinosaurs and carrion-feeding birds; short-necked, short-limbed semiaquatic crocodylians; and aerial raptors (Fig. 4). The darter (*Anhinga melanogaster*), a shallow diving suliform, plots close to spinosaurids, given its similar proportions (Fig. 4, number 38). Also known as snakebirds for their elongate necks, darters hunt at the surface with head intermittently above the water, plunge diving with rapid neck extension to impale prey on their elongate, pointed beaks (*69*, *70*). Like cormorants and grebes, the darter is a volant, foot-propelled (webbed) diver that has retained a longer skull and hind limb and more symmetrical pes for perching than other more specialized nonvolant divers such as penguins. With their large body size, spinosaurids do not need the proportionately elongate hind limbs of avian waders to hunt effectively in shallow water, plotting just outside their minimum convex hull (Fig. 4).

The long-necked but broad-snouted semiaquatic shoe-billed stork (*Balaeniceps rex*) clustered with terrestrial theropods including *T. rex* (Fig. 4, number 31). Its broad snout of modest length is very unusual among extant avians that hunt as waders in shallow water environments. At prey capture, the shoe-billed stork often captures vegetation along with its prey, unlike the more targeted prey capture of longer-snouted waders.

Phylogenetic analysis and definitions

We performed maximum parsimony phylogenetic analysis (TNT v1.6) of a data matrix composed of 159 characters statements scored in six outgroup species and 16 spinosaurid taxa or described specimens. Forty-one new character statements were added to a previous spinosaurid matrix (*3*), representing ~25% of the data. A total data analysis resulted in 42 minimum-length trees with the new species nested among derived spinosaurines. After a posteriori pruning of four poorly known unstable taxa and specimens identified with the iterPCR subroutine, the analysis yielded a single minimum-length tree showing the divergence of spinosaurids into baryonychine and spinosaurine subclades with increasing resolution (Fig. 5B). Phylogenetic definitions of spinosauroid taxa are summarized with recognition of Spinosaurini Stromer 1915 for the final suite of transatlantic spinosaurids (for decay and Bayesian analyses, see the "Phylogenetic definitions and analysis" section in the supplementary materials).

REFERENCES AND NOTES

1. E. Stromer, *Ergebnisse der Forschungsreisen Prof. E. Stromer in den Wüsten Ägyptens. II. Wirbeltier-Reste der Baharîje-Stufe (unterstes Cenoman). 3. Das Original des Theropoden Spinosaurus aegyptiacus nov. gen., nov. spec.* (De Gruyter Brill, 1915).
2. N. Ibrahim *et al.*, Semiaquatic adaptations in a giant predatory dinosaur. *Science* **345**, 1613–1616 (2014). doi: 10.1126/science.1258750; pmid: 25213375
3. P. C. Sereno *et al.*, *Spinosaurus* is not an aquatic dinosaur. *eLife* **11**, e80092 (2022). doi: 10.7554/eLife.80092; pmid: 36448670
4. R. Motani, The evolution of marine reptiles. *Evolution (N. Y.)* **2**, 224–235 (2009). doi: 10.1007/s12052-009-0139-y
5. D. W. E. Hone, T. Holtz Jr., Evaluating the ecology of *Spinosaurus*: Shoreline generalist or aquatic pursuit specialist? *Palaeontol. Electronica* **24**, 1–28 (2021). doi: 10.26879/1110
6. N. P. Myhrvold *et al.*, Diving dinosaurs? Caveats on the use of bone compactness and pFDA for inferring lifestyle. *PLOS ONE* **19**, e0298957 (2024). doi: 10.1371/journal.pone.0298957; pmid: 38446841
7. N. Ibrahim *et al.*, Tail-propelled aquatic locomotion in a theropod dinosaur. *Nature* **581**, 67–70 (2020). doi: 10.1038/s41586-020-2190-3; pmid: 32376955
8. M. Fabbri *et al.*, Subaqueous foraging among carnivorous dinosaurs. *Nature* **603**, 852–857 (2022). doi: 10.1038/s41586-022-04528-0; pmid: 35322229
9. T. Beevor *et al.*, Taphonomic evidence supports an aquatic lifestyle for *Spinosaurus*. *Cretac. Res.* **117**, e104627 (2021). doi: 10.1016/j.cretres.2020.104627
10. N. Ibrahim *et al.*, Geology and paleontology of the Upper Cretaceous Kem Kem Group of eastern Morocco. *ZooKeys* **928**, 1–216 (2020). doi: 10.3897/zookeys.928.47517; pmid: 32362741
11. M. Benyoucef *et al.*, Overabundance of piscivorous dinosaurs (Theropoda: Spinosauridae) in the mid-Cretaceous of North Africa: The Algerian dilemma. *Cretac. Res.* **55**, 44–55 (2015). doi: 10.1016/j.cretres.2015.02.002
12. H. Faure, *Reconnaissance Géologique des Formations Sédimentaires Post-Paléozoïques du Niger Oriental* (République du Niger Ministère des Travaux Publics, des Transports, des Mines et de l'Urbanisme, Direction des Mines et de la Géologie, 1966).
13. R. T. J. Moody, "The Iullemmeden Basin" in *Sedimentary Basins of the World*, vol. 3, R. C. Selley, Ed. (Elsevier, 1997), pp. 89–103.
14. J. Ph. Lefranc, R. Guiraud, The continental intercalaire of northwestern Sahara and its equivalents in the neighbouring regions. *J. Afr. Earth Sci. Middle East* **10**, 27–77 (1990). doi: 10.1016/0899-5362(90)90047-I
15. P. Taquet, *Géologie et Paléontologie Du Gisement de Gadoufaoua (Aptien Du Niger)* (Éditions du Centre National de la Recherche Scientifique, 1976).
16. A. F. Pascal, B. J. Mathey, K. Alzouma, J. Lang, C. Meister, "Late Cenomanian-Early Turonian shelf ramp, Niger, West Africa" in *Cretaceous Carbonate Platforms*, J. A. T. Simo, R. W. Scott, J.-P. Masse, Eds. (American Association of Petroleum Geologists, 1993), pp. 145–154. doi: 10.1306/M56578C12
17. P. C. Sereno *et al.*, Predatory dinosaurs from the Sahara and Late Cretaceous faunal differentiation. *Science* **272**, 986–991 (1996). doi: 10.1126/science.272.5264.986; pmid: 8662584
18. P. Taquet, *Dinosaur Impressions: Postcards from a Paleontologist* (Cambridge Univ. Press, 1998).
19. P. C. Sereno *et al.*, A long-snouted predatory dinosaur from africa and the evolution of spinosaurids. *Science* **282**, 1298–1302 (1998). doi: 10.1126/science.282.5392.1298; pmid: 9812890
20. L. Faure-Denard, M. Servant, O. Faure, L. Ortlieb, J.-L. Probst, Hugues Faure, 1928–2003: The unique adventure of his life. *Global Planet. Change* **72**, 248–256 (2010). doi: 10.1016/j.gloplacha.2010.04.001
21. L. M. Adamu, N. G. Obaje, J. A. Adeoye, R. G. Oladimeji, I. Yusuf, Trans-Saharan seaway connection between the South Atlantic and the Tethys Sea during the Coniacian–Turonian: Evidence from bibliographical synthesis, field mapping, and seismic interpretation. *Geosyst. Geoenviron.* **3**, e100243 (2024). doi: 10.1016/j.geogeo.2023.100243
22. Y.-X. Li *et al.*, Enhanced ocean connectivity and volcanism instigated global onset of Cretaceous Oceanic Anoxic Event 2 (OAE2) ~94.5 million years ago. *Earth Planet. Sci. Lett.* **578**, 117331 (2022). doi: 10.1016/j.epsl.2021.117331
23. A. Charig, A. C. Milner, *Baryonyx walkeri*, a fish-eating dinosaur from the Wealden of Surrey. *Bull. Nat. Hist. Mus. Geol. Ser.* **53**, 11–70 (1997).
24. C. T. Barker *et al.*, New spinosaurids from the Wessex Formation (Early Cretaceous, UK) and the European origins of Spinosauridae. *Sci. Rep.* **11**, e19340 (2021). doi: 10.1038/s41598-021-97870-8; pmid: 34588472
25. T. L. Green, P. M. Gignac, Osteological comparison of casque ontogeny in palaeognathous and neognathous birds: Insights for selecting modern analogues in the study of cranial ornaments from extinct archosaurs. *Zool. J. Linn. Soc.* **199**, 10–25 (2023). doi: 10.1093/zoolinnean/zlad016
26. G. Mayr, A survey of casques, frontal humps, and other extravagant bony cranial protuberances in birds. *Zoomorphology* **137**, 457–472 (2018). doi: 10.1007/s00435-018-0410-2
27. D. Angst, J. Barnoud, R. Cornette, A. Chinsamy, Sex and Ontogenetic Variation in the crest of *Numida meleagris*: Implications for crested vertebrates. *Anat. Rec. (Hoboken)* **303**, 1018–1034 (2020). doi: 10.1002/ar.24275; pmid: 31702115
28. T. L. Green, D. I. Kay, P. M. Gignac, Intraspecific variation and directional casque asymmetry in adult southern cassowaries (*Casuarius casuarius*). *J. Anat.* **241**, 951–965 (2022). doi: 10.1111/joa.13733; pmid: 35933695
29. A. D. Marsh, T. B. Rowe, A comprehensive anatomical and phylogenetic evaluation of *Dilophosaurus wetherilli* (Dinosauria, Theropoda) with descriptions of new specimens from the Kayenta Formation of northern Arizona. *J. Paleontol.* **94**, 1–103 (2020). doi: 10.1017/jpa.2020.14
30. N. D. Smith, P. J. Makovicky, W. R. Hammer, P. J. Currie, Osteology of *Cryolophosaurus ellioti* (Dinosauria: Theropoda) from the Early Jurassic of Antarctica and implications for early theropod evolution. *Zool. J. Linn. Soc.* **151**, 377–421 (2007). doi: 10.1111/j.1096-3642.2007.00325.x
31. O. W. M. Rauhut, A. C. Milner, S. Moore-Fay, Cranial osteology and phylogenetic position of the theropod dinosaur *Proceratosaurus bradleyi* (Woodward, 1910) from the Middle

Jurassic of England. *Zool. J. Linn. Soc.* **158**, 155–195 (2010). doi: 10.1111/j.1096-3642.2009.00591.x
32. J. H. Madsen, S. P. Welles, *Ceratosaurus (Dinosauria, Theropoda): A Revised Osteology* (Utah Geological Survey, 2000).
33. S. D. Sampson, L. M. Witmer, Craniofacial anatomy of *Majungasaurus crenatissimus* (Theropoda: Abelisauridae) from the Late Cretaceous of Madagascar. *J. Vertebr. Paleontol.* **27** (sup2), 32–104 (2007). doi: 10.1671/0272-4634(2007)27[32:CAOMCT]2.0.CO;2
34. X.-J. Zhao, P. J. Currie, A large crested theropod from the Jurassic of Xinjiang, People's Republic of China. *Can. J. Earth Sci.* **30**, 2027–2036 (1993). doi: 10.1139/e93-178
35. J. M. Clark, M. A. Norell, T. Rowe, Cranial Anatomy of *Citipati osmolskae* (Theropoda, Oviraptorosauria), and a reinterpretation of the Holotype of *Oviraptor philoceratops*. *Am. Mus. Novit.* **3364**, 1–24 (2002). doi: 10.1206/0003-0082(2002)364<0001:CAOCOT>2.0.CO;2
36. M. A. Cerroni, J. I. Canale, F. E. Novas, The skull of *Carnotaurus sastrei* Bonaparte 1985 revisited: Insights from craniofacial bones, palate and lower jaw. *Hist. Biol.* **33**, 2444–2485 (2021). doi: 10.1080/08912963.2020.1802445
37. D. W. E. Hone, D. Naish, I. C. Cuthill, Does mutual sexual selection explain the evolution of head crests in pterosaurs and dinosaurs? *Lethaia* **45**, 139–156 (2012). doi: 10.1111/j.1502-3931.2011.00300.x
38. D. W. E. Hone, D. Naish, The 'species recognition hypothesis' does not explain the presence and evolution of exaggerated structures in non-avialan dinosaurs. *J. Zool.* **290**, 172–180 (2013). doi: 10.1111/jzo.12035
39. A. C. R. Lackey, J. W. Boughman, Divergent sexual selection via male competition: Ecology is key. *J. Evol. Biol.* **26**, 1611–1624 (2013). doi: 10.1111/jeb.12173; pmid: 23859471
40. T. M. S. Arden, C. G. Klein, S. Zouhri, N. R. Longrich, Aquatic adaptation in the skull of carnivorous dinosaurs (Theropoda: Spinosauridae) and the evolution of aquatic habits in spinosaurids. *Cretac. Res.* **93**, 275–284 (2019). doi: 10.1016/j.cretres.2018.06.013
41. R. Vullo, R. Allain, L. Cavin, Convergent evolution of jaws between spinosaurid dinosaurs and pike conger eels. *Acta Palaeontol. Pol.* **61**, 825–828 (2016). doi: 10.4202/app.00284.2016
42. S. Smart, M. Sakamoto, Using linear measurements to diagnose the ecological habitat of *Spinosaurus*. *PeerJ* **12**, e17544 (2024). doi: 10.7717/peerj.17544; pmid: 38881866
43. J. A. Kushlan, "*Feeding ecology of wading birds in wading birds, research report 7, A. Sprunt IV*," in J. C. Ogden, S. Winckler, Eds. (National Audubon Society, 1978), pp. 249–292.
44. L. S. Forbes, Feeding behaviour of great blue herons at Creston, British Columbia. *Can. J. Zool.* **65**, 3062–3067 (2011). doi: 10.1139/z87-464
45. M. Schade, O. Rauhut, C. Foth, O. Moleman, S. Evers, A reappraisal of the cranial and mandibular osteology of the spinosaurid *Irritator challengeri* (Dinosauria: Theropoda). *Palaeontol. Electronica* **26**, 1–116 (2023). doi: 10.26879/1242
46. M. A. F. Sales, C. L. Schultz, Spinosaur taxonomy and evolution of craniodental features: Evidence from Brazil. *PLOS ONE* **12**, e0187070 (2017). doi: 10.1371/journal.pone.0187070; pmid: 29107966
47. A. Cau, The assembly of the avian body plan: A 160-million-year long process. *Boll. Soc. Paleontol. Ital.* **57**, 1–25 (2018).
48. A. Serrano-Martínez *et al.*, New theropod remains from the Tiourarén Formation (?Middle Jurassic, Niger) and their bearing on the dental evolution in basal tetanurans. *Proc. Geol. Assoc.* **126**, 107–118 (2015). doi: 10.1016/j.pgeola.2014.10.005
49. E. B. Machado, "Description of a new example of Spinosauridae (Dinosauria, Theropoda) from the Romualdo Formation (Araripe Basin), northeast Brazil," thesis, Universidade Federal do Rio de Janeiro, Rio de Janeiro (2010).
50. H.-D. Sues, E. Frey, D. M. Martill, D. M. Scott, *Irritator challengeri*, a spinosaurid (Dinosauria: Theropoda) from the Lower Cretaceous of Brazil. *J. Vertebr. Paleontol.* **22**, 535–547 (2002). doi: 10.1671/0272-4634(2002)022[0535:ICASDT]2.0.CO;2
51. T. Aureliano *et al.*, Semi-aquatic adaptations in a spinosaur from the Lower Cretaceous of Brazil. *Cretac. Res.* **90**, 283–295 (2018). doi: 10.1016/j.cretres.2018.04.024
52. C. R. A. Candeiro, S. L. Brusatte, A. L. de Souza, Spinosaurid dinosaurs from the Early Cretaceous of North Africa and Europe: Fossil record, biogeography and extinction. *Anuário IGEO UFRJ* **40**, 294–302 (2018). doi: 10.11137/2017_3_294_302
53. E. Malafaia *et al.*, A new spinosaurid theropod (Dinosauria: Megalosauroidea) from the upper Barremian of Vallibona, Spain: Implications for spinosaurid diversity in the Early Cretaceous of the Iberian Peninsula. *Cretac. Res.* **106**, e104221 (2020). doi: 10.1016/j.cretres.2019.104221
54. O. Mateus, D. Estraviz-López, A new theropod dinosaur from the early cretaceous (Barremian) of Cabo Espichel, Portugal: Implications for spinosaurid evolution. *PLOS ONE* **17**, e0262614 (2022). doi: 10.1371/journal.pone.0262614; pmid: 35171930
55. R. Allain, T. Xaisanavong, P. Richir, B. Khentavong, The first definitive Asian spinosaurid (Dinosauria: Theropoda) from the Early Cretaceous of Laos. *Naturwissenschaften* **99**, 369–377 (2012). doi: 10.1007/s00114-012-0911-7; pmid: 22528021
56. E. Malafaia, J. M. Gasulla, F. Escaso, I. Narvaéz, F. Ortega, An update of the spinosaurid (Dinosauria: Theropoda) fossil record from the Lower Cretaceous of the Iberian Peninsula: distribution, diversity, and evolutionary history. *J. Iber. Geol.* **46**, 431–444 (2020). doi: 10.1007/s41513-020-00138-9
57. A. Santos-Cubedo, C. de Santisteban, B. Poza, S. Meseguer, A new spinosaurid dinosaur species from the Early Cretaceous of Cinctorres (Spain). *Sci. Rep.* **13**, e6471 (2023). doi: 10.1038/s41598-023-33418-2; pmid: 37202441
58. A. Samathi, P. M. Sander, P. Chanthasit, A spinosaurid from Thailand (Sao Khua Formation, Early Cretaceous) and a reassessment of *Camarillasaurus cirugedae* from the Early Cretaceous of Spain. *Hist. Biol.* **33**, 3480–3494 (2021). doi: 10.1080/08912963.2021.1874372
59. D. W. E. Hone, T. R. Holtz Jr., A century of spinosaurs - A review and revision of the Spinosauridae with comments on their ecology. *Acta Geol. Sin. Engl. Ed.* **91**, 1120–1132 (2017). doi: 10.1111/1755-6724.13328
60. P. C. Sereno, H. C. Larsson, C. A. Sidor, B. Gado, The giant crocodyliform *Sarcosuchus* from the Cretaceous of Africa. *Science* **294**, 1516–1519 (2001). doi: 10.1126/science.1066521; pmid: 11679634
61. M. Arai, Aptian/Albian (Early Cretaceous) paleogeography of the South Atlantic: A paleontological perspective. *Braz. J. Geol.* **44**, 339–350 (2014). doi: 10.5327/Z2317-4889201400020012
62. W. Dummann, P. Hofmann, J. O. Herrle, M. Frank, T. Wagner, The early opening of the Equatorial Atlantic gateway and the evolution of Cretaceous peak warming. *Geology* **51**, 476–480 (2023). doi: 10.1130/G50842.1
63. M. Medeiros, Large theropod teeth from the Eocenomanian of northeastern Brazil and the occurrence of Spinosauridae. *Rev. Bras. Paleontol.* **9**, 333–338 (2006). doi: 10.4072/rbp.2006.3.08
64. A. W. A. Kellner, S. A. K. Azevedo, E. B. Machado, L. B. Carvalho, D. D. R. Henriques, A new dinosaur (Theropoda, Spinosauridae) from the Cretaceous (Cenomanian) Alcântara Formation, Cajual Island, Brazil. *An. Acad. Bras. Cienc.* **83**, 99–108 (2011). doi: 10.1590/S0001-37652011000100006; pmid: 21437377
65. P. Taquet, D. A. Russell, New data on spinosaurid dinosaurs from the Early Cretaceous of the Sahara. *Earth. Planet. Sci.* **327**, 347–353 (1998).
66. M. Benyoucef *et al.*, The "mid"-Cretaceous (Lower Cenomanian) continental vertebrates of Gara Samani, Algeria. Sedimentological framework and palaeodiversity. *Front. Earth Sci. (Lausanne)* **10**, 927059 (2022). doi: 10.3389/feart.2022.927059
67. D. C. D'Amore, E. Johnson-Ransom, E. Snively, D. W. E. Hone, Prey size and ecological separation in spinosaurid theropods based on heterodonty and rostrum shape. *Anat. Rec. (Hoboken)* **2024**, 1–18 (2024). pmid: 39205383
68. A. W. A. Kellner, Y. Tomida, Description of a new species of Anhangueridae (Pterodactyloidea) with comments on the pterosaur fauna from the Santana Formation (Aptian-Albian), Northeastern Brazil. *Nat. Sci. Mus. Monogr.* **17**, 137 (2000).
69. K. Hustler, Buoyancy and its constraints on the underwater foraging behaviour of reed cormorants *Phalacrocorax africanus* and darters *Anhinga melanogaster*. *Ibis* **134**, 229–236 (1992). doi: 10.1111/j.1474-919X.1992.tb03804.x
70. P. Read, Anhinga near Delaware, Ontario. *Ontario Birds* **18**, 97–105 (2000).
71. C. R. Scotese, "Atlas of Early Cretaceous Paleogeographic Maps, PALEOMAP Atlas for ArcGIS, volume 2, The Cretaceous, Maps 23 - 31, Mollweide Projection, PALEOMAP Project, Evanston, IL" (PALEOMAP Project, 2014), Technical Report; https://doi.org/10.13140/2.1.4099.4560.
72. B. Mathey *et al.*, Unusual faunal associations during the Upper Cenomanian-Lower Turonian floodings on the Niger ramp (central West Africa). *Palaeogeogr. Palaeoclimatol. Palaeoecol.* **119**, 63–75 (1995). doi: 10.1016/0031-0182(95)00060-7

ACKNOWLEDGMENTS

We thank O. Zant for comments on the manuscript, MorphoSource for archiving CT scans, and the Niger Republic for access to the field and for loan of fossil material to the University of Chicago. This study represents the views of the authors; any opinions, findings, or conclusions are not those of the US Federal Government. **Funding:** This work was supported by an anonymous gift to the University of Chicago to P.C.S., Marie Sklodowska Curie Actions Grant EvoSaurAf 101068861 of the European Commission to D.V, and a Santander-UNED FPI predoctoral grant to M.C.R. **Author contributions:** Conceptualization: P.C.S, D.V., E.J.-R., E.T.S.; Data curation: D.V., P.C.S., E.J.-R.; Fossil curation: T.M.K. and E.C.F.; Funding proposals: P.C.S., D.V., M.C.R., L.L.B.; Investigation – field work: P.C.S., D.V., N.S.F., M.C.R., S.L.B., B.A., E.C.F., R.A.S.L., A.V.D.-P., A.S., F.G.-L., A.L., ~~A.G.~~, C.V.B., V.R., R.V., F.B., ~~A.G.~~, G.K.-B., J.R.; Investigation – fossils: P.C.S., D.V., T.M.K., J.C.M., R.M.L.; Investigation – recent specimens: S.L.B. and T.L.G.; PCA analysis: E.J.-R. P.C.S, E.T.S.; Phylogenetic analysis: D.V.; Visualization: P.C.S., D.V., L.L.B., M.C.R, T.M.K., E.C.F.; Writing – original draft: P.C.S.; Writing – review & editing: D.V., N.P.M., E.T.S, A.S.L.R., S.L.B., T.L.G., D.B.D., R.A.S.L., A.V.D.-P., V.R., C.V.B., R.M.L, J.C.M., J.R. **Competing interests:** The authors declare no competing interests. **Data, code, and materials availability:** All reconstructions and data supporting the findings in this study are available within the main text or the supplementary materials. CT scans and 3D models are available on MorphoSource under project ID 000749095 (https://www.morphosource.org/projects/000749095?locale=en).

SUPPLEMENTARY MATERIALS

science.org/doi/10.1126/science.adx5486
Supplementary Text; Figs. S1 to S22; Tables S1 to S10; References (*73*–*100*); Data S1 to S4

Submitted 18 March 2025; resubmitted 1 July 2025; accepted 21 January 2026
10.1126/science.adx5486

Science
AAAS

Supplementary Materials for

Scimitar-crested *Spinosaurus* species from the Sahara caps stepwise spinosaurid radiation

Paul C. Sereno *et al.*

Corresponding authors: Paul C. Sereno, dinosaur@uchicago.edu; Daniel Vidal, eoalulavis@gmail.com

DOI: 10.1126/science.adx5486

The PDF file includes:

Other Supplementary Material for this manuscript includes the following:

Science
AAAS

Supplementary Materials for

New scimitar-crested *Spinosaurus* species from the Sahara caps stepwise spinosaurid radiation

Paul C. Sereno[1,2*], Daniel Vidal[1,3*], Nathan P. Myhrvold[4], Evan Johnson-Ransom[1], María Ciudad Real[3], Stephanie L. Baumgart[5], Noelia Sánchez Fontela[6], Todd L. Green[7], Evan T. Saitta[1], Boubé Adamou[8], Lauren L. Bop[1], Tyler M. Keillor[1], Erin C. Fitzgerald[1], Didier B. Dutheil[9], Robert A. S. Laroche[10], Alexandre V. Demers-Potvin[11], Álvaro Simarro[3], Francesc Gascó-Lluna[12], Ana Lázaro[13], Arturo Gamonal[3], Charles V. Beightol[14], Vincent Reneleau[9], Rachel Vautrin[9], Filippo Bertozzo[15], Alejandro Granados[16], Grace Kinney-Broderick[17], Jordan C. Mallon[18], Rafael M. Lindoso[19], Jahandar Ramezani[20]

***Corresponding authors:** dinosaur@uchicago.edu (P.C.S.); eoalulavis@gmail.com (D.V.)

The PDF file includes:

Supplementary Text

Contents

1. Provenance of *Spinosaurus mirabilis* sp. nov

1.1 Localities

The specimens of *Spinosaurus mirabilis* sp. nov. in this report (Table S1) were found in the Farak Formation from two fossil areas (Fig. 1A), Iguidi (17° 56′ N, 5° 37′ E) and Jenguebi (16° 40′ N, 10° 15′ E). See the next section for discussion of the history and identification of the formation. The holotype specimen (MNBH JEN1) comes from the Jenguebi fossil area at a site called Sirig Taghat.

1.2 Holotype

The bones composing the holotype of *Spinosaurus mirabilis* (MNBH JEN1) include a right premaxilla, portions of both maxillae, the base and the bottom one-half of the fused nasal-prefrontal crest (including the flattened crest process of both prefrontals), the alveolar edge of the right dentary, and five teeth found near the maxillae. All were found in a small area near the right premaxilla, which was preserved *in situ* and collected in a field jacket (Fig. S1A, B).

No.	Specimen	Description
Jenguebi fossil area		
1	MNBH JEN1 (holotype)	Right premaxilla, both maxillae, nasal crest and a portion of the alveolar edge of a right dentary, and five maxillary teeth (*in situ*)
2	MNBH JEN2	Partial left maxilla, nasal crest, partial anterior-mid cervical and mid-posterior dorsal vertebrae, partial lt. ischium, partial proximal end of the left femur
3	MNBH JEN3	Nasal crest missing distal tip (*in situ*)
4	MNBH JEN4	Partial right dentary, posterior caudal vertebrae, left tibia, pedal phalanges (*in situ*)
5	MNBH JEN5	Left maxilla (*in situ*)
6	MNBH JEN6	Three isolated crowns (a-c) (*in situ*)
7	MNBH JEN7	Anterior dorsal vertebra (D3) preserving a partial centrum and base of the neural arch, isolated
8	MNBH JEN8	Posterior dorsal centrum with base of spine (2 pieces)
9	MNBH JEN9	Anterior caudal vertebra with partial centrum and neural arch and distal end of a chevron
Iguidi fossil area		
10	MNBH IGU11	Anterior dorsal centrum (D1)
11	MNBH IGU25	Two articulated anterior dorsal centra (D1, D2) with the base of the neural arches attached
12	MNBH IGU38	50 isolated crowns
13	MNBH IGU39	Mid caudal centrum and base of neural arch
14	MNBH IGU40	Pedal proximal phalanx II-1

Table S1. Holotype and 13 select referred specimens of *S. mirabilis*, sp. nov. Specimens come from two fossil areas in Niger, Jenguebi (JEN) and Iguidi (IGU). D, dorsal vertebra; MNBH, Musée National Boubou Hama (MNBH).

1.3 Referred specimens

Many additional teeth as well as associated and isolated bones are provisionally referred to *S. mirabilis* from the Jenguebi (JEN) and Iguidi fossil areas (IGU) (Table S1). MNBH JEN2 (Fig.

S1C) represents a subadult individual smaller than the holotype that preserves the nasal crest in association with other cranial fragments, several vertebrae, proximal portions of the femur and a fragmentary left ischium. MNBH JEN3 (Fig. S1D) represents a third subadult individual also smaller than the holotype that preserves the fused nasal crest found *in situ* but in isolation. MNBH JEN4 is another specimen from another locality in the Jenguebi fossil area that preserves most of one dentary in association with other bones including most of the left tibia and posterior caudal centra (Fig. S2A). Several key measurements are given in Table S2.

Bone	Collection No.	Dimension	Measurement (cm)
Premaxilla	MNBH JEN1	Maximum length	27.5
		Maximum height	14.7
Maxilla	MNBH JEN1	Maximum length	54.8
		Anterior ramus, height	14.5
		Mid-section, height	9.8
Nasal	MNBH JEN1	Crest base, anteroposterior length	21.0
		Crest mid height, anteroposterior length	13.7
Tibia	MNBH JEN4	Maximum length	54.6
		Proximal end, anteroposterior	(6.9)
		Mid shaft, transverse width	5.1
		Distal end, maximum transverse width	11.0

Table S2. Measurements for select bones of *S. mirabilis* sp. nov. Measurements for the right premaxilla and maxilla (MNBH JEN1) and left tibia (MNBH JEN4) of subadult individuals. Parentheses indicate estimated measurement.

1.4 Associated data and specimen access

Age. Approximately 95 Mya based on the close overlap in fauna with the better dated Cenomanian Douira Formation of Morocco (*17*).

Taxonomic justification. The new species is based on the dramatic extension and scimitar form of the cranial crest and other subtle features that differentiate it from its closest relative, *Spinosaurus aegyptiacus* (*2*, *3*). We erect a new species, *S. mirabilis* sp. nov., in the genus *Spinosaurus*, given its close resemblance to the type species, *Spinosaurus aegyptiacus*.

Authentication. The new species is easily differentiated on cited features. Its distinction from previously known spinosaurids is not controversial.

Collectors. One of the authors (P. C. S.) lead expeditions to Niger in 2000, 2019 and 2022, when the material in this report was collected. Most of the authors of this report participated in one or more of these expeditions.

Collection. The maxillae and partial dentary of the holotype (MNBH JEN1) and all specimens from the Iguidi fossil area are on temporary loan to the Fossil Lab at the University of Chicago (5437 S. Wabash Avenue, Chicago, IL 60615). For examination, contact Tyler Keillor (Lab Manager, tkeillor@uchicago.edu). Other bones of the holotype and all referred specimens from Jenguebi fossil area are in Niger Republic under the care of Prof. Oumarou Ide of Abdou Moumouni University of Niamey (oumarou.ide5@gmail.com).

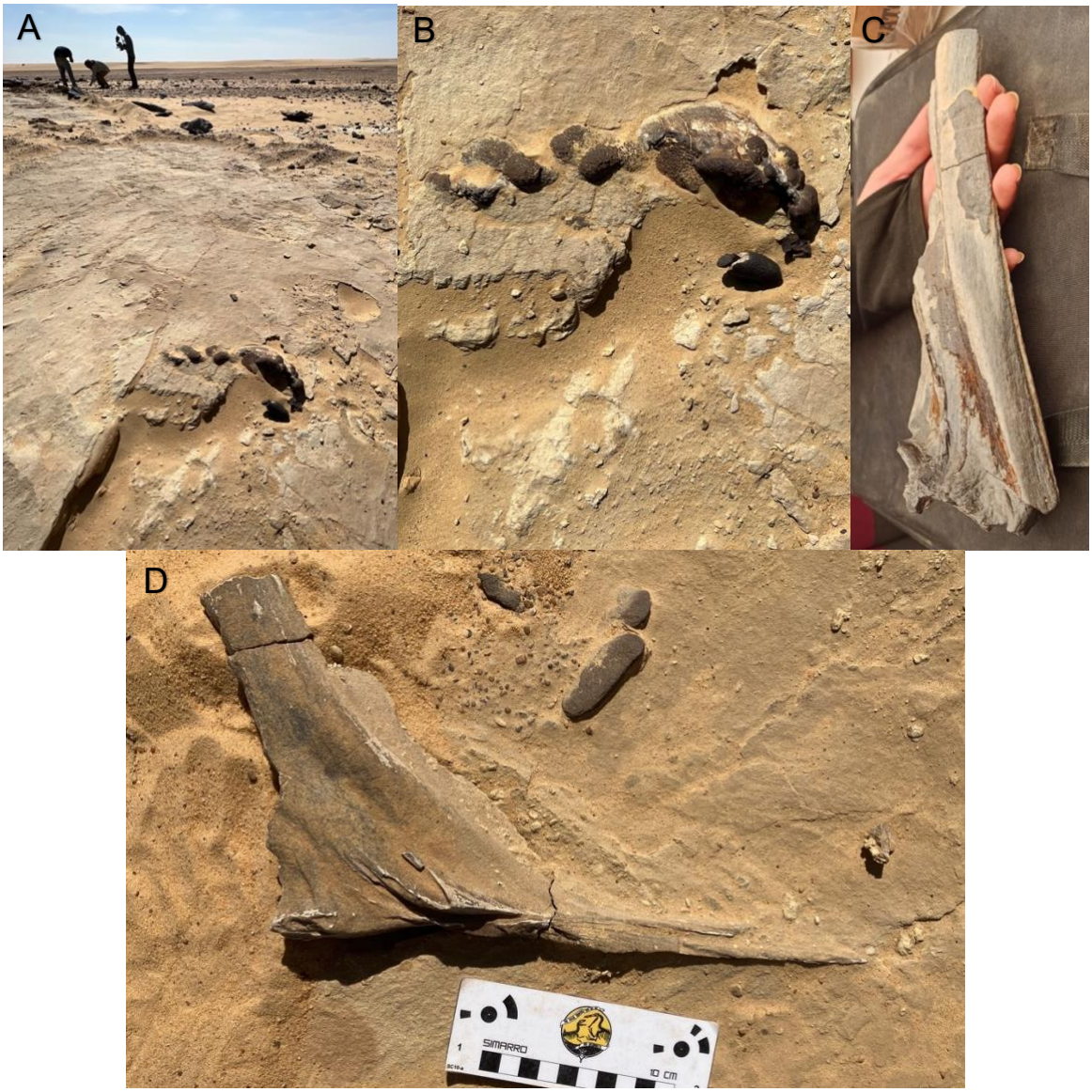

Fig. S1. *Spinosaurus mirabilis* sp. nov. premaxilla and nasal crest at Sirig Taghat. (**A**) Right premaxilla in cross-bedded sandstone (MNBH JEN1, holotype). (**B**) Closer view of right premaxilla showing hematitic concretions adhering to portions of the specimen. (**C**) Fused nasal crest of a second subadult individual (MNBH JEN2). (**D**) *In situ* fused nasal crest of a third subadult individual (MNBH JEN3).

2. Local stratigraphy and associated fauna

2.1 Geologic setting

We briefly describe the two basins and the Jurassic and Cretaceous sediments that are relevant to understanding the geologic setting for the fossils described as *Spinosaurus mirabilis* sp. nov. from Jenguebi and Iguidi fossil areas. Based on our field work, we identify the strata in these two fossil areas as the Farak Formation (previously identified as the Echkar Formation). The Farak

Formation is the fossil-bearing unit preserving the remains of *S. mirabilis* and its associated Early-Middle Cenomanian vertebrate fauna (*Carcharodontosaurus*, etc.).

Fig. S2. *Spinosaurus mirabilis* sp. nov. referred specimen and crocodyliform from other localities in the Jenguebi fossil area. (**A**) Left subadult tibia of *Spinosaurus mirabilis* sp. nov. MNBH JEN4. (**B**) Cranial bones pertaining to a large-bodied crocodyliform.

Basins. The sediments of Gadoufaoua, Iguidi and Jenguebi fossil areas were deposited in the Iullemmeden Basin (*13, 73*, 74). A northwest-southeast rift zone has been recognized more recently by petroleum geologists as the East Niger Rift Basin, which lies immediately to the east of Gadoufaoua and Jenguebi fossil areas. Its northwest end is a rectangular graben called the Téfidet (*75*) on the perimeter of the Aïr Massif floored by rocks of the Elrhaz Formation

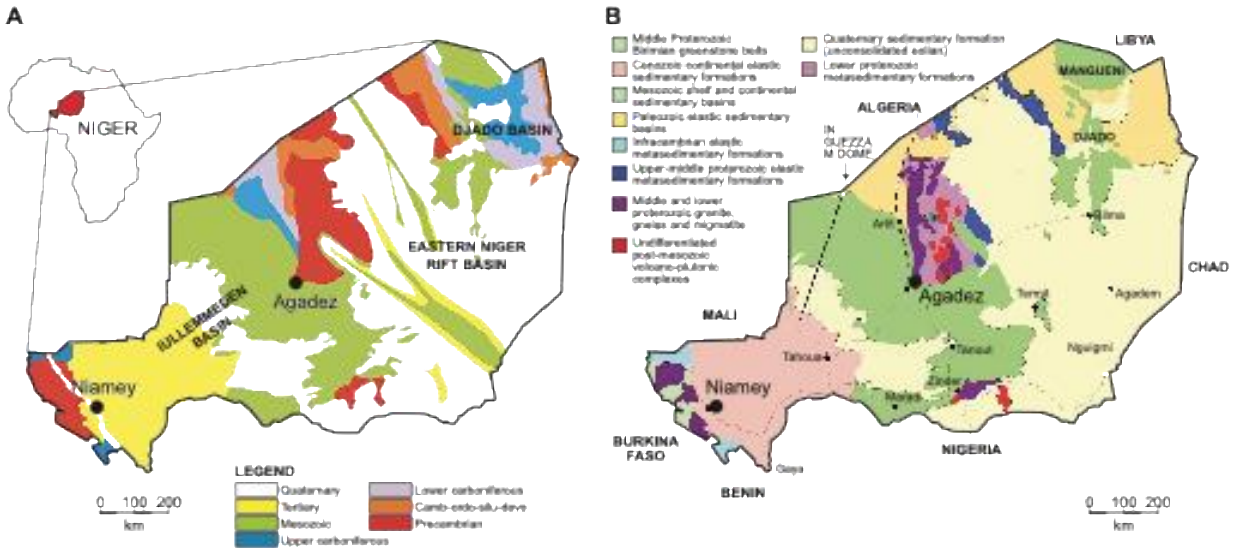

Fig. S3. General geologic and structural maps of Niger. (**A**) Map of Niger showing principal basins (after *73*). (**B**) General geologic map of Niger (after *74*).

comparable to those in Gadoufaoua. These grabens also began to receive sediments by mid Cretaceous time (Fig. S3A).

Jurassic and Cretaceous sediments. Jurassic and Cretaceous sedimentary strata with fossiliferous horizons are exposed in outcrops across a broad, diagonal band from northwest to southeast passing south of Agadez and the Aïr Highlands (Fig. S3). These sediments have been referred to traditionally as the "Continental intercalaire" and "Continental hamadien," the former the "between" rocks and the latter the "plateau" rocks initiated by the cliff-forming Upper Cenomanian-Turonian limestone. Both have been subdivided into series or groups and then subdivided further into formations, although often without precise definitions or designated stratotype sections (*15*).

As a result, there has been some confusion and discussion of the lower boundary of the "Continental intercalaire,' the composition of groups or series, and the correlation between formations listed for different regions within this broad package of strata (*10*, *14*, *15*, *74*). Taquet (*15*) summarized the sequence as understood in 1976 (Table S3), dividing the Tégama Series into three formations (Tiguedi-Tazolé, Elrhaz, Echkar) and eight GAD levels, the latter recognized by uranium survey geologists (*76*).

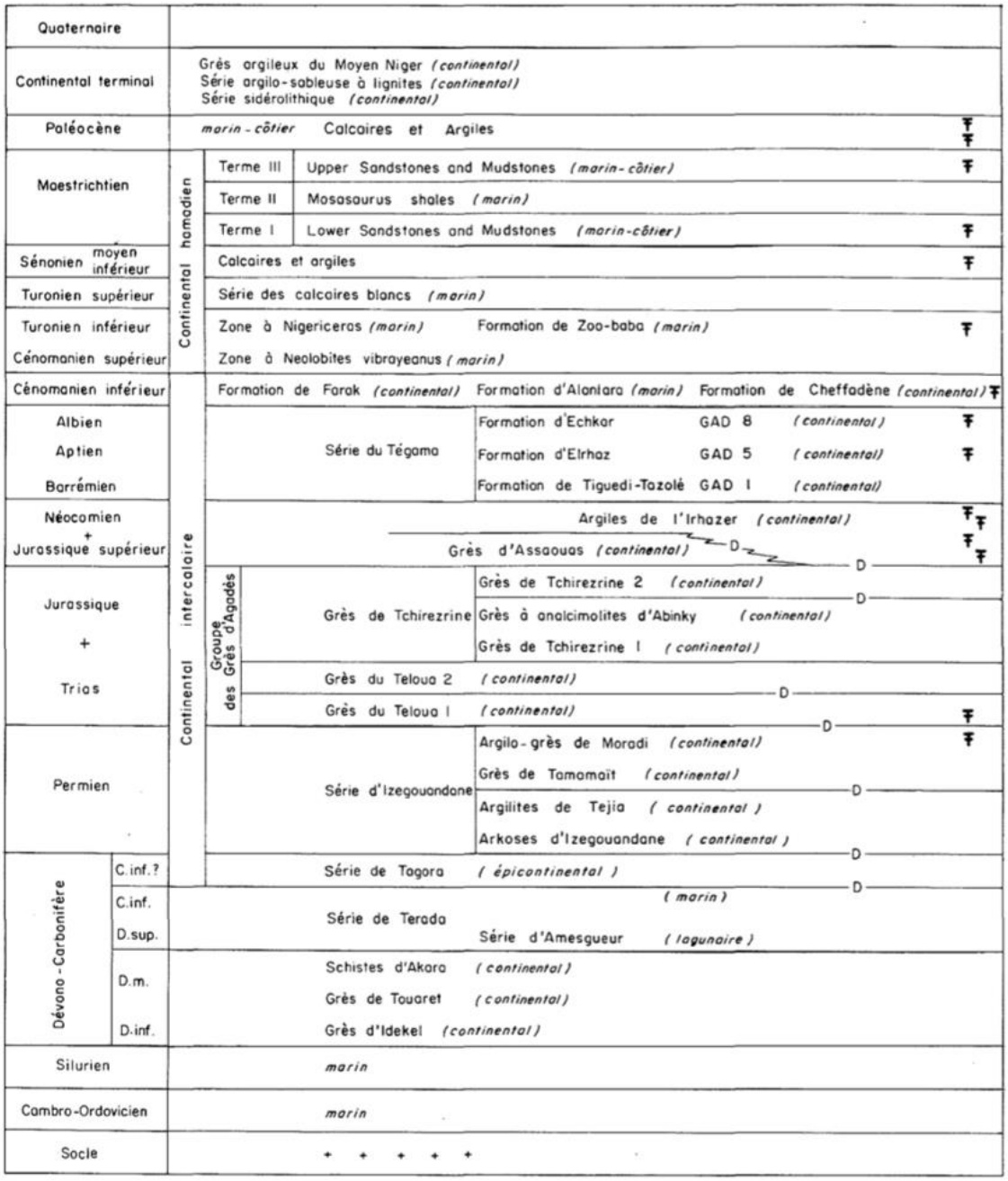

Table S3. Stratigraphic summary of formations and sediment in Niger. Sedimentary succession in Niger (*15*).

More recently geologists and paleontologists have abandoned the large historical divisions and organized the strata into a series of groups and formations [Fig. S4; (77–81)]. Following Taquet (*15*), the Tégama Group was divided into three formations (Tazolé, Elrhaz, Echkar) ending in the Albian and followed by a fourth formation (Farak) underlying the marine platform and regarded as Cenomanian. Two of these formations yielded considerable vertebrate faunas and two are barren. The famous fossil area Gadoufaoua and its increasingly diversified vertebrate fauna have uniformly been regarded as the Elrhaz Formation (GAD5) and assigned the general age of Aptian-

Albian. The cliff-forming Tazolé Formation (Falaise de Tiguedi) at the base of the Tégama Group serves as a regional marker horizon and contains abundant fossil wood including trunks of the gymnosperm *Araucaria* (Jurassic to Recent), but it has not yielded any vertebrate remains.

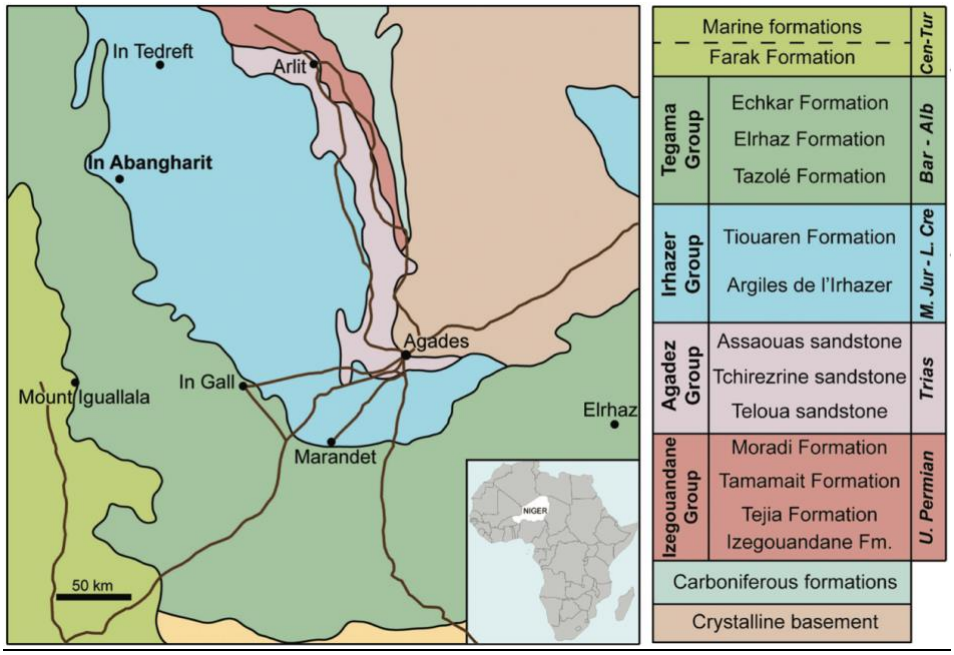

Fig. S4. Groups and formations for Mesozoic strata of the Iullemeden Basin of Niger. Map and Table (from *79* after *15*).

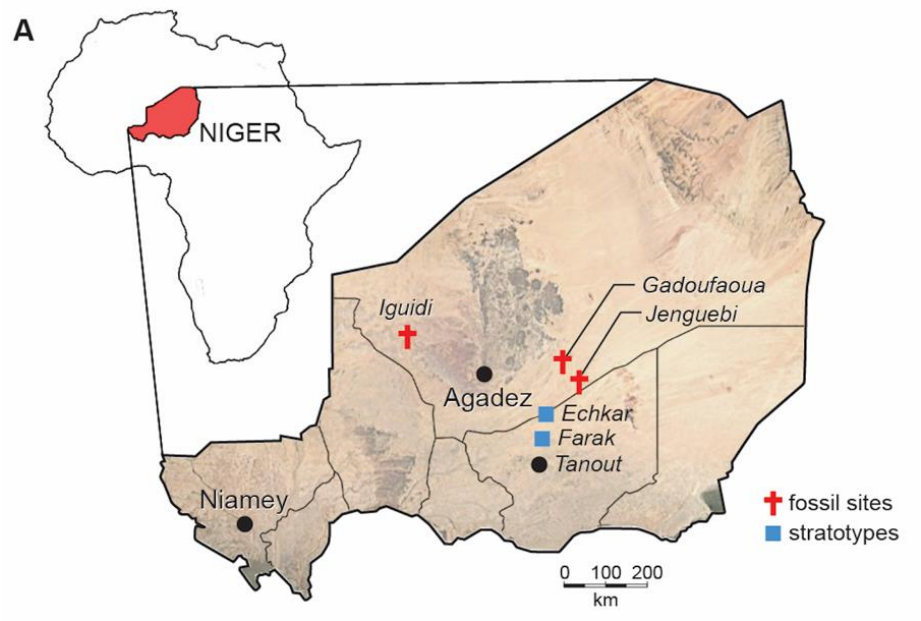

Fig. S5. Map of Niger showing key locations. Fossil areas (red crosses) and stratotype sections for the Echkar and Farak Formations (also Fig. 1A).

The Iguidi area lies west of the transiently inhabited location of In Abangharit. Two crocodylians [*Kaprosuchus* and *Laganosuchus* (*78*)], an abelisaurid theropod [*Rugops* (*79*)], and a species of *Carcharodontosaurus* (*80*) were described from Iguidi with their localities attributed to the Echkar Formation. The obvious similarities to the Cenomanian age Kem Kem Group in Morocco were underscored, but no justification was given for the assignment of the Iguidi exposures to the Echkar, rather than the Farak, Formation.

More recently Young et al. renamed a crocodylian lower jaw collected in the 1950s from the Iguidi area [*Fortignathus* (*81*)]. They attributed the fossil to the Echkar Formation over the Farak Formation and posited an age of "upper Albian to lower Cenomanian age" but offered no reasoning for either the formational assignment or the age designation (Fig. S4). They remarked that no shared species had yet been described from both the Kem Kem Group and the Iguidi area, a possible indication they were different in age.

We argue here that it is impossible to make an assignment of formation to the outcrops in either Iguidi or Jenguebi areas without reference to the sections Faure described for each formation north of Tanout [Fig. S5, (*12*)]. Second, a latitudinal distance of approximately 2,500 km separates the Moroccan Kem Kem Group from the fossil sites in Niger. This equals latitudinal differences separating some realms among ammonites (*82*). Finding dissimilarity at the species level between faunas, thus, is not surprising versus the similarity of vertebrate faunas along similar latitude on the northern coast of Africa (*83*). Third, there are overlapping species in both Niger and Moroccan sites, including teeth of the widespread Cenomanian sawfish *Onchopristis numidus*.

None of the terrestrial Cretaceous formations in either Morocco or Niger have been radioisotopically dated, and so their absolute ages are open to debate. There are only two less speculative relative dates for these beds based on ammonites (*82*, *84*) or widespread elasmobranchs correlated with ammonite zonation (*17*). In Niger the Upper Cenomanian-Turonian platform (*16*, *70*) and its ammonite zonation (*82*, *84*) are well studied near Tanout in the region where our new fossils were discovered (Fig. S3, also Fig. 1A). The age of the Cenomanian-Turonian stage boundary has been well established globally at 93.9 ± 0.2 Mya (*85*, *86*), with a slightly older age (~94.5 Mya) for the peak of the Cenomanian-Turonian transgression (*22*). Thus, the age of terrestrial sediments underlying the platform in both Morocco and Niger that contain fossil vertebrates including *Spinosaurus* would be estimated to be ~95 Mya or older, as they are situated at least a short distance in-section below the limestone.

The relative age of the Douira Formation of the Kem Kem Group was assessed based on the teeth of nine elasmobranchs of Cenomanian age obtained from several microvertebrate localities, with seven of the nine species also recorded in the Bahariya Formation in Egypt (*17*). Articulated remains of *Spinosaurus aegyptiacus*, *Carcharodontosaurus saharic*us and *Deltadromeus agili*s were discovered as singularly intact specimens in a deltaic facies dominated by transported fossil bone and teeth (*10*). The conformable contact between the Douira Formation and the overlying carbonate platform argues against an appreciable temporal gap between the two formations. Thus, vertebrate biostratigraphic correlation suggests an Early to Middle Cenomanian age for both the Kem Kem Group in Morocco and the Iguidi and Jenguebi fossil areas in Niger.

2.2 Upper Cretaceous stratigraphic sequence

Cenomanian-Turonian limestone. We visited the stratigraphic section in exposures near Tanout including the Cenomanian-Turonian limestone and name-bearing sections for both Farak and Echkar Formations (Fig. 1A). In a section of the limestone platform, we found three

ammonites including the Late Cenomanian ammonite *Metengonoceros dumbli* [Fig. S6; (*82*, *84*)].

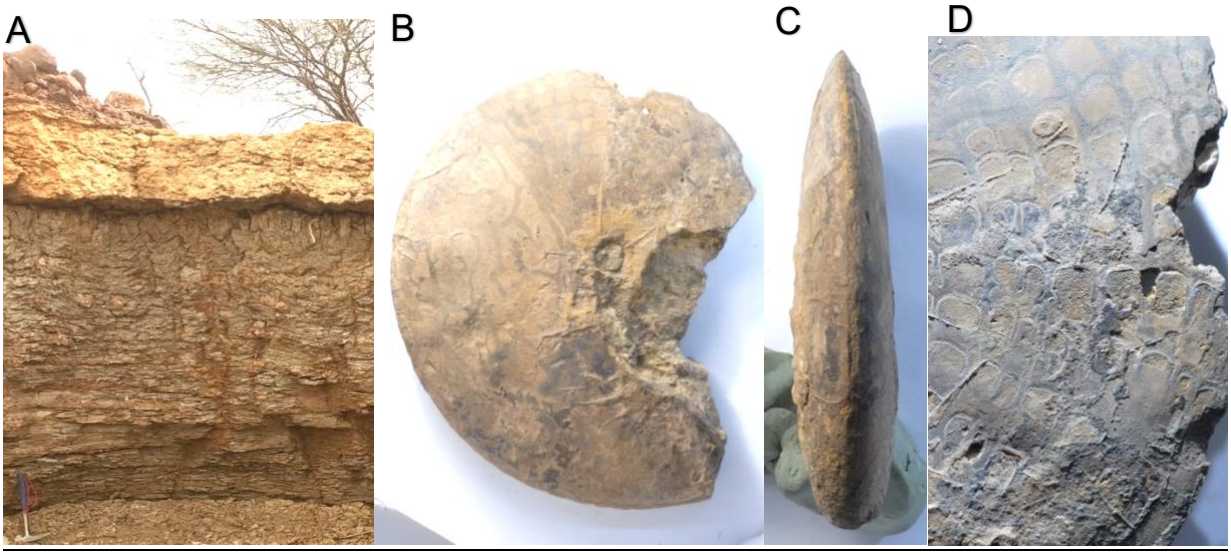

Fig. S6. Ammonite *Metengonoceras dumbli* from the Cenomanian-Turonian limestone near Tanout. (**A**) Section. (**B**, **C**) Steinkern in lateral and posterior view showing the narrow, unornamented external margin. (**D**) Sutural pattern between chambers.

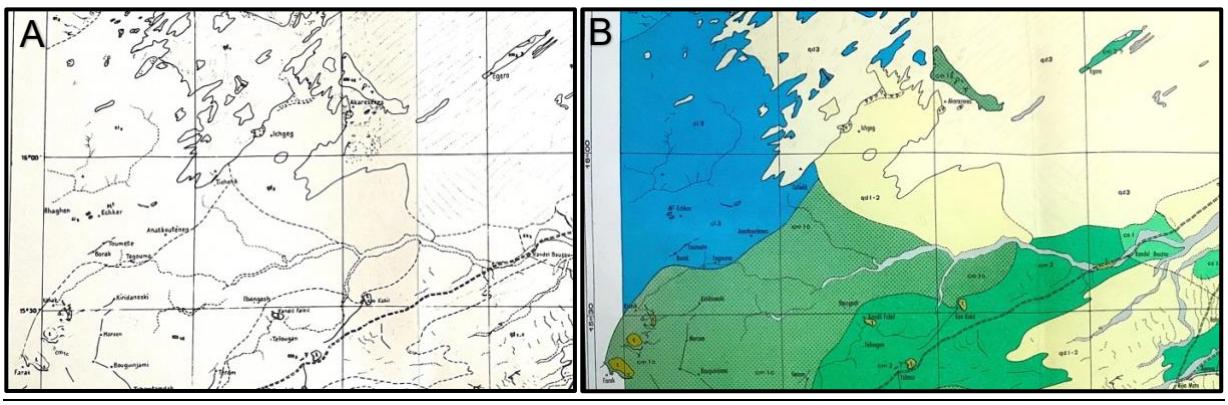

Fig. S7. Maps of the Jenguebi fossil area northeast of Tanout. (**A**) Political map showing Farak and Echkar sites (southwest corner), the Akarazeras locality (central north), and the Jenguebi fossil area north of Égaro (northeast corner). (**B**) Geological map corresponding to the political map. Maps are cropped from originals (*12*).

Farak Formation. Using a piste heading northeast out of Tanout (Fig. S7), we moved down-section from the Cenomanian-Turonian limestone to the Farak falaise, which crosses the piste (12). Sections described by Faure in the area did not yield vertebrate fossils but did preserve abundant fossil wood including tree trunks. The sediments varied between cross-bedded sandstone of medium grain to finer siltstones with intercalated mudstone layers. Like Faure we also did not encounter vertebrate fossils in the sections adjacent to the piste.

Farther northeast, Faure (*12*) describes the outcrop Akarazeras near a small well, which we eventually located. Like Faure we discovered a rich vertebrate fauna there, including teeth of *Carcharodontosaurus* and *Spinosaurus*, titanosaurian vertebrae and ribs, crocodylians and lungfish. We found bones of this fauna at localities surrounding Akarazeras, identifying a fossiliferous zone trending northeast-southwest. This trend parallels the many localities of Gadoufaoua (GAD5) with barren sandstones of the Echkar Formation (GAD6–8) in between.

Exploring north of an exposure known as Égaro, we discovered the fossiliferous Jenguebi area comprising a suite of small exposures on the edge of a vast erg (Fig. S7). We interpret these outcrops as pertaining to the Farak Formation with a vertebrate fauna overlapping that from Akarazeras and from Iguidi west of Agadez. The outcrop at Jenguebi lies along an arcuate band extending west and then arearing again to the north in the Iguidi fossil area. These strata underlie the Cenomanian-Turonian limestone, which is exposed to the south and west of Jenguebi and Iguidi, respectively (Fig. S4).

Echkar Formation. We visited the section of the Echkar Formation described by Faure at Mount Echkar (*12*, p. 127), a butte with a well exposed section. He described light-colored, cross-bedded sandstones, recording some white silicified wood but no vertebrate fossils. The section accurately described the outcrop of uniform cross-bedded sandstone. After considerable prospection, we were unable to find fossils of any kind on Mount Echkar including petrified wood. The only fossils Faure recorded in several other sections he regarded as the Echkar Formation occurred to the north, where he mentioned nondescript vertebrate bone in an intercalated layer of mudstone (*12*, p. 125).

Taquet (15) attributes GAD6-8 to the Echkar Formation, the stratotype section of which lies southeast of Gadoufaoua. Crisscrossing this region of cross-bedded sandstone has turned up one eroded bone, even though the sandstone is indistinguishable to the eye from fossiliferous sandstones of GAD5 at Gadoufaoua. The sandstone in this section resembles that in Gadoufaoua but appears to be reworked and hence without vertebrate remains. We never encountered intercalated mudstone layers. There is less variability of sedimentation than observed in the Farak falaise, at Akarazeras or the Jenguebi fossil area. Based on this and other field observations, we suggest that the barren Echkar Formation lies at the top of the Tegama Series (GAD7, 8) below the fossiliferous Farak Formation, as Faure (*12*) described in his composite section northeast of Tanout.

2.3 Jenguebi fossil area and the Sirig Taghat local section

The outcrops in the Jenguebi fossil area are topographically low except for a few cliff-edged valleys (figs. S8, S9). Exposures are typically low ridges of cross-bedded, laminated, poorly cemented, medium-grained sandstone with some parts hardened by secondary ferruginous cement. Although fossil wood and carbonized plant traces are rare, the outcrop uniformly suggests a fluvial setting in a riparian environment with deposition in pulses preserving associated vertebrate remains.

Unlike the mud-dominated Douira Formation that underlies the Cenomanian-Turonian limestone in Morocco, there are no significant mudstone layers in the Farak Formation, and taxa common to brackish or marginal marine settings, such as the sawfish Onchopristis numidus, are rare. We did not recover hybodontids or teeth representing other elasmobranchs, and we never encountered paludal or intertidal sediments. Unlike Cenomanian formations along the northern coast of Africa, bones and partial skeletons of large-bodied herbivores such as sauropods are

common rather than truly exceptional. In sum, we found no evidence to suggest that a marine shoreline was nearby. Prior to the Late Cenomanian-Turonian transgression that laid down the limestone platforms, the nearest shoreline would have been in the Benue Trough to the southeast (*21*), approximately 500 kms from Jenguebi and 1,000 kms form Iguidi.

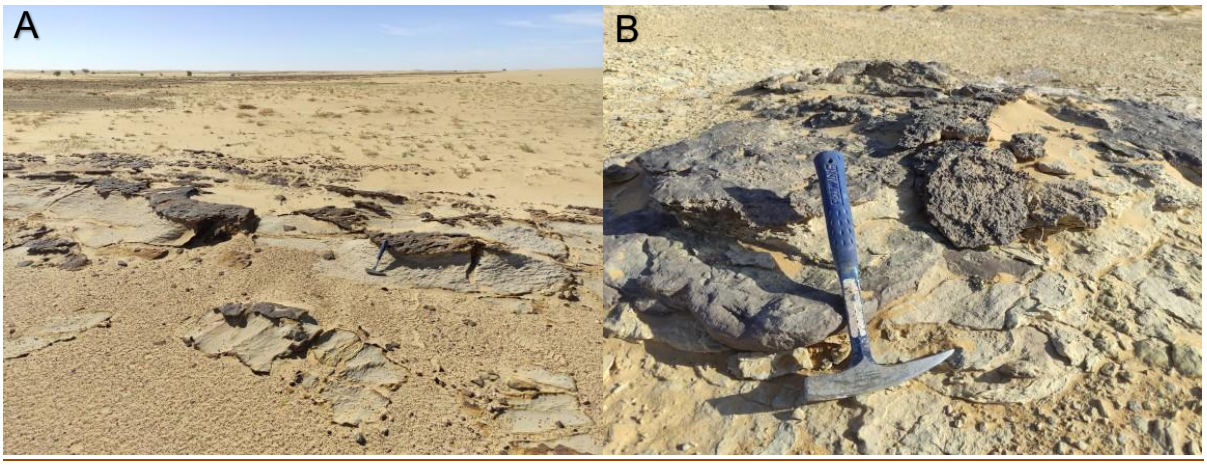

Fig. S8. Jenguebi fossil area exposures. Outcrops are low, cross-bedded sandstones (**A**) hardened in local areas by ferruginous cement (**B**).

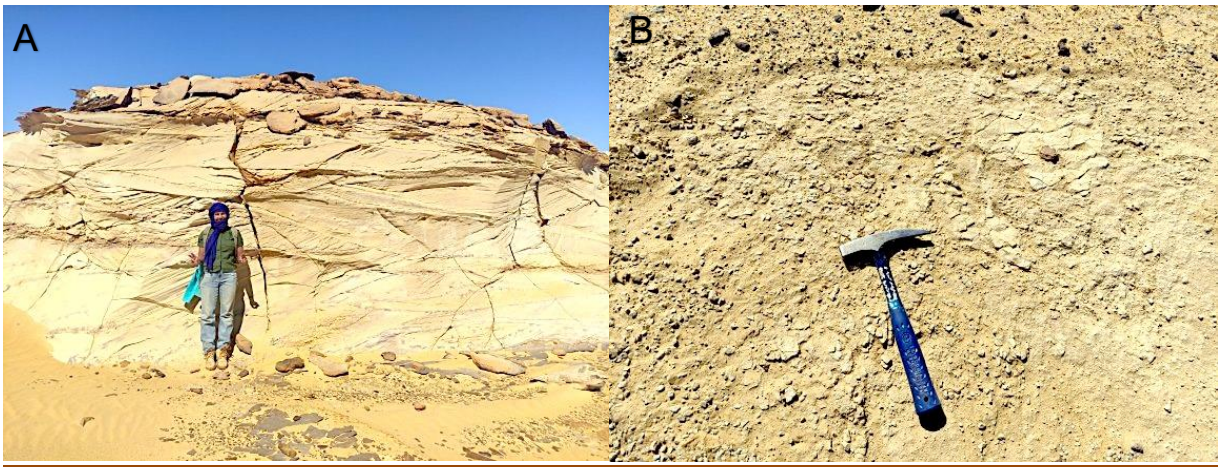

Fig. S9. Jenguebi fossil area exposures. (A) Prominent cliff outcrop showing largescale cross-bedded sandstones. (**B**) Crumbly siltstone encasing the partial skull and postcranial skeleton of a the tetanuran theropod *Carcharodontosaurus* sp. (see Fig. 1A, left column).

The stratigraphic section in the Jenguebi fossil area is composed almost exclusively of medium-to-fine grained sandstones and siltstones (Fig. S10, left column). The local section at Sirig Taghat, the type locality of S. mirabilis sp. nov., is similar (Fig. S10, right column). The type locality preserves multiple associated fossil vertebrates in a relatively small area interred in approximately 60 cm of sediment. The preservation and physical proximity of multiple specimens of *S. mirabilis* and titanosaurian and rebbachisaurid sauropods suggests that they were contemporary inhabitants of a riparian paleoenvironment.

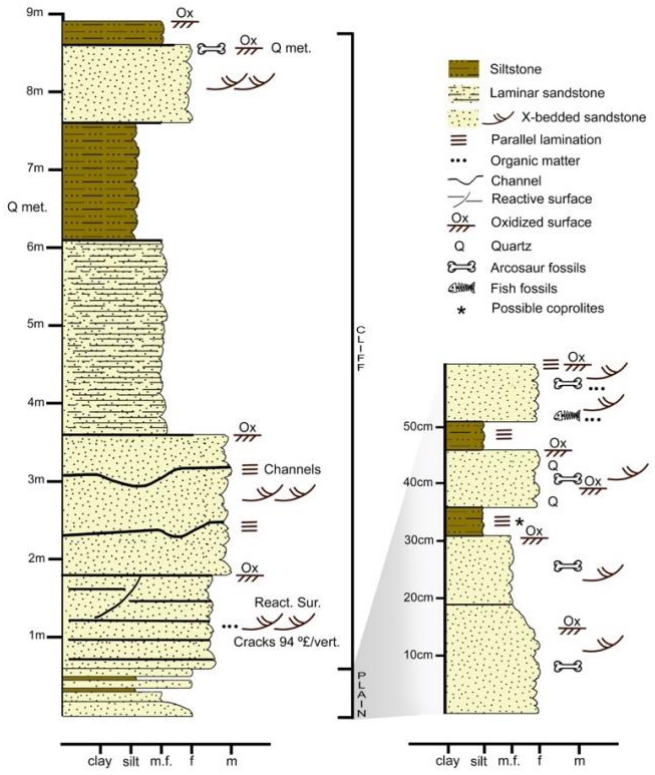

Fig. S10. Stratigraphic section in the Jenguebi fossil area. Composite section within the Farak Formation showing further detail in the basal 60 cm at the type locality Sirig Taghat.

2.4 Associated vertebrate fauna

A general list is given here of the vertebrate fauna collected from Jenguebi fossil area localities. Precise identification awaits laboratory preparation and study of fossil materials.

Chondrichthyes
- *Onchopristis numidus*

Osteichthyes
- Polypteridae, indet.

Testidines
- Family indet.

Crocodyliformes
- Families indet. (three taxa)

Pterosauria
- Azdarchoidea indet.

Dinosauria
- Rebbachisauridae, indet.
- Titanosauria
  - Families indet. (two taxa)
- Abelisauridae indet.
- Carcharodontosauridae
  - *Carcharodontosaurus* sp.
- Spinosauridae
  - *Spinosaurus mirabilis* sp. nov.

3. Skeletal reconstruction

3.1 Skull reconstruction

The skull of *S. mirabilis* was reconstructed from four specimens from Jenguebi (MNBH JEN1–4) with other portions of the skull based first on *Spinosaurus aegyptiacus* (*3*) and then *Irritator challengeri* (*45*). We first scaled and combined Jenguebi specimens, fitting to this composite skull the well-preserved remains of the snout of *S. aegyptiacus* and occiput of *I. challengeri* (Fig. S11).

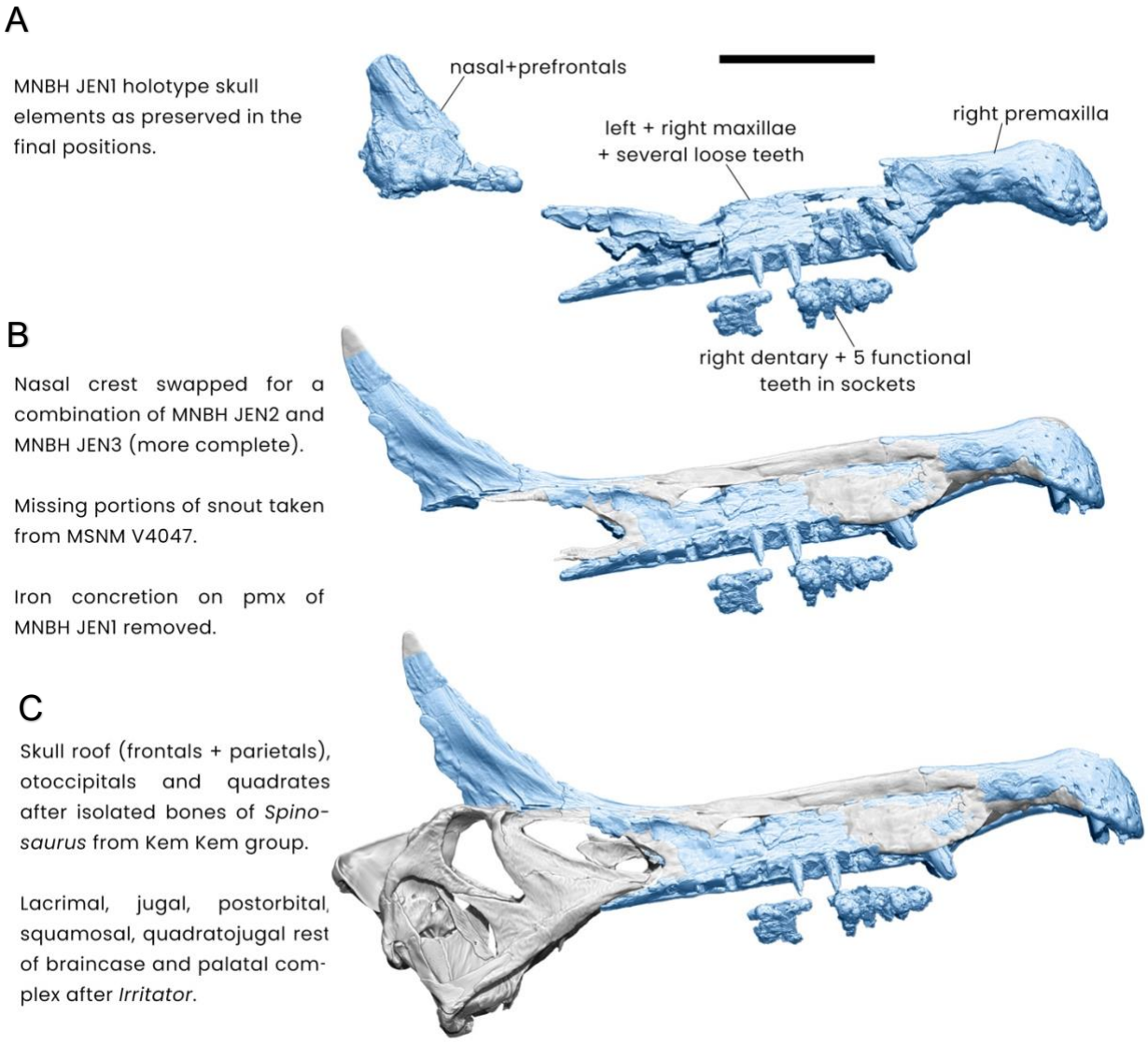

Fig. S11. Cranial reconstruction of *S. mirabilis* sp. nov. (**A**) Preserved snout and crest bones from Jenguebi. (**B**) Missing portions of the snout added from *S. aegyptiacus*. (**C**) Posterior end of the cranium added from *S. aegyptiacus* and *I. challengeri.*

The nasal-prefrontal crest differs markedly between *S. mirabilis* and *S. aegyptiacus*, both reconstructed based on multiple specimens (Fig. S12). In the three available specimens of the nasal crest in *S. mirabilis*, a lateral eminence and shallow linear grooves sweep upward and backward from the thicker base of the crest (Fig. S12A). The crest of the holotype of *S. mirabilis* also preserves the tongue-shaped articular processes of prefrontal on each side of the nasal crest.

Two new specimens preserving sections of the nasal crest in *S. aegyptiacus* were discovered in the Kem Kem Group that document the posterior portion of the base, a relatively transversely narrow crest, and the lateral triangular articular facet for participation of the prefrontal (Fig. S12B). The broader base, fluting and lack of a lateral eminence differentiate the crest from *S. mirabilis*, even though its thinning dorsal edge is not completely preserved.

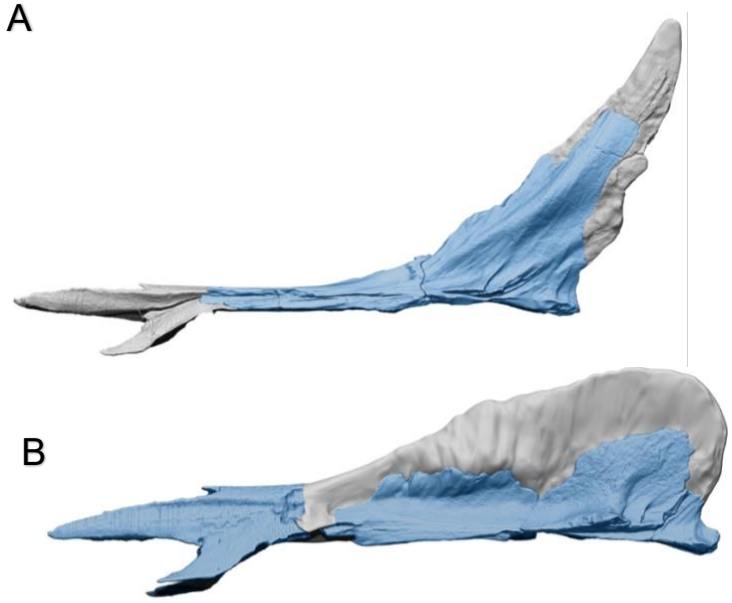

Fig. S12. Nasal crests in *Spinosaurus* species. (**A**) Nasal crest of *S. mirabilis* (MNBH JEN 3 in blue) with anterior end based on evidence from the maxilla and crest augmented from other specimens (MNBH JEN1, JEN2) with its tip restored. (**B**) Composite nasal crest of *S. aegyptiacus* (preserved portions in blue).

3.2 Skeletal reconstruction

The postcranial skeleton of *S. mirabilis* is incompletely known from available specimens. Bones of the axial column, which include cervical, dorsal and mid caudal vertebrae from Iguidi and Jenguebi fossil areas, preserve enough detail to show derived similarities to *S. aegyptiacus* (e.g., squat anterior dorsal centrum proportions with hypertrophied ventral keel, tall striated, parallel-sided dorsal neural spines, subquadrate centrum faces on relatively short mid caudal centra) as well as a few autapomorphies of *S. mirabilis* (e.g., relatively larger cervical pleurocoels).

One specimen (MNBH JEN4) preserves most of the dentary and a nearly complete tibia (Fig. S13), allowing size and relative length comparison to specimens of *S. aegyptiacus* [Fig. S13, Table S4; (*3*)]. The dentary in *S. mirabilis* has a more angular anterior end compared to the more rounded end in *S. aegyptiacus*. The tibia maintains a modest medullary cavity (Fig. 3H) like the Albian spinosaurine from Brazil, unlike the infilled shaft of the neotype of *S. aegyptiacus* (*3*). The articular depression for the ascending process is more limited in *S. mirabilis*. The length of the tibia relative

to the dentary is greater in *S. mirabilis* than in *S. aegyptiacus*, suggesting hind limb length was slightly greater in *S. mirabilis* than *S. aegyptiacus*.

Table S4. Scaling in *Spinosaurus*. Comparative reconstructed skeletal length in specimens of *S. aegyptiacus* and *S. mirabilis* sp. nov.

No.	Taxon	Specimen	Maturity	Relative axial skeleton length (%)	Description
1	*S. aegyptiacus*	BSPG 1912 VIII 19	Subadult	76	Holotype (destroyed) preserving dentaries, presacral, sacral and caudal vertebrae including the dorsal sail (Stromer, 1915)
2	*S. aegyptiacus*	FSAC-KK 11888	Subadult	76	Neotype preserving skull bones, partial limbs, dorsal said, and most of the tail (Ibrahim et al., 2014, 2020)
3	*S. aegyptiacus*	MSMN V4047	Adult	100	Isolated snout with broken teeth (Dal Sasso et al., 2005); large size and co-ossified sutures indicate maturity
4	*S. mirabilis*	MNBH JEN1	Subadult	61	Holotype preserving premaxilla, maxillae, dentary, and nasal crest
5	*S. mirabilis*	MNBH JEN2	Subadult	61	Partial skeleton with jaw fragments (including teeth), nasal crest, 5 cervical neural arches, 1 dorsal vertebra, fragments of dorsal spines, fragments of femur
6	*S. mirabilis*	MNBH JEN3	Subadult	46	Partial skeleton with right dentary, posterior caudal vertebrae, left tibia, and pedal elements

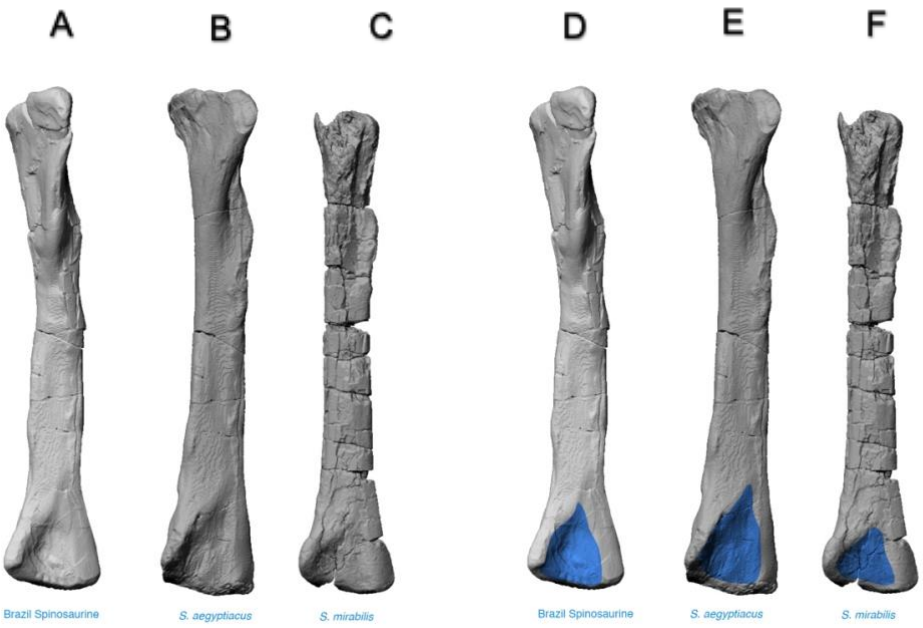

Fig. S13. Tibiae in the new Brazilian spinosaurine and *Spinosaurus*. Left tibiae in anterior view (A–C) with the articular surface of the ascending process of the astragalus highlighted in blue (D–F) in the Albian-age Brazilian spinosaurine (**A**, **D**) and the Cenomanian-age neotype of *S. aegyptiacus* (**B**, **E**) and a referred specimen (MNBH JEN4) of *S. mirabilis* (**C**, **F**).

4. Cranial crests in *Spinosaurus mirabilis* and extant avians

4.1 Cranial crest in *Spinosaurus mirabilis*

The nasal-prefrontal crest in *S. mirabilis* is known in the subadult holotype (MNBH JEN1) and in two subadult referred specimens of individuals of smaller size (Fig. S14; MNBH JEN1, JEN2). In all the nasals are completely coossified, whereas the nasal-prefrontal suture remains open. Nasal coossification must occur early in spinosaurid ontogeny followed by growth, as all known examples are fused. All show asymmetry as well, which is most profound in the more robust crest of the larger holotypic specimen, which deviates markedly from the midline toward to the left side (Fig. S14A). The central axis and shape of the crest in lateral view in *S. mirabilis* also appears to vary between specimens, the holotypic specimen with a slightly more upright crest than the other two (Fig. S14).

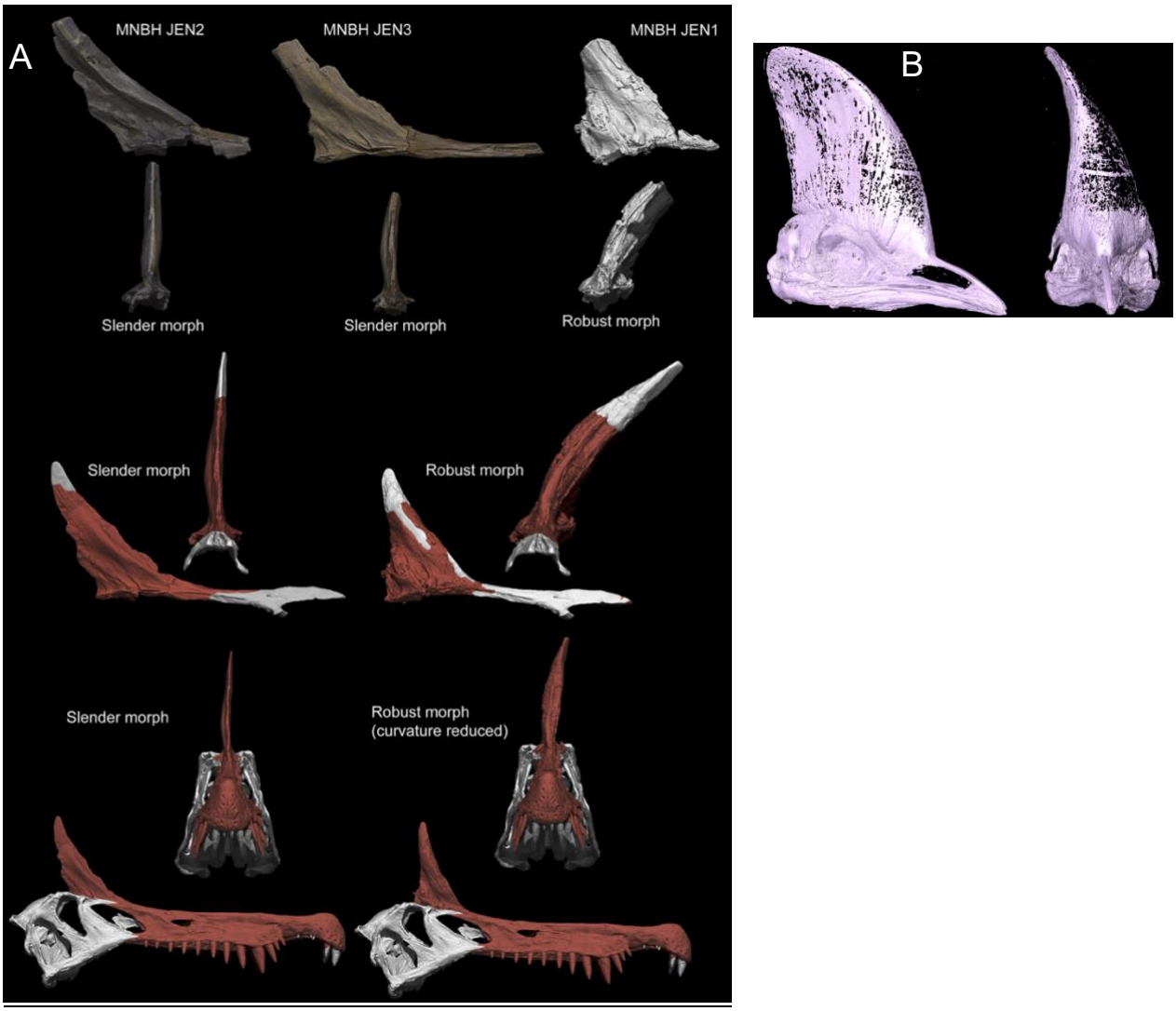

Fig. S14. Asymmetry in cranial ornaments. (**A**) Asymmetry in three nasal crests in *S. mirabilis* sp. nov. (**B**) Asymmetry in the cranial casque in the Southern Cassowary (*Casuarius casuarius* TLG C069).

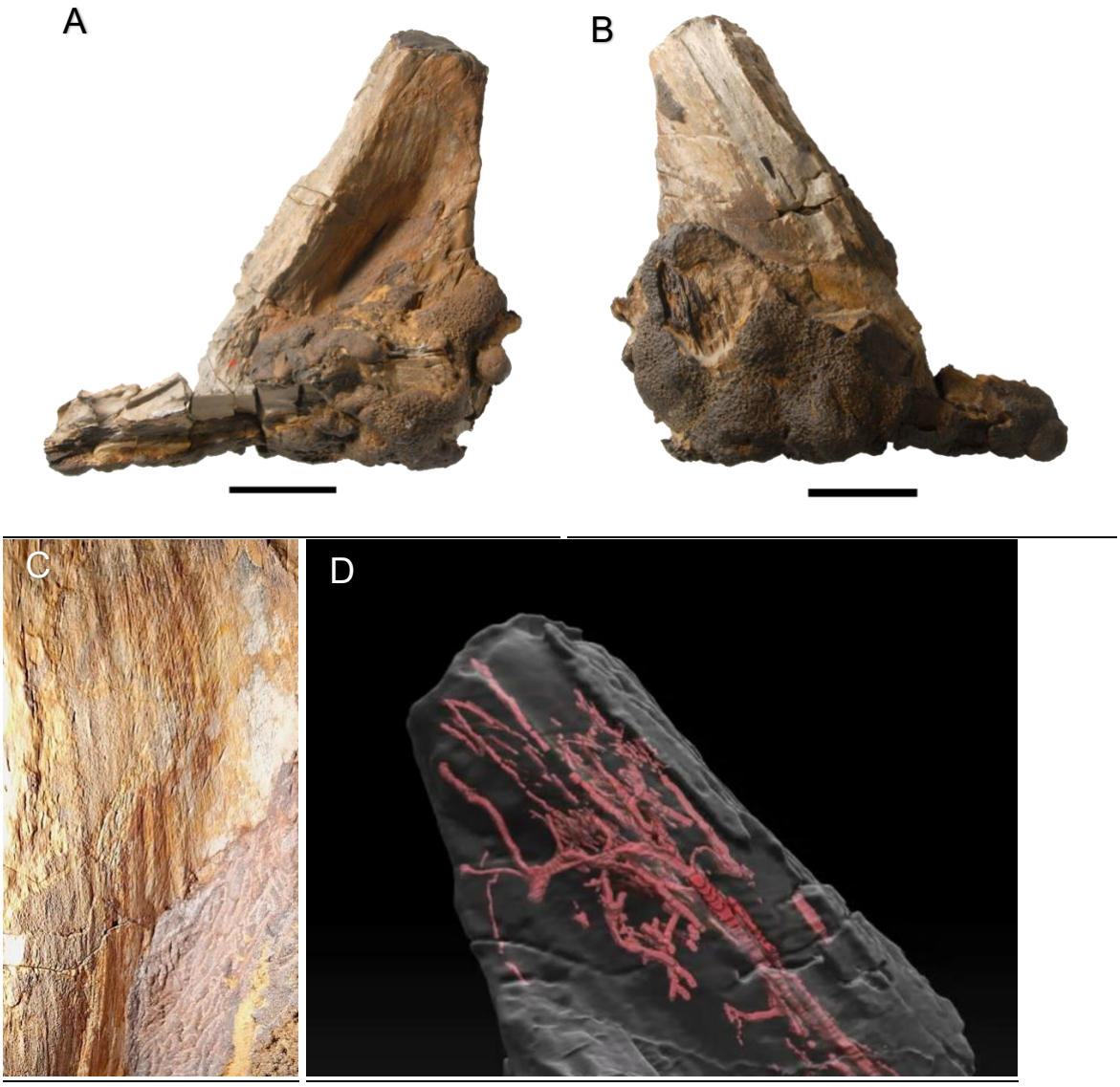

Fig. S15. Surface detail and internal vascular canals of the crest in *Spinosaurus mirabilis* sp. nov. Nasal-prefrontal crest of the holotypic specimen (MNBH JEN1). (**A, B**), Left and right lateral views of the nasal-prefrontal crest. (**C**) Close-up of the surface of the left side of the crest showing crisscrossed texture (center) and longitudinal striations and grooves. (**D**) Internal vascularity passing distally and ramifying within the mid-section of the crest as reconstructed from a microCT scan. Scale bar, 5 cm.

The surface texture, which is well-preserved on both sides of the holotypic nasal-prefrontal crest (Fig. S15C), shows a variety of textures consistent with attachment of a keratinous sheath and generally trending parallel to the long axis of the scimitar-shaped crest. These include longitudinal striations, crisscrossed striations, and longitudinal grooves. The bone of the crest is dense with vascular canals passing posterodorsally along the axis of the crest before ramifying (Fig. S15D). There are few canals that exit onto the surface of the crest, suggesting that the keratinous cover sheath had a separate vascular supply on the surface of the bony crest, possibly accommodated by the longitudinal grooves.

4.2 Cranial crests and casques in extant avians

Extant avians have evolved a variety cranial crests and casques for visual display (Fig. S16, Table S5). We use *crest* to denote a "cornified or keratin-sheathed, laterally compressed, sagittal or parasagittal cranial ornament underlain by bone with little or no pneumatization" and *casque* to denote a "keratin-sheathed, rarely feathered, cranial ornament underlain by highly pneumatized bone in birds and nonavian theropods" (*87*). Development of both structures in extant avians has recently been clarified (*25*, *26*, *88*) along with species-specific variation in crest shape in *Casuarius* (*89*).

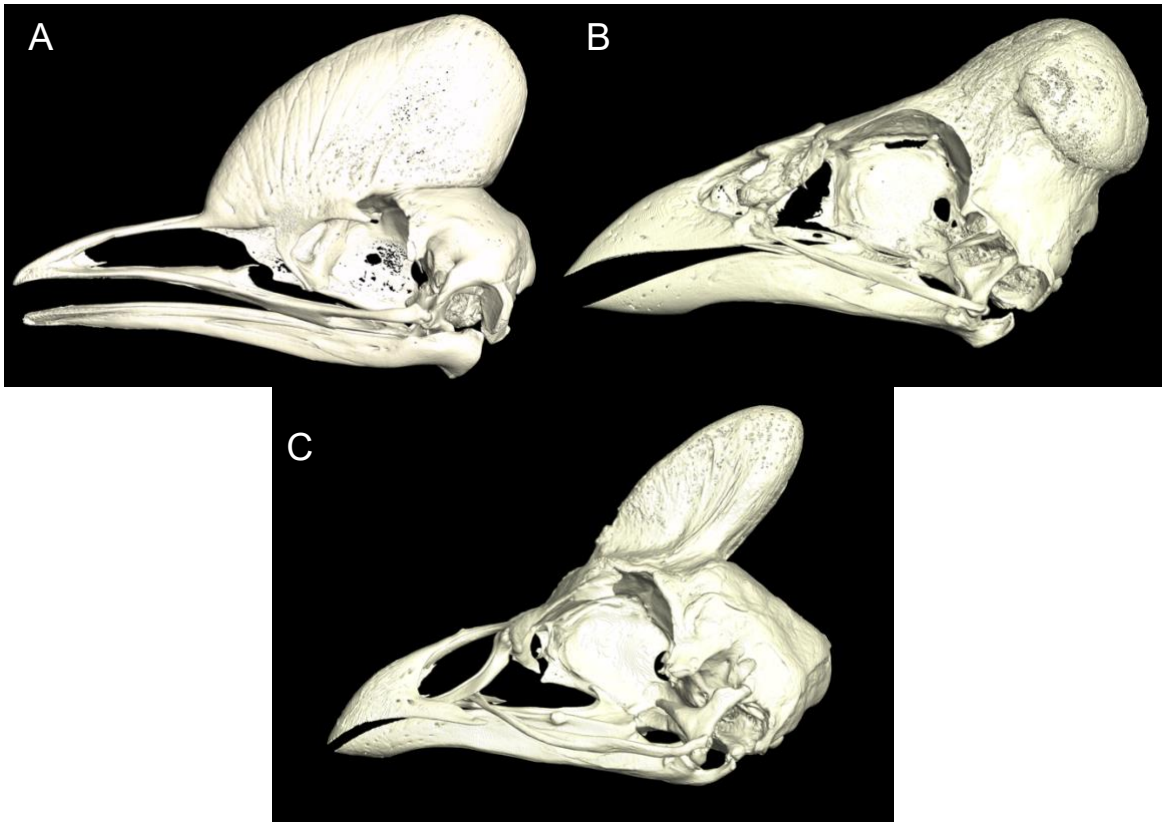

Fig. S16. CT renderings of extant avian skulls with cranial crests/casques. (**A**) Southern cassowary, *Casuarius casuarius* (AMNH 962). (**B**) Maleo, *Macrocephalon maleo* (TLG MM006). (**C**) Helmeted guinea fowl, *Numida meleagris* (TLG NM007).

Vascularization of these highly pneumatized casques consists of small-diameter vessels that pass internally into the pneumatized bone. Vascular support of the keratinous sheath, in contrast, consists of larger-diameter vessels that sometimes track in grooves on the outer surface of the casque (Fig. S16). They ramify and tend to decrease in diameter toward the margins of the ornament.

Table S5. Five extant avians with bony cranial ornamentation. Examples of bony casques in extant palaeognathous and neognathous avians.

No.	Taxon	Crest form	Notes
1	Cassuaridae *Casuarius casuarius* Southern cassowary		Keratinous outer sheath, thin cortical bone, and highly pneumatized internal space with loosely spaced trabecular bone; casque composed of following cranial elements: paired nasals, lacrimals, frontals and unpaired mesethmoid and median casque element (*88*)
2	Bucerotidae *Ceratogymna atrata* Black-casqued hornbill		Keratinous outer sheath, thin cortical bone, and highly pneumatized internal space with loosely spaced trabecular bone; casque composed of paired premaxillae (*25*)
3	Megapodiidae *Macrocephalon maleo* Maleo	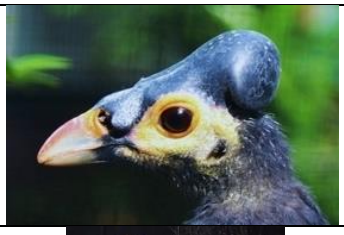	Cornified outer skin, thin cortical bone, and highly pneumatized internal space with loosely spaced trabecular bone; casque composed of paired frontals and parietals (*25*, *26*)
4	Numididae *Numida meleagris* Helmeted guinea fowl	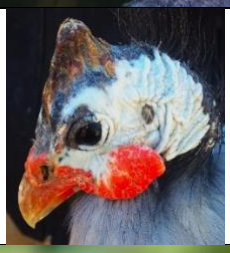	Keratinous outer sheath, relatively thin cortical bone, and pneumatized internal space with trabecular bone; casque composed of paired frontals (*25*)
5	Cracidae *Oreophasis derbianus* Horned guan	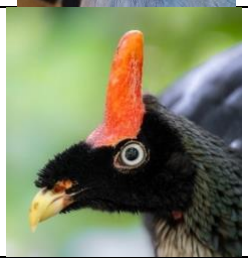	Cornified outer skin, relatively thin cortical bone, and pneumatized internal space with trabecular bone; casque composed of paired frontals (*25*)

5. Principal component analysis (PCA)

5.1 Measurements and taxon sampling

We took 7 measurements (Fig. S17) in 43 extant and extinct carnivorous archosaurs (extant crocodilians, extinct non-avian dinosaurs, extant avians; Table S6). As numbered in the table, these include two spinosaurids *Spinosaurus aegyptiacus* and *Suchomimus tenerensis* (1, 2), 18 additional nonavian dinosaurs (3 to 20), two terrestrial birds of prey/scavengers (21, 22), four aerial birds of prey (23 to 26), five long-necked semiaquatic birds (27 to 32), seven diving birds (33 to 38) and five crocodylians (39 to 43). These predators involve five prey capture modes: long-neck semiaquatic, short-neck semiaquatic, diving, terrestrial and aerial (Fig. 4). Our seven linear

morphological variables capture key aspects of head shape and body proportions (neck, hind limb) critical to these hunting modes. This simple and intuitive set of variables effectively partitions predatory mode. Skull or snout shape alone is insufficient to effectively separate crocodylians from long-snouted waders or divers (*5*, *42*). We plotted the two spinosaurids as 'unknown' regarding predation mode.

Sampled archosaurian predators range in body size across four orders of magnitude (*Accipiter nisus*, ~0.2 kg; *Tyrannosaurus rex*, ~8,000–9,000 kg), which is why body size garners most of the variance in PC1 (Fig. S18). To address skewness when considering such profound scaling, we $\log_{10}$-transformed the dataset to linearize the relationship between variables. Next, we normalized the measurements by standardizing each variable to unit variance (i.e., mean of zero, standard deviation of 1), before running PCA with R version 4.4.1 [setting scale=TRUE in the command prcomp()]. Doing so ensures that in PCA no single morphometric variable has an outsized influence over other variables.

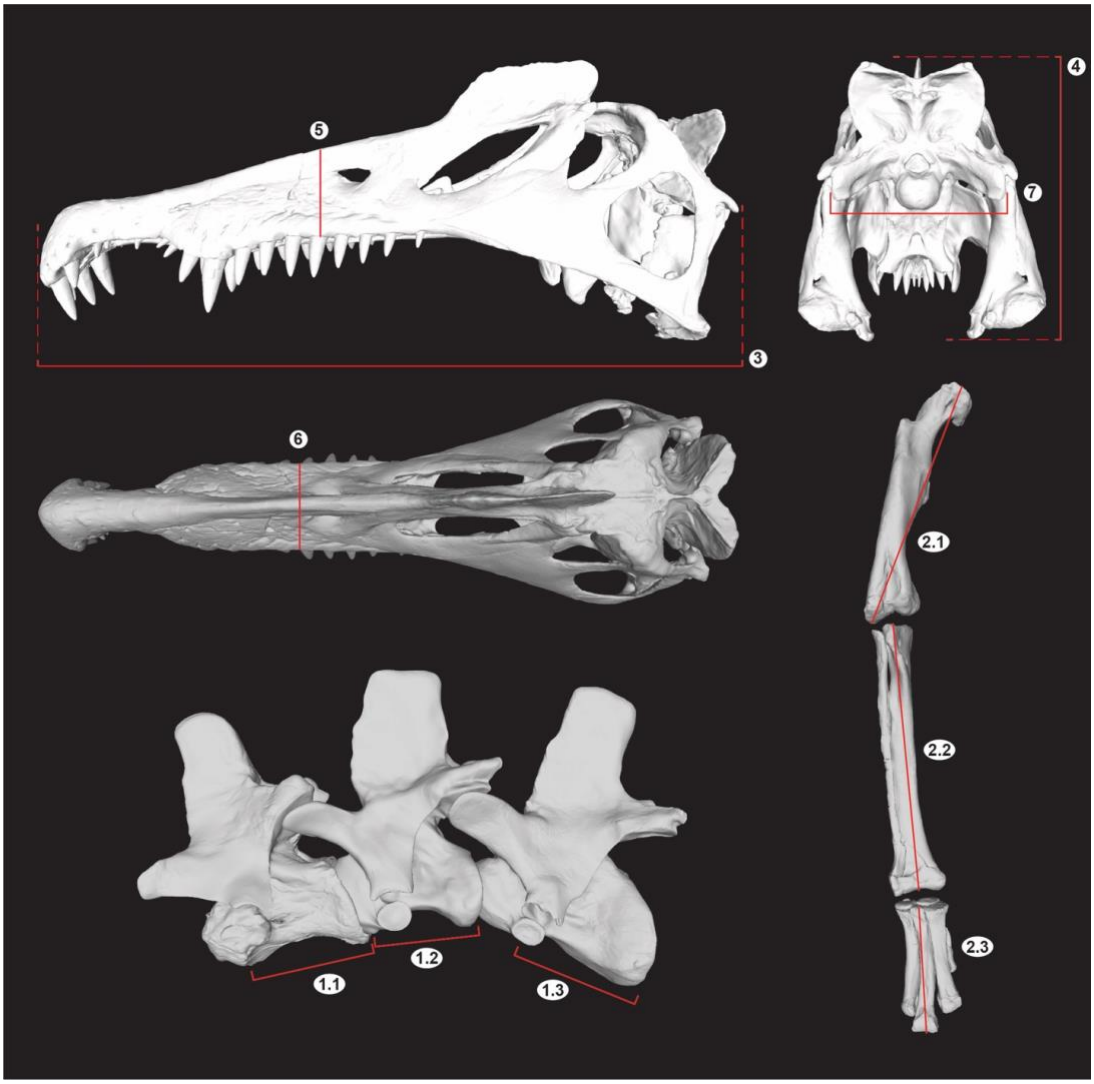

Fig. S17. Measurements for principal components analysis. Seven measurements form the skull, neck and hind limb as exemplified in a reconstruction of skull and skeletal parts in *Spinosaurus aegyptiacus*. 1-*Neck length*, sum of centrum length of the axis through the most

posterior cervical vertebra measured at mid height from anterior to posterior rim; 2-*Hind limb length*, sum of maximum length of the femur, tibia plus proximal tarsals (or tibiotarsus) and metatarsal 3. 3-*Cranium length*, anterior end of the snout to the posterior end of the quadrate condyle; 4-*Cranium height*, top of the nuchal crest to the bottom of the transverse midpoint of the quadrate condyle; 5-*Mid-snout height*, vertical height measured at the midpoint of the snout (halfway between snout tip and most anteriormost orbital margin) from the top of the snout (excluding crests) to the alveolar margin; 6-*Mid-snout width*, maximum width of the snout at its midpoint; 7-*Occiput width*, maximum width measured across the paroccipital processes.

Table S6. Principal component analysis measurements. Seven measurements (cm) in 2 spinosaurids (1, 2 in red), 18 other nonavian dinosaurs (3–20 in purple), 2 terrestrial birds of prey/scavengers (21, 22 in red), 4 aerial birds of prey (23–26 in red), 5 long-necked semiaquatic birds (27–31 in light blue), 7 diving birds (32–38 in dark blue) and 5 crocodylians (39–43 in green). Taxon text color matches predatory mode minimum convex hulls in Fig. 4. Museum abbreviations: AMNH, American Museum of Natural History, New York City, USA; FMNH, Field Museum of Natural History, Chicago, USA; FSAC, Aïn Chock Faculty of Sciences in Casablanca, Casablanca, Morocco; GM, Ganzhou Museum, Ganzhou City, China; IVPP, Institute of Vertebrate Paleontology and Paleoanthropology, Beijing, China; KMV, Kunming City Museum, Kunming, China; LDM, Lufeng Dinosaur Museum, Lufeng County, China; MACN, Argentine Museum of Natural Sciences Bernardino Rivadavia, Buenos Aires, Argentina; MAGNT, Museum and Art Gallery of the Northern Territory, Darwin, Australia; MCCM, Museum of Sciences of Castilla-La Mancha, Plaza de la Merced, Spain; MCZ, Museum of Comparative Zoology, Cambridge, USA; MMCH, Ernesto Bachmann Paleontological Museum, El Chocón, Argentina; MNBH, Boubou Hama National Museum, Niamey, Niger; MNHN, The French National Museum of Natural History, Paris, France; MPC, Institute of Paleontology and Geology of the Mongolian Academy of Sciences, Ulaanbaatar, Mongolia; MSNM, Milan Natural History Museum, Milan, Italy; NHMUK, Natural History Museum London, London, UK; PVSJ, Museum of Natural Sciences and the National University of San Juan, San Juan, Argentina; UA, University of Antananarivo, Antananarivo, Madagascar; TCMI, The Children's Museum of Indianapolis, Indianapolis, USA; UF, Florida Museum of Natural History, Gainesville, USA; UMZC, Cambridge University Museum of Zoology, Cambridge, UK; USNM, United States National Museum of Natural History, Washington D.C., USA; YPM, Yale Peabody Museum of Natural History, New Haven, USA; ZCDM, Zhucheng Dinosaur Museum, Shandong, China.

No.	Species	Clade Specimen(s)	Neck	Hind limb	Cranium				
			1-Neck length	2-Hind limb length	3-Cranium length	4-Cranium height	5-Mid-snout height	6-Mid-snout width	7-Occiput width
1	*Spinosaurus aegyptiacus*	Spinosauridae FSAC-KK 1888 scaled up to MSNM v4047	211.70	229.60	167.80	53.64	23.96	22.15	31.49
2	*Suchomimus tenerensis*	Spinosauridae MNBH GAD70, GAD500	135.00	199.20	101.10	28.26	15.35	8.40	25.59
3	*Tyrannosaurus rex*	Tyrannosauridae FMNH PR2081	91.00	303.00	144.00	65.95	41.00	37.00	63.89
4	*Gorgosaurus libratus*	Tyrannosauridae TCMI 2001.89.1	86.00	263.20	102.00	51.00	28.00	30.00	52.00

5	*Qianzhousaurus sinensis*	Tyrannosauroidea GM F10004	61.00	192.00	85.50	23.62	15.00	14.74	21.36
6	*Yutyrannus huali*	Tyrannosauroidea ZCDM V5000	71.17	197.30	90.90	40.10	26.98	22.60	30.17
7	*Ceratosaurus nasicornis*	Ceratosauria USNM 5278	57.00	140.00	67.00	25.00	20.00	19.00	18.00
8	*Carnotaurus sastrei*	Abelisauridae MACN-Pv Ch 894	105.00	219.00	69.00	40.00	27.00	16.00	24.00
9	*Majungasaurus crenatissimus*	Abelisauridae FMNH PR 2100, UA 8678	94.23	149.10	60.00	31.90	20.34	24.53	27.76
10	*Skorpiovenator bustingorryi*	Abelisauridae MMCH-PV 48K	98.00	215.00	67.00	33.00	26.18	21.45	27.00
11	*Allosaurus fragilis*	Allosauroidae USNM 4734	74.00	167.00	70.88	30.28	21.38	19.08	23.75
12	*Concavenator corcovatus*	Carcharodontosauridae MCCM-LH 6666	57.00	126.90	61.00	23.18	16.92	13.65	21.85
13	*Meraxes gigas*	Carcharodontosauridae MMCH-PV 65	139.00	267.00	140.20	50.70	44.00	26.00	45.00
14	*Sinraptor dongi*	Metricanthosauridae IVPP 10600	77.00	187.80	83.50	34.05	25.00	19.73	29.38
15	*Velociraptor mongoliensis*	Dromaeosauridae MPC-D 100/25	26.97	54.81	21.60	6.53	3.91	2.17	7.03
16	*Deinonychus antirrhopus*	Dromaeosauridae YPM 5232, AMNH 5210	33.63	92.80	40.20	11.57	9.00	3.91	10.85
17	*Sinosaurus triassicus*	Tetanurae LDM-L10, KMV 8701	65.42	129.80	52.90	19.40	12.39	20.00	14.77
18	*Coelophysis bauri*	Coelophysidae AMNH 7224	20.71	22.93	9.40	2.83	1.62	1.39	2.22
19	*Eodromaeus murphi*	Theropoda PVSJ 562	25.84	39.22	14.40	4.96	3.80	2.90	4.95
20	*Herrerasaurus ischigualastensis*	Herrerasauridae PVSJ 407	46.54	70.25	28.02	8.45	6.61	4.18	8.02
21	*Vultur gryphus*	Accipitriformes FMNH 104696	18.95	46.83	13.30	3.52	1.78	2.40	4.08
22	*Sagittarius serpentarius*	Accipitriformes FMNH 85779	15.26	62.42	8.90	3.64	1.77	1.39	2.95
23	*Pandion haliaetus*	Accipitriformes FMNH 375972	7.60	23.51	5.90	2.90	1.16	1.20	3.21
24	*Accipiter nisus*	Accipitriformes NHMUK S1982.149.1	3.65	18.72	3.50	1.98	0.65	0.58	1.46
25	*Aquila chrysaetos*	Accipitriformes MNHN 1930-152	10.20	28.55	8.10	4.27	2.05	1.50	2.97
26	*Haliaeetus leucocephalus*	Accipitriformes MNHN A-4056	9.27	32.13	9.60	3.00	2.38	2.17	3.26
27	*Ciconia ciconia*	Ciconiiformes NHMUK ZOO S/2007.107.1	22.49	58.28	21.60	3.76	1.37	1.26	2.11
28	*Ardea herodias*	Ciconiiformes FMNH 464301	40.96	57.53	20.32	2.54	1.27	1.02	2.54
29	*Plegadis falcinellus*	Pelicaniformes UMZC 327AA	9.96	24.44	10.84	1.97	0.45	0.42	1.52
30	*Leptoptilos crumeniferus*	Ciconiiformes FMNH 339240	37.59	69.22	33.02	4.06	2.54	1.91	4.57
31	*Balaeniceps rex*	Pelicaniformes FMNH 104644	33.11	70.85	26.30	6.20	5.68	7.96	4.48
32	*Pelecanus occidentalis*	Pelicaniformes NHMUK ZOO S/1973.66.16	45.33	27.25	40.50	5.96	1.36	1.96	2.92
33	*Aptenodytes forsteri*	Sphenisciformes FMNH 105018	33.15	37.719	17.145	5.08	1.27	1.905	5.08
34	*Eudyptes crestatus*	Sphenisciformes FMNH 432601	15.24	20.32	8.26	3.81	0.64	1.27	3.175
35	*Spheniscus demersus*	Sphenisciformes FMNH 104434	16.00	20.57	10.16	3.43	0.89	1.27	3.81
36	*Sula bassana*	Suliformes FMNH 506415	26.29	21.59	17.15	3.81	1.52	1.52	4.45

37	*Phalarocorax auritus*	Suliformes FMNH 441561	27.43	23.50	12.7	3.18	1.02	0.64	2.79
38	*Anhinga anhinga*	Suliformes FMNH 491374	26.54	16.51	10.80	1.90	0.64	0.64	1.52
39	*Alligator mississippiensis*	Alligatoridae AMNH R-40582	19.51	43.49	38.50	7.26	3.62	14.72	12.79
40	*Crocodylus porosus*	Crocodylidae MAGNT reptile R38573	45.62	71.92	69.40	15.36	11.20	27.80	24.48
41	*Gavialis gangeticus*	Gavialidae UF 119998	24.27	35.28	52.90	7.02	2.33	3.20	13.96
42	*Tomistoma schlegelii*	Gavialidae MCZ R-12459	27.35	46.68	58.30	7.51	2.10	4.96	15.17
43	*Crocodylus niloticus*	Crocodylidae USNM 64011	13.86	21.35	31.20	6.90	4.43	7.44	11.81

5.2 PC1 versus PC2 plot

Capturing the wide range of body size in the dataset, PC1 captures most of the variation (90.79%; Fig. S18). All seven morphometric variables have a negative loading of -0.357 to -0.391 (Table S7). PC2 (=4.32% total variance) and PC3 (=2.51% total variance) captures the range in cranium, neck and hind limb proportions. With increasing PC2 scores, neck and hind limb length increase, whereas mid-snout width and occiput width decrease. Thus, PC2 is useful for distinguishing semiaquatic crocodylians with wide heads and short necks and hind legs from semiaquatic wading birds, with narrow heads and long necks and hind legs. For PC3 cranial and neck length weight positively, whereas snout height and hind limb length weight negatively. Thus, PC3 is useful for distinguishing tall-snouted, long-legged aerial and terrestrial predators from long/low-snouted, shorter-legged semiaquatic predators.

Spinosaurids (*Suchomimus, Spinosaurus*) plot among long and *narrow-snouted, long-necked, long legged semiaquatic wading piscivores* well separated from other (terrestrial) nonavian dinosaurs (Fig. 4). The morphometric analysis supports the interpretation of spinosaurids as engaging a prey capture mode quite distinct among nonavian dinosaurs and like that in extant herons that typically wade in shallow water to ambush prey striking from above, rather than using subaqueous ambush predation as in crocodylians. Gross indices of skull shape alone are insufficient to distinguish crocodylian and avian semiaquatic modes.

The well separated minimal polygons suggest that these seven variables of skull shape and neck and hind limb length also distinguish other recognized modes of predation including a generalized terrestrial mode for other nonavian dinosaurs and a few extant avians, divers, and aerial predators (Fig. 4).

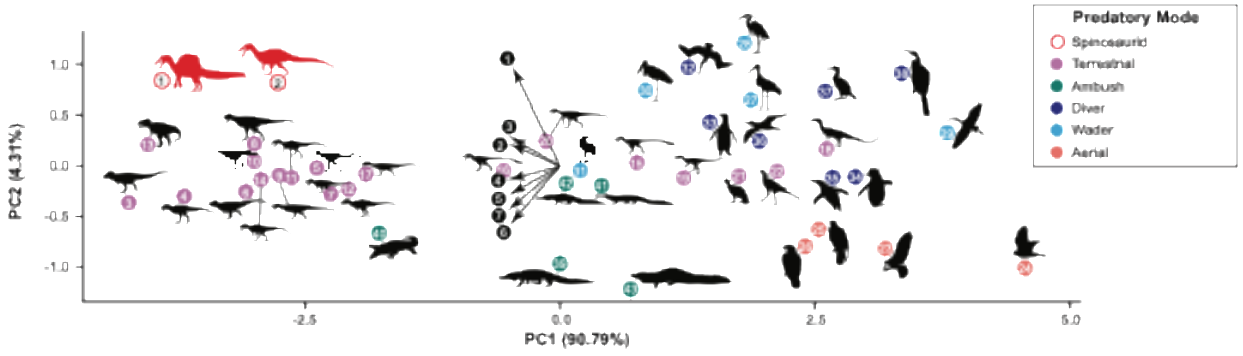

Fig. S18. Plot of PC1 vs. PC2. PC1 captures body size, whereas PC2 captures g cranium, neck, and hind limb length variation in extant and extinct archosaurs categorized by prey capture mode. Vectors show the variable loadings. Taxa are identified by number and color in Table S6.

Table S7. PCA loadings. The loadings of each morphometric variable on the first three principal component axes. The proportion of variance in the data that each principal component explains is show in parentheses.

No.	Variable	PC1 (90.79%)	PC2 (4.32%)	PC3 (2.51%)
1	Neck length	-0.3570036	0.75136081	0.09504645
2	Hind limb length	-0.3745348	0.16397055	-0.6732050
3	Cranium length	-0.3775639	0.22517203	0.54568904
4	Cranium height	-0.3907991	-0.1028003	-0.0775349
5	Mid-snout height	-0.3855824	-0.2163933	-0.3397133
6	Mid-snout width	-0.3775778	-0.4391665	0.1424145
7	Occiput width	-0.3817786	-0.328035	0.31350592

The close position of the darter (*Anhinga*) to spinosaurids indicates that, at smaller body size at least, surface diving is not incompatible with head and body proportions similar to those of waders. However, wading and any mode of diving (surface, plunge) do not mix among extant avians; there are no birds that hunt for prey while wading that also dive in pursuit of prey.

Darters (anhingas) often float with their head above water (hence their alternative nickname "snakehead") when hunting for prey, followed by short and often shallow dives in pursuit of prey (*69, 70*). To enhance diving, their skeletons are apneumatic to reduce buoyancy. As they frequently perch on branches near water to scout for prey and dry their wings, their foot is the least modified among divers in terms of its symmetry and size. Unlike its close relative the cormorant and other nonvolant divers like penguins that have elongated the pedal phalanges as scaffold to a substantial asymmetrical paddle (with the outside digit IV longer than III), anhingas have a smaller symmetrical foot paddle with the third the longest. Their quick stabbing pursuit of prey on short, shallow dives is possible with a smaller foot paddle in a bird that maintains both the ability to fly and perch on branches of small diameter. Interdigital webbing is always present in divers and often present in waders and other waterbirds that paddle or plunge-fed at the surface (e.g., Anatidae).

We grouped the brown pelican (*Pelecanus occidentalis*) among divers as it secures prey by plunge diving at high speed followed by underwater pursuit. Despite similar morphology and proportions, the white pelican (*Pelecanus erythrorhynchos*) does not dive and instead preys in social groups on fish near the surface. We grouped the Andean condor (*Vultur gryphus*) with terrestrial predators that ground feed on carrion rather than aerial predators that attack live prey from the air and transport carrion for roost feeding.

6. Phylogenetic definitions and analysis

6.1 Phylogenetic definitions

Stromer (*1*) erected Spinosauridae as a monotypic (redundant) taxon for *Spinosaurus aegyptiacus*, which by the Principle of Coordination of the International Code of Zoological Nomenclature (*90*) confers nominal authorship to all family-group names (Table S8; Spinosauroidea, Spinosaurinae, Spinosaurini). Similarly, Charig and Milner (*23*) erected Baryonychidae as a monotypic (redundant) taxon for *Baryonyx walkeri*, and thus they are the nominal authors of other family-

group derivatives (e.g., Baryonychinae). Sereno (*91*, *92*) used Spinosauroidea, Torvosauridae and Spinosauridae as a node-stem triplet (*93*, *94*) to anchor the taxonomy of a clade of increasing diversity within a larger array of basal tetanuran theropods. Baryonychinae and Spinosaurinae were defined as stem-based taxa (*19*), highlighting a basal split among spinosaurids that has been repeatedly determined in more recent phylogenetic studies including the present analysis.

Holtz et al. (*95*, p. 95) adopted all the definitional types specified above except for Spinosauroidea, offering a stem-based definition "*Spinosaurus aegyptiacus* and all taxa sharing a more recent common ancestor with it than with *Passer domesticus*". This definitional type identifies the same clade as the original node-based definition on their reference phylogenetic tree (*95*, Fig. 4.20). Nonetheless, given the lack of consensus over the phylogenetic relationships of basal tetanurans, we feel the original node-based definition for Spinosauroidea (*91*) better limits the possible future content of the taxon (Table S8).

Table S8. Phylogenetic definitions for Spinosauroidea and ingroups. Phylogenetic definitions and authorship for suprageneric taxa used in this study.

Taxon	Nominal Author	Definitional type	Revised Definition	Definitional author
Spinosauroidea	Stromer, 1915	node	Least inclusive clade that contains *Spinosaurus aegyptiacus* and *Torvosaurus tanneri*	(*91*)
Spinosauridae	Stromer, 1915	stem	Most inclusive clade that contains *Spinosaurus aegyptiacus* but not *Torvosaurus tanneri*	(*91*)
Baryonychinae	Charig and Milner, 1986	stem	Most inclusive clade that contains *Bayronyx walkeri* but not *Spinosaurus aegyptiacus*	(*19*)
Spinosaurinae	Stromer, 1915	stem	Most inclusive clade that contains *Spinosaurus aegyptiacus* but not *Bayronyx walkeri*	(*19*)
Spinosaurini	Stromer, 1915	stem	Most inclusive clade that contains *Spinosaurus aegyptiacus* but not *Irritator challengeri*	this paper

6.2 Phylogenetic analysis

We used (TNT v. 1.6) to analyze a data matrix of 159 morphological characters divided roughly evenly between cranial and postcranial features and scored in 22 terminal species or specimens (6 outgroup, 16 ingroup; Table S9). Many of the taxa or unnamed specimens scored in the matrix are poorly known (Table S10). All analyses were done using a traditional search of 1000 Wagner trees with 10 tree bisection reconnection (TBR) replicates per tree with equally weighted characters. Maximum parsimony yielded 42 minimum length trees (222 steps; CI = 0.762; RI = 0.845), when including all ingroup taxa/specimens (Fig. S19).

Table S9. Taxa and morphological characters. Phylogenetic analysis using maximum parsimony was applied to 159 character statements across these taxa. *, pruned unstable taxon/specimen from final phylogenetic tree (Fig. 5B).

Outgroup taxa	Ingroup taxa	Character sum, %			
		Cranial	Dental	Axial	Appendicular
Ceratosaurus nasicornis *Allosaurus fragilis* *Debreuillosaurus valesdunensis* *Afrovenator abakensis* *Torvosaurus tanneri* *Eustreptospondylus oxoniensis*	*Riojavenatrix lacustris* *Camarillosaurus cerugidae* *Phu Wiang spinosaurid B *Ceratosuchops inferodios* **Iberospinus naratioi* **Prothatlitus cinctorrensis* *Suchomimus tenerensis* *Baryonyx walkeri* *Ichthyovenator laoensis* *Vallibonavenatrix cani* *Irritator challengeri* *SM-KK-14 Brazil spinosaurine (UFMA ITA1) *Oxalaia quilombensis* *Spinosaurus aegyptiacus* *Spinosaurus mirabilis* sp. nov.	62 39%	16 10%	44 28%	37 23%

Table S10. Terminal taxa/specimens. List of terminal entities scored and sources for scoring. BSPG, Bayerischen Staatssammlung für Paläontologie und Geologie, Munich, Germany; BYU, Bringham Young Museum of Paleontology, Provo, USA; FSAC, Faculté des sciences Aïn Chock Casablanca, Casablanca, Morocco; MNBH, Musée National Boubou Hama, Niamey, Niger; SM, ML, Museu Lourinhã, Lourinhã, Portugal; MN, Museu Nacional do Brasil, Rio de Janiero, Brazil; MPG, Museo Paleontológico de Galve, Galve, Spain; MSNM, Museo di Storia Naturale di Milano, Milano, Italy; NHMUK, Natural History Museum, London, UK; SM, Sirindhorn Museum; SMNS, Staatliches Museum für Naturkunde Stuttgart, Stuttgart, Germany; UFMA, Universidade Federal do Maranhão, São Luis, Brazil.

No.	Taxon/specimen	Source	% scored
1	*Ceratosaurus nasicornis*	Madsen et al., 2000	87.4
2	*Allosaurus fragilis*	Gilmore, 1920; Madsen, 1976	88.7
3	*Eustreptospondylus oxoniensis*	Bakker et al., 1992, Carrano & Benson, 2012	68.5
4	*Torvosaurus tanneri*	BYU 2002, Dry Mesa referred specimens, Britt, 1991	74.8
5	*Dubreuillosaurus valesdunensis*	Allain & Taquet ,2002, 2005	38.3
6	*Afrovenator abakensis*	MNBH TIG1, Sereno et al., 1994	57.2
7	Phu Wiang Spinosaurid B	Samathi et al., 2021	8.2
8	SM-KK-14	SM-KK-14, Samathi et al., 2019	18.2
9	*Riojavenatrix valesdunensis*	Isasmendi et al., 2024	10.0
10	*Iberospinus naratioi*	ML1190; Mateus & Estraviz-Lopez, 2022	18.2
11	*Prothatlitus cinctorrensis*	Right maxilla (8ANA-109), 5 caudals (3ANA83, 4ANA43, 4ANA69, 4ANA76, 5ANA78); Santos-Cubedo et al., 2023	20.7
12	*Baryonyx walkeri*	NHMUK VP R9951; Charig & Milner, 1997	76.1
13	*Suchomimus tenerensis*	MNBH GAD500, GAD501, GAD70, GAD71, Sereno et al., 1998	92.5
14	*Ceratosuchops inferodios*	Barker et al., 2021	37.7
15	*Ichthyovenator laoensis*	Allain et al., 2012	29.5
16	*Camarillasaurus cerugidae*	MPG-KPC1-46; Sanchez-Hernandez & Benton, 2014; Malafaia et al., 2020	12.6
17	*Vallibonavenatrix cani*	Malafaia et al., 2019; 2020	21.4
18	*Irritator challengeri*	SMNS 58022 (Sues et al., 2002), SMNS 58023 (partial sacrum), MN4819-V (D13, sacrum and C1, pelvis, partial manus), LPP-PV-0042 (partial tibia)	53.5
19	*Oxalaia quilombensis*	MN 6117-V cast (University of Chicago); Kellner et al., 2011	5.6
20	Brazil spinosaurine	UFMA ITA1 unpublished	27.7
21	*Spinosaurus aegyptiacus*	BSPG 1912 VIII; Stromer, 1915 FSAC-KK 11888; Ibrahim et al., 2014, 2020 FSAC-KK11889 MSNM V4047; Dal Sasso et al., 2005	84.3
22	*Spinosaurus mirabilis* sp. nov.	MNBH JEN1–JEN9	45.3

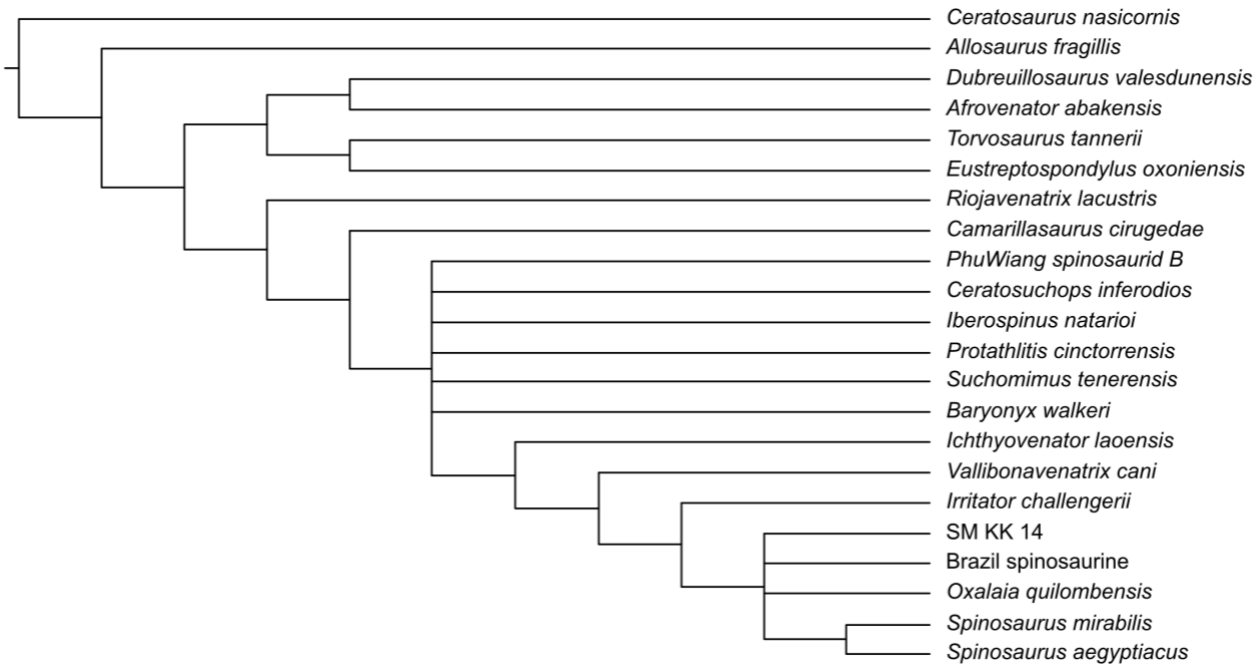

Fig. S19. Parsimony analysis with all scored taxa and specimens included. Strict consensus tree of all included species/specimens summarizing 42 minimum-length trees. Tree determined with TNT and rendered with FigTree.

The initial traditional parsimony analysis was followed by a "New Technology Search" in TNT using sectorial searches, drift, and tree fusing, with their consensus stabilized five times. The resulting trees were then rearranged with tree bisection–reconnection. This was performed using equally-weighted characters as the 'Traditional Search' and using extended implied weighting (*96*) with concavity values "k" of 3, 6 and 9 to test different homoplasy weights. Using equally weighted characters we found 42 most parsimonious trees as well (222 steps; CI = 0.779; RI = 0.860) with a strict consensus tree of identical topology (Fig. S19). Using "extended implied weights" we also found 42 most parsimonious trees with k=3 (11.28 score; CI = 0.779; RI = 0.860), k=6 (6.62 score; CI = 0.779; RI = 0.860) and k=9 (4.69 score; CI = 0.779; RI = 0.860) with a strict consensus tree of identical topology (Fig. S19).

Four poorly known taxa/specimens result in the loss of resolution of a baryonychine clade at the base of the spinosaurid tree. These include two recently described taxa from the Iberian Peninsula, *Protathlitis cinctorrensis* (*57*) and *Iberospinus natarioi* (*54*), and two unnamed specimens from Thailand, the Phu Wiang spinosaurid B (*97*) based on associated vertebrae and the Khok Kruat spinosaurid SM-KK-14 (*97*) based on a partial but as yet undescribed skeleton. Three of these are identified as wildcard taxa by the iterPCR (iterative Positional Congruence Reduced) subroutine in TNT [(*98*, *99*); Fig. S20].

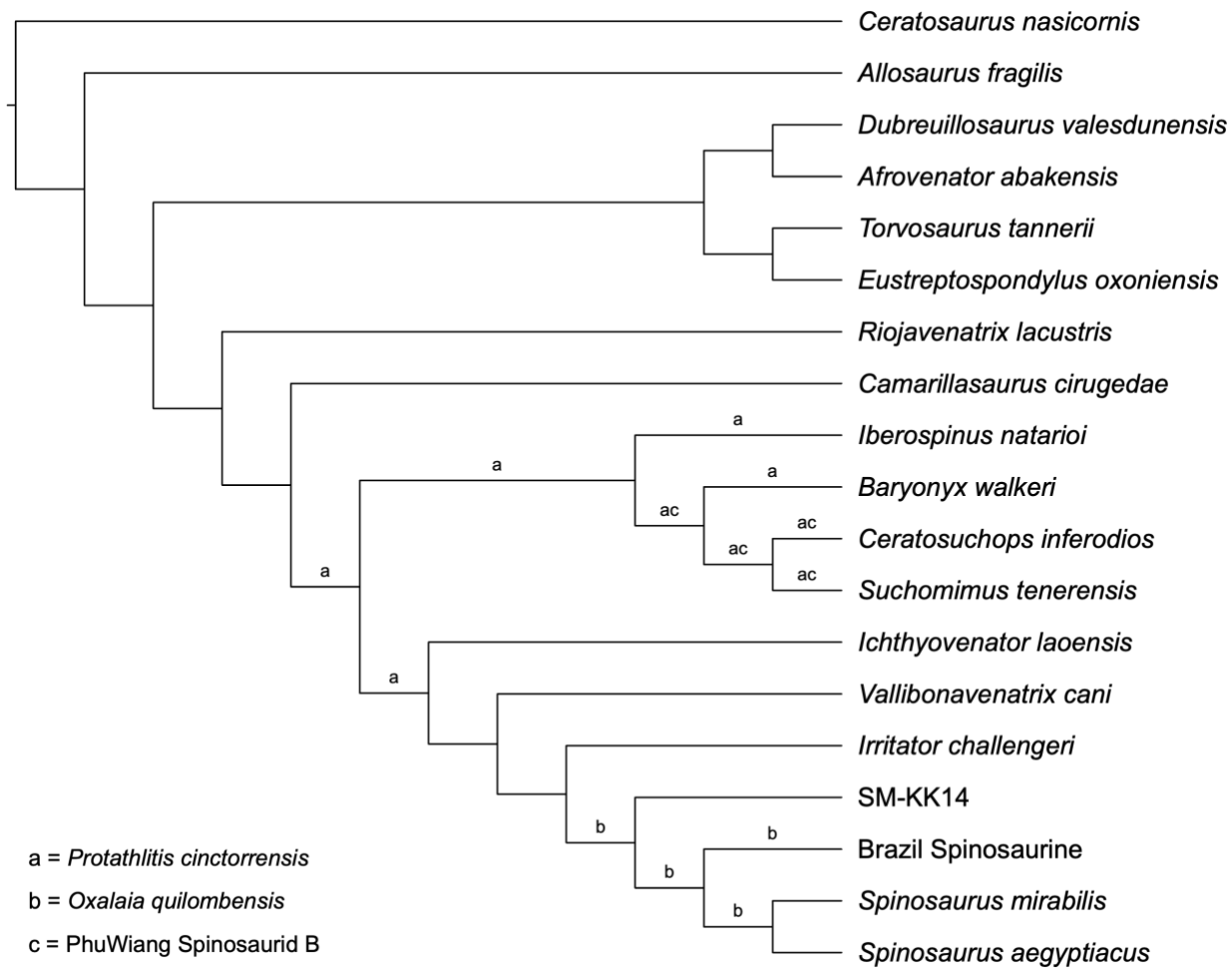

Fig. S20. Phylogenetic tree with *a posteriori* pruning of poorly known taxa/specimens. Strict consensus showing the variable positions of three unstable ingroup taxa/specimens in 42 minimum-length trees. Tree determined with TNT and rendered with FigTree.

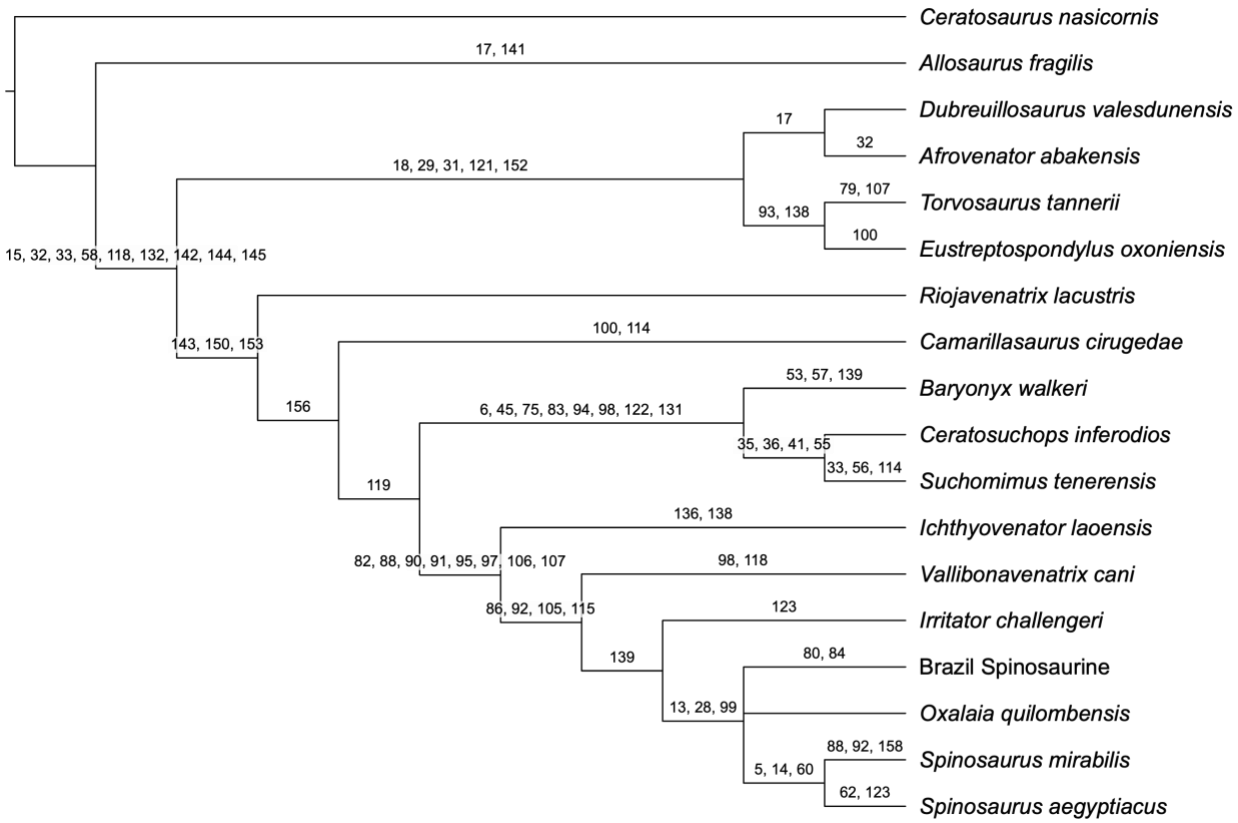

Fig. S21. Analysis with pruned ingroup showing synapomorphies. Unambiguous synapomorphies are plotted on a single minimum-length tree after pruning of four poorly known species/specimens. Tree determined with TNT and rendered with FigTree.

Iberospinus natarioi (*54*) is the fourth poorly constrained taxon resulting in considerable loss of character resolution. Pruning this taxon increases unambiguous character support for spinosaurines from one to the eight synapomorphies shown and listed below (Fig. S21; Synapomorphy list).

Finally, a tip-dated Bayesian analysis was performed to include both morphological and temporal data and to account for phylogenetic uncertainty (*100*). All characters were regarded as independent and unordered. The MkV likelihood model of evolution was assumed to account for ascertainment bias. Asymmetric rates of state changes with gamma distribution governing rate variation were also implemented into the model. A birth-death-skyline serial sampling was assumed with a relax-clock with lognormal distribution of sampled rates. The stratigraphic range of each terminal taxon was sampled from an assumed uniform distribution. The XML files were constructed using BEAUti2 to run in BEAST v2.7.7. The MCMC ran for a total of 20 million generations, a sufficient duration for the sampling process which reached convergence relatively early, with sampling occurring every 1,000 generations. The first 20% of sampled trees were discarded to eliminate the initial burn-in phase of the analysis prior to reaching convergence in TreeAnotator v2.7.7.

The resulting tree (Fig. S22) has a very similar topology to the pruned consensus tree (Fig. S20), the only major differences being the position of *Riojavenatrix* as a Baryonychine spinosaurid instead of the outgroup to Baryonychinae+Spinosaurinae and SM-KK-14 as sister taxon to

Vallibonavenatrix outside Spinosaurini. The wildcard taxa "Phu Wiang spinosaurid B" is positioned as a sister to *Ceratosuchops*; *Protathlitis* is positioned as the sister taxon of *Iberospinus*; and *Oxalaia* is basal to other Spinosaurini. Regardless of the type of phylogenetic analysis or the weighting of characters in parsimony analysis, we always find *Spinosaurus mirabilis* and *Spinosaurus aegyptiacus* as sister taxa.

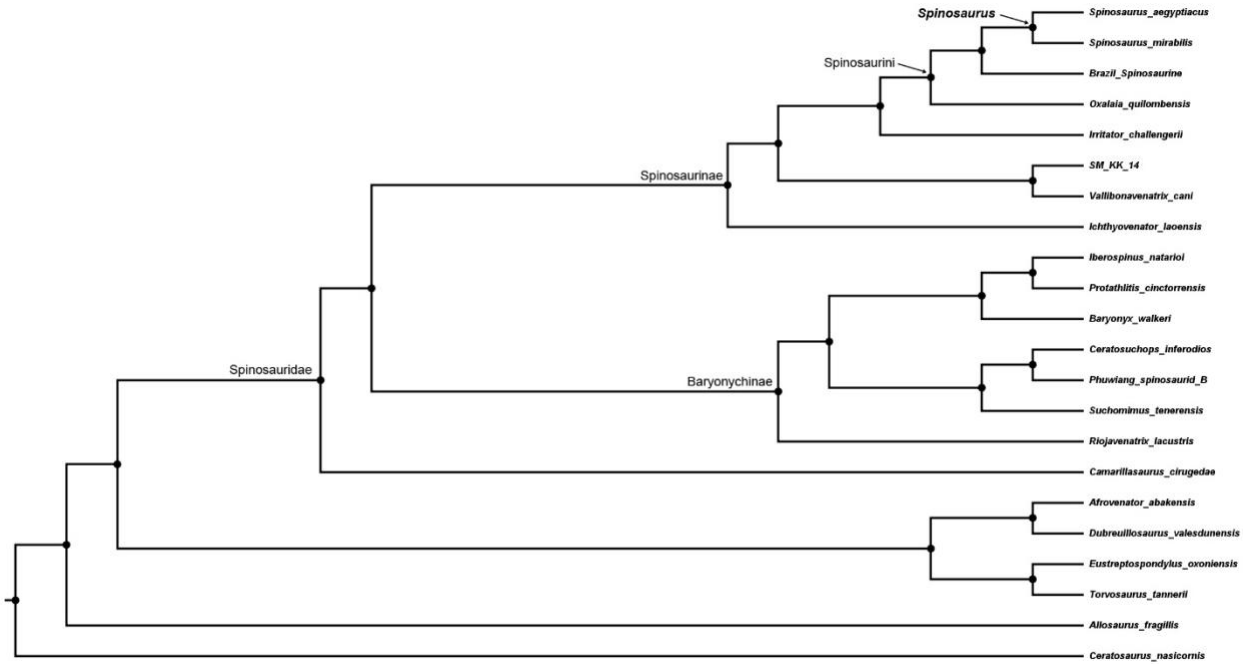

Fig. S22. Bayesian analysis with all scored taxa and specimens included. Maximum clade credibility tree for variable-rates tip-dated Bayesian phylogenetic analysis.

Data S1. Character and synapomorphies lists

Character list

159 character statements are listed below with several modified from cited sources (shaded beige) and 41 others that are new to spinosaurid phylogenetic analysis (shaded green).

Cranial

1. Snout (preorbital region of skull), length relative to antorbital fenestra length: less (0) or more (1) than three times. (Sereno et al., 1998, char. 7)
2. Snout (premaxillae, maxillae and nasals), dorsal surface morphology: low and round (0), acute sagittal crest (1). (after Sales and Schultz 2017).
3. Snout (premaxillae and nasals), dorsal surface ornamentation: rugose (0); smooth (1).
4. Jaws (premaxillae and dentary), anterior end, form: convergent (0); expanded into a premaxillary/ dentary rosette (1). (Sereno et al., 1998, char. 6)
5. Upper jaws (premaxillae and maxillae), festooning along the alveolar margin: absent (0); present (1).
6. Premaxilla, form of premaxilla-nasal suture: V-shaped (0); W-shaped (1). (Carrano et al., 2012, char. 5)
7. Premaxilla, external nares, proportions and position: shorter than premaxilla ventral to nares, angle between anterior and alveolar margins >75° (0); longer than body ventral to nares (1). (Carrano et al., 2012, char. 6)
8. Premaxillae, inter-premaxillary suture at maturity, form: open (0); fused (1). (Sereno et al., 1998, char. 10)
9. Premaxilla-maxilla articulation, form: scarf or butt joint (0); interlocking (1). (Sereno et al., 1998, char. 11)
10. Premaxilla-maxilla suture, lateral surface, subnarial foramen, shape: foramen (0); dorsoventrally directed channel (1). (Carrano et al., 2012, char. 10)
11. Premaxilla, ventral margin, shape in lateral view: straight to convex (0); concave (1). (Cau, 2018, char. 1485)
12. Premaxilla, lateral and dorsal surface, extensive pitting of neurovascular foramina: absent (0); present (1). (Barker et al., 2021, char. 1796)
13. Premaxilla, notch for dentary tooth 1 at the height of premaxillary alveoli 2: absent (0); present (1).
14. Premaxillae, shape of rosette anterior expansion: continuous, oval-shaped (0); abrupt with a constriction by the third premaxillary alveolus, mushroom-shaped (1) (after Sales and Schultz 2017).
15. Maxilla, anterior ramus, length relative to maximum depth: 70% (0); 100% or more (1). (Sereno et al., 1998, char. 1)
16. Maxilla, antorbital fossa, width of ventral margin relative to depth of posterior ramus of maxilla: more (0) or less (1) than 30%. (Sereno et al., 1998, char. 40)
17. Maxilla, antorbital fossa, anterior margin: rounded (0); squared (1). (Carrano et al., 2012, char. 23)
18. Maxilla, subcircular depression in the anterior corner of the antorbital fossa: absent (0); present (1). (Sereno et al., 1998, char. 41)
19. Maxilla, anteromedial process, shape: fluted prong (0); plate (1). (Sereno et al., 1998, char. 12)
20. Maxilla, anteromedial process, anterior extension: as far as (0); far anterior to (1) the anterior margin of the maxilla; or reaching the premaxillary symphysis (2). (modified from Sereno et al., 1998, char. 13)
21. Maxillae, intermaxillary contact: absent (vomer connects both maxillae) (0); present (maxillae form a “secondary palate”) (1).
22. Maxillae, intermaxillary contact, extension: anterior to half of the tooth row (0); extensive, until or posterior to half the tooth row (1).
23. Maxilla, antorbital fossa, size relative to orbit: larger (0); smaller (1). (Sereno et al., 1998, char. 9)

24. Maxilla, anteroventral margin, curvature: not curved (0); dorsomedially curved (1). (modified from Cau, 2018, char. 731; Tykoski, 2005)
25. Nasal, posterior process, overlap of frontal in articulation: absent or limited (0); extensive, in particular medially, on almost or all the process dorsal surface (1). (modified from Cau, 2018, char. 1500)
26. Nasal sagittal crest (posterior dorsal projection above the lacrimal, frontal and prefrontal contact): absent (0); present (1).
27. Nasal crest, height relative to widest point: lower or subequal (0); greater (1).
28. External naris, position of anterior margin relative to maxillary tooth row: anterior past anteriormost maxillary tooth (0); anterior, but not reaching anteriormost maxillary tooth (1); posterior to halfpoint of maxillary tooth row (2).
29. Jugal, posterior ramus, depth relative to orbital ramus: less (0); more (1). (Sereno et al., 1998, char. 43)
30. Lacrimal, anterior and ventral rami, angle of divergence: 75° to 90° (0); 30° to 45° (1). (Sereno et al., 1998, char. 15)
31. Lacrimal foramen, position relative to ventral process: near the base (0); at mid-height (1). (Sereno et al., 1998, char. 42)
32. Lacrimal, anterior ramus, length relative to ventral ramus: more (0) or less (1) than 65%. (Sereno et al., 1998, char. 2)
33. Postorbital, ventral process, cross section of distal half: subcircular (0); U-shaped (1). (Sereno et al., 1998, char. 44)
34. Postorbital, supraorbital shelf (boss) formed mostly by palpebral: absent (0); present (1). (modified from Carrano et al., 2012, char. 61)
35. Frontal, postorbital facet, anterior depth: less than 2/5 facet length (0); more than 2/5 facet length (1). (Barker et al., 2021, Source data 2)
36. Frontal, shape of the lateral margin in dorsal view: describes a smooth transition between the anterior half and the postorb ital process (0); an abrupt transition between the anterior half and the postorbital process (1). (Senter et al., 2010, char. 44)
37. Frontal, interfrontal suture versus orbital margin depth: subequal (0), or twice or more (1) as deep.
38. Frontal, anterior process, tongue-shaped, very long, underlying nasal: absent (0); present (1).
39. Frontals, midline ridge (or fused crest): absent (0); present (1) (modified from Schade et al., 2023)
40. Frontal, attachment surface anterior to supratemporal fossa, shape: semicircle (0); narrow edge (1).
41. Prefrontal, boss-like process: absent (0); present (1). (Barker et al., 2021, Source data 2)
42. Prefrontal, mediolateral extension: small, within a great margin from the midline (0); large, almost reaching the midline at the posterior end of the nasal (1).
43. Prefrontal, ventral process length: short, barely surpassing its anteroposterior length (0); deep, several times longer than its anteroposterior length (1).
44. Parietal, length: less than 3/4 of the frontal (0); subequal or more than 3/4 of the frontal (1); Parietal much longer than the frontal (2). (modified from Cau, 2018, char. 78)
45. Quadrate, head, shape: oval (0); subquadrate (1). (Sereno et al., 1998, char. 27)
46. Quadrate, foramen, size: foramen (0); broad fenestra (1). (Sereno et al., 1998, char. 28)
47. Quadrate, medial foramina adjacent to condyles: absent (0); present (1). (Carrano et al., 2012, char. 84)
48. Quadrate, foramen margin, placement: at mid-height or dorsal (0); ventral, close to mandibular condyles (1). (modified from Loewen et al., 2013, char. 158)
49. Basisphenoid, width of the interbasipterygoidal web: thin; 40% of occipital condyle width or less (0); thick, more than 40% occipital condyle width (1). (modified from Barker et al., 2021, Source data 1)
50. Basisphenoid, basipterygoid process, exposure of the ventral surface in lateral view: broad (0); reduced (1). (Barker et al., 2021, Source data 2)

51. Basisphenoid, basipterygoid process, shape of lateral margin in ventral view: flat or slightly concave (0); convex (1). (Barker et al., 2021, Source data 2)
52. Basioccipital, position of subcondylar recess: dorsoventrally tall, recess reaches the occipital condyle neck (0); ventrally restricted, surface directly below condyle convex (1). (Barker et al., 2021, Source data 2)
53. Basioccipital, width of subcondylar recess relative to occipital condyle width: narrow, 0.5 times or less (0); wide, greater than 0.5 times (1). (modified from Barker et al., 2021, Source data 2)
54. Basioccipital, thick crests bordering subcondylar recess laterally: present (0); absent (1). (Barker et al., 2021, Source data 2)
55. Basioccipital, contribution to foramen magnum: large, exoccipitals widely separated (0); reduced, exoccipitals closely placed (1). (Barker et al., 2021, Source data 2)
56. Basioccipital, proportions relative to basisphenoid (measured along midline ventral to occipital condyle to interbasipterygoidal web), in posterior view: shorter (0); longer (1). (Barker et al., 2021, Source data 2)
57. Otoccipitals, angle of projection of paroccipital processes: posterolaterally (0); laterally or subhorizontal (1). (Barker et al., 2021, Source data 2)
58. Splenial foramen, size: small (0); large (1). (Sereno et al., 1998, char. 16)
59. Dentary, shape of anterior end in lateral view: blunt and unexpanded (0); dorsoventrally expanded, rounded and slightly upturned (1); squared off in lateral view via anteroventral process (2). (Carrano et al., 2012, char. 120)
60. Premaxilla and anterior dentary, interdental septa spacing: regular (0); alternate (alveoli result paired) (1). (modified from Cau, 2018, char. 1614)
61. Dentary, deflection of posterior ramus after symphyseal articulation: at dentary tooth 1 (0); at dentary tooth 3 to 4 (1); posterior to the mid length of the dentary (2).
62. Dentary, shape of the anterior edge in lateral view: posteriorly directed, with dentary tooth 1 being the anteriormost point (0); with a chin process protruding beyond dentary tooth 1 (1).

Dental

63. Teeth, distal, curvature: present, marked (0); reduced or non-curved (1). (Sereno et al., 1998, char. 35; modified after Hendrickx et al., 2019)
64. Teeth, maxillary and dentary, serrations: present (0); absent (1). (Sereno et al., 1998, char. 17)
65. Teeth, distal, midcrown cross-section: elliptical (0); circular (1). (Sereno et al., 1998, char. 36; modified after Hendrickx et al., 2019)
66. Teeth, distal, crown striations (flutes/apicobasal ridges): absent (0); present (1). (Sereno et al., 1998, char. 18; modified after Hendrickx et al., 2019)
67. Teeth, enamel ornamentation: absent (0); present (1). (modified from Carrano et al., 2012, char. 143)
68. Teeth, enamel ornamentation type: extending as bands across labial and lingual tooth surfaces (0); pronounced marginal enamel wrinkles (1); pronounced deeply veined/anastomous texture (2). (modified from Carrano et al., 2012, char. 143)
69. Teeth, basalmost root shape: broad (0); strongly tapered (1). (Sereno et al., 1998, char. 21)
70. Premaxilla, tooth count: 3 or 4 (0); 6 or 7 (1). (Sereno et al., 1998, char. 19)
71. Premaxillary tooth 1, size: slightly smaller (0) or much smaller (1) than crowns 2 and 3. (Sereno et al., 1998, char. 38)
72. Premaxilla, diastemata within the premaxillary rosette: narrow (0); broad (1). (Sereno et al., 1998, char. 39)
73. Maxillary teeth, mid-tooth spacing: adjacent (0); with intervening space/diastemata (1). (Sereno et al., 1998, char. 20)
74. Maxilla, tooth count: up to 15 (0) less than 15 (1) 20 or more (2).
75. Dentary, tooth count: up to 15 (0); ≥15 (1). (Sereno et al., 1998, char. 26)
76. Dentary teeth, spacing: adjacent (0); with intervening space (1). (Sereno et al., 1998, char. 37)
77. Dentary tooth 1, size: subequal or slightly smaller (0) or markedly smaller (1) than crowns 2 and 3.
78. Paradental laminae: present (0); absent (1). (Sereno et al., 1998, char. 14)

Axial

79. Cervical vertebrae, middle, shape of anterior pneumatic foramina: round (0); anteroposteriorly elongate (1). (Carrano et al., 2012, char. 169)
80. Cervical vertebrae, posteriormost, ventral keel: absent or developed as a weak ridge (0); pronounced, around 1/3 the height of centrum and inset from lateral surfaces (1). (Sereno et al., 2022)
81. Cervical vertebrae, prezygapophyseal facets, elongation related to width: as long as wide (0); longer than wide (1); wider than longer (2). (Sereno et al., 2022)
82. Cervical vertebrae, middle and posterior centra width relative to centra height: taller than wide or round (0); wider than tall (1). (Sereno et al., 2022)
83. Cervical vertebrae, anterior post-axial neural spines in lateral view: longer than tall (0); taller than long (1). (Cau, 2018, char. 212)
84. Dorsal vertebrae, anterior centra, depth of ventral keel relative to total centrum height: absent or less than ¼ (0); blade-shaped, more than ¼ (1). (Sereno et al., 1998, char. 22)
85. Dorsal vertebrae, anterior centra, ventral process projecting anterior to the keel (hypapophysis): poorly developed (0); strongly developed (1). (modified from Cau, 2018, char. 225; from Rauhut, 2003)
86. Dorsal vertebrae, middle, centra length relative to height: 1.4 < times centrum height (0); ≥1.4 times centrum height (1). (Sereno et al., 2022)
87. Dorsal vertebrae, anterior parapophyses, size: less (0) or more (1) than half-depth of anterior facet of centrum. (Cau, 2018, char. 1740)
88. Dorsal vertebrae, anterior centra, pneumatic foramen, size relative to parapophysis: larger or equal (0); smaller (1). (Sereno et al., 2022)
89. Dorsal vertebrae, anterior, prezygapophyseal facets, elongation related to width: as long as wide (0); longer than wide (1); wider than longer (2). (Sereno et al., 2022)
90. Dorsal vertebrae, mid-posterior, excavated prezygoparadiapophyseal fossa delimited by the paradiapophyseal lamina: absent (0); present (1). (Sereno et al., 2022) (after Malafaia et al., 2020)
91. Dorsal vertebrae, middle and posterior neural arches, notched spinoprezygapophyseal lamina in lateral view: absent (0); present (1).
92. Dorsal vertebrae, middle and posterior centra, pneumatic foramina: absent (0); present (1). (modified from Cau, 2018, char. 1350)
93. Dorsal vertebrae, height of neural spines relative to centrum height: low,<1.3× (0); moderate, 1.3–1.8× (1); tall, <1.8× (2). (modified from Carrano et al., 2012, char. 193)
94. Dorsal vertebrae, posterior neural spines, basal webbing: absent (0); present (1). (Sereno et al., 1998, char. 24)
95. Dorsal vertebrae, mid and posterior neural spines, ornamentation: smooth (0); strong longitudinal striations (1).
96. Dorsal vertebrae, middle and posterior, neural spine anteroposterior length at base relative to centrum length: subequal (0); shorter (1). (Sereno et al., 2022)
97. Dorsal vertebrae, middle-posterior parapophyses, development: distinct elevated process (0); reduced, knob-shaped (1). (Sereno et al., 2022)
98. Dorsal vertebrae, accessory centrodiapophyseal lamina: absent (0); present (1). (Sereno et al., 1998, char. 25)
99. Dorsal vertebrae, posterior centra, articular surface: platycoelous/amphicoelous (0); opisthocoelous (1).
100. Sacrum, centrum pneumaticity: absent (0); present (1). (modified from Carrano et al., 2012, char. 196)
101. Sacrum, centrum pneumaticity type: pleurocoelous fossae (0); pneumatic foramina (1). (modified from Carrano et al., 2012, char. 196)
102. Sacrum, neural spines: without distal anteroposterior expansion (0); with distal expansion contacting adjacent spines (1). (Sereno et al., 2022)

103. Caudal vertebrae, anterior, morphology of ventral surface: flat (0); groove (1); ridge (2). (Carrano et al., 2012, char. 202)
104. Caudal vertebrae, ventral groove on centra, width: narrow (0); wide (1).
105. Caudal vertebrae, anterior, well-marked spinodiapophyseal lamina: absent (0); present (1). (Sereno et al., 2022)
106. Caudal vertebrae, anterior neural arches, ventral rib laminae: absent (0); present (1). (Cau, 2018, char. 358)
107. Caudal vertebrae, anterior neural arches, anterolateral surface, deep triangular prezygocostal fossa delimited by two laminae: absent (0); present (1). (Cau, 2018, char. 1605; modified from Brusatte et al., 2010)
108. Caudal vertebrae, anterior neural arches, hyposphene: absent (0); present (1). (Cau, 2018, char. 359)
109. Caudal vertebrae, position of transition point (caudofemoralis and ilio-ischiocaudalis mm. correlates): at or beyond CA20 (0); around CA15-19 (1). (Sereno et al., 2022)
110. Caudal vertebrae, middle, height of neural spines relative to centrum height: low, ≥1.3× (0); moderate, 1.3–2.0× (1); tall, 2.0–4.0× (2); extreme elongation >4× (3). (Sereno et al., 2022)
111. Caudal vertebrae, distal, height of neural spines relative to centrum height: low, ≥1.3× (0); moderate, 1.3–2.0× (1); tall, 2.0–4.0× (2); extreme elongation >4× (3). (Sereno et al., 2022)
112. Caudal vertebrae, middle and posterior, neural spines length versus width (lateral view): longer than wide (0); subequal (1); wider than long (2).
113. Caudal vertebrae, middle and posterior neural spines, orientation: vertical (0); posteriorly directed (1).
114. Caudal vertebrae, middle and posterior neural spines, neural spine base not extending (0) or extending (1) up to prezygapophyses.
115. Caudal vertebrae, middle, centrum length relative to height: elongate (> 1.6) (0); not elongate (≤ 1.6) (1). (Sereno et al., 2022)
116. Caudal vertebrae, middle and posterior, centrum shape in anterior or posterior view: circular (0); subquadrate (1).
117. Caudal vertebrae, middle and posterior, prezygapophyses: elongated, projected beyond the anterior rim of the centrum (0); shortened, barely reaching the anterior rim of the centrum (1). (Sereno et al., 2022) (after observations in Samathi et al., 2021)
118. Chevrons, anterior and posterior longitudinal groove: absent (0); present (1). (Sereno et al., 2022)
119. Chevrons, anterior and posterior surfaces: without distinctive features (0); with longitudinal groove widened as a fossa (1). (Sereno et al., 2022)
120. Chevrons, posterior elongation compared with anterior and middle ones: shorter (0); as elongated (1). (Sereno et al., 2022)
121. Chevrons, anterior process: absent (0); present (1). (Carrano et al., 2012, char. 217)

Appendicular

122. Coracoid, posterior process, shape: low and rounded (0); crescentic (1). (Sereno et al., 1998, char. 29)
123. Appendicular bones, marrow cavity: present (0); reduced to barely present (1). (Sereno et al., 2022)
124. Humerus, deltopectoral crest, length relative to humeral length: less (0) or more (1) than 45%. (Sereno et al., 1998, char. 3)
125. Humerus, deltopectoral crest, orientation of apex: anterior (0), lateral (1). (Sereno et al., 1998, char. 31)
126. Humerus, trochanters, size: low and rounded (0); hypertrophied and pointy (1). (Sereno et al., 1998, char. 30)
127. Humerus, internal tuberosity, size: low and rounded (0); hypertrophied (1). (Sereno et al., 1998, char. 32)
128. Ulna, olecranon process, size: weakly developed (0); well-developed (1); hypertrophied (2). (Novas et al., 1992)
129. Ulna, olecranon process, mediolateral width: broad (0); thin (1). (modified from Calvo et al., 1997)

130. Ulna, olecranon process, shape in lateral view: tapering distally (0); squared (1).
131. Ulna, robusticity index (proximo-distal length relative to anteroposterior length of proximal epiphysis including the olecranon): slender, more than 2 (0); robust, less than 2 (1).
132. Radius (forearm), length relative to humeral length: more (0) or less (1) than 50%. (Sereno et al., 1998, char. 4)
133. Radius, external tuberosity and ulnar internal tuberosity, size: low and rounded (0); hypertrophied (1). (Sereno et al., 1998, char. 33)
134. Manual digit I–ungual, length relative to the depth of proximal end: 2.5 (0) or 3 (1) times. (Sereno et al., 1998, char. 5)
135. Manual unguals, curvature (articular socket held vertical, lateral view): tip ventral (0) or level with (1) ventral margin of flexor tubercle.
136. Ilium, ventrolateral development of supraacetabular crest: extended, pendant (0); reduced and shelf-like (1). (Carrano et al., 2012, char. 267)
137. Ilium, lateral vertical crest dorsal to the acetabulum: absent (0); present (1). (Rauhut, 2003, char. 6)
138. Ilium, shape of posterior margin of postacetabular process: convex (0); concave (1); straight (2); with prominent posterodorsal process but lacking posteroventral process (3). (Carrano et al., 2012, char. 280)
139. Ilium, orientation of pubic peduncle: mostly ventral (0); mostly anterior or 'kinked' double facet with anterior and ventral components (1). (Carrano et al., 2012, char. 268)
140. Ilium, pubic peduncle length to width ratio: greater than or equal to 1 (0); 1–2 (1); greater than 2 (2). (modified from Carrano et al., 2012, char. 272)
141. Ilium, brevis fossa, lateral and medial margins, orientation in ventral view and development of fossa: subparallel, narrow fossa (0); posteriorly diverging, expanded fossa (1). (modified by Cau, 2018, char. 592; Holtz, 2000; Rauhut, 2003)
142. Pubis, pubic foot, posteromedial ramus size: moderate to large (0); reduced to a small flange (1). (modified from Sereno et al., 1998, char. 34)
143. Pubis, pubic foot, lateral process: absent (0); present (1) (Note: This character describes the condition present in most spinosaurids)
144. Pubis, pubic foot projection: anteriorly and posteriorly (0); posteriorly (1) (modified from Norell et al. 2001).
145. Pubis, pubic foot, distal face shape: elongate with subparallel margins (0); triangular (1); L-shaped (2) (modified from Choiniere). Note: polarity of states 0 and 1 reversed and a second derived state added to account for the morphology present in many spinosaurids.
146. Pubis, pubic foramen distal to apron and proximal to pubic symphysis: absent (0); present (1).
147. Pubis, pubic foramen, size relative to the distance between the most proximal extent of apron to distalmost extent of symphysis: large, a third or more (0); small, less than a third (1).
148. Puboischiadic plate, foramina/notches: closed along midline, 3 fenestrae (0); open along midline, 1 fenestra (obturator foramen of pubis) and 1–2 notches (1); open along midline, 0 fenestrae, 1–2 notches (2). (Carrano et al., 2012, char. 281)
149. Pubis, length relative to ischium: longer (0); subequal or shorter (1). (Sereno et al., 2022)
150. Ischium, distal half, cross section: laminar, strongly mediolaterally compressed (0); robust, rod-like (1). (Cau, 2018, char. 425)
151. Femur, fourth trochanter position of distalmost end: proximal most 1/3 (0); almost at the half of the femur (1). (Sereno et al., 2022)
152. Femur, oblique ligament groove on posterior surface of head: shallow, groove bounding lip does not extend past posterior surface of head (0); deep, bound medially by well-developed posterior lip (1). (Carrano et al., 2012, char. 304)
153. Femur, orientation of long axis of medial condyle in distal view: anteroposterior (0); posterolateral (1). (Carrano et al. 2012).

154. Femur, distal end, length of the crista tibio-fibulatis (cft) relative to the medial femoral condyle: shorter than half femoral condyle length (0); as long or longer than half the femoral condyle length (1).
155. Femur (or tibia), length: more (0) or less (1) than five times posterior dorsal centrum length. (Cau, 2018, char. 245)
156. Tibia, proximal diaphysis, length-width ratio: smaller than 2 (0); greater than 2 (1). (Sereno et al., 2022) (after Samathi et al., 2021)
157. Tibia, distal end, lateral malleolus: projecting as a distinct process (0); barely projecting, not really distinguishing from diaphysis (1).
158. Astragalus, ascending process, height relative to its posterior dorsoventral height: lower (0); higher (1); more than twice (2). (modified from Rauhut et al., 2003)
159. Pedal ungual phalanges, ventral side: concave (0); flat (1). (Sereno et al., 2022)

Synapomorphy list

Unambiguous synapomorphies ("C#" is character number) are listed below for clades in the minimum-length tree.

Spinosauridae

- Pubis, pubic foot, lateral process (C142): absent --> present
- Ischium, distal half, cross sectionion (C149): robust, rod-like--> laminar, strongly mediolaterally compressed
- Femur, orientation of long axis of medial condyle in distal view (C152): anteroposterior --> posterolateral

***Camarillasaurus* + Baryonychinae + Spinosaurinae**

- Tibia, proximal diaphysis, length-width ratio (155): smaller than 2 --> 2 or greater

Baryonychinae

- Premaxilla, form of premaxilla-nasal suture (C6): W-shaped --> V-shaped
- Quadrate, articular head, shape (C45): oval --> subquadrate
- Dentary, tooth count (C75): 15 or less --> 16-30
- Cervical vertebrae, anterior post-axial neural spines in lateral view (C83): taller than long --> longer than tall
- Dorsal vertebrae, posterior neural spines, extensive basal webbing (C94): absent --> present
- Dorsal vertebrae, accessory centrodiapophyseal lamina (C98): absent --> present
- Coracoid, posterior process, shape (C122): crescentic --> 2
- Ulna, robusticity index (proximo-distal length relative to anteroposterior length of proximal epiphysis including the olecranon) (C131): slender, more than 2 --> robust, less than 2

Spinosaurinae

- Cervical vertebrae, middle and posterior centra width relative to centra height (C82): taller than wide or as tall as wide (round) --> wider than tall
- Dorsal vertebrae, anterior centra, pneumatic foramen, size relative to parapophysis (C88): larger or equal --> smaller
- Dorsal vertebrae, mid-posterior, excavated prezygo-para-diapophyseal fossa (prpadf) delimited by ppdl (C90): absent --> present
- Dorsal vertebrae, middle and posterior neural arches, notched spino-prezygapophyseal lamina (sprl) in lateral view (C91): absent --> present
- Dorsal vertebrae, posterior, neural spine antero-posterior length at base relative to centrum length (CX95): subequal --> shorter
- Dorsal vertebrae, middle-posterior parapophyses, development (C97): distinct and well-developed --> small, knob-like
- Caudal vertebrae, anterior neural arches, ventral rib laminae (centro-costal laminae, ?acpl? and ?pcpl?) (C106): absent --> present
- Caudal vertebrae, anterior neural arches, anterolateral surface, deep triangular prezygocostal fossa delimited by two laminae (C107): absent --> present

***Vallibonavenatrix* + *Irritator* + Spinosaurini**

- Dorsal vertebrae, middle, centrum length relative to height (C86): less than 1.4 times centrum height --> equal or greater than 1,4 times centrum height

- Dorsal vertebrae, mid-posterior centra, pneumatic foramina (C92): absent --> present
- Caudal vertebrae, anterior, well-marked spinodiapophyseal lamina (C105): absent or very faint at base of spine --> present
- Caudal vertebrae, middle, centrum elongation relative to centrum height (C115): elongated, greater than 1.6 times --> not elongated, 1.6 times or shorter

***Irritator* + Spinosaurini**

- Ilium, orientation of pubic peduncle (C138): mostly anterior or kinked double facet with anterior and ventral components --> mostly ventral

Spinosaurini

- Premaxilla, notch for dentary tooth 1 at the height of premaxillary alveoli 2 (C13): absent --> present
- External naris, position of anterior margin relative to maxillary tooth row (C28): anterior, but not reaching anteriormost maxillary tooth --> posterior to half point of maxillary tooth row
- Dorsal vertebrae, posterior centra, articular surface (C99): platycoelous or amphycoelus --> strongly opisthocoelous

Spinosaurus

- Upper jaws (premaxillae and maxillae), festooning along the alveolar margin (C5): absent --> present
- Premaxillae, shape of rosette anterior expansion (C14): continuous, oval-shaped --> abrupt with a constriction by the third premaxillary alveolus, mushroom-shaped
- Premaxilla and anterior dentary, interdental septa spacing (C60): regular --> alternate (alveoli result paired)